AD 739946

AD

USAAMRDL TECHNICAL REPORT 71-69

AN INVESTIGATION OF THE QUANTITATIVE APPLICABILITY OF MODEL HELICOPTER ROTOR WAKE PATTERNS OBTAINED FROM A WATER TUNNEL

By

Anton J. Landgrebe

Elton D. Bellinger

December 1971

EUSTIS DIRECTORATE

U. S. ARMY AIR MOBILITY RESEARCH AND DEVELOPMENT LABORATORY

FORT EUSTIS, VIRGINIA

Reproduced by
NATIONAL TECHNICAL
INFORMATION SERVICE
Springfield, Va 22151

CONTRACT DAAJ02-70-C-0009

UNITED AIRCRAFT CORPORATION

RESEARCH LABORATORIES

EAST HARTFORD, CONNECTICUT

Approved for public release;
distribution unlimited.

U. S. ARMY MATERIEL COMMAND

DISCLAIMERS

The findings in this report are not to be construed as an official Department of the Army position unless so designated by other authorized documents.

When Government drawings, specifications, or other data are used for any purpose other than in connection with a definitely related Government procurement operation, the United States Government thereby incurs no responsibility nor any obligation whatsoever; and the fact that the Government may have formulated, furnished, or in any way supplied the said drawings, specifications, or other data is not to be regarded by implication or otherwise as in any manner licensing the holder or any other person or corporation, or conveying any rights or permission, to manufacture, use, or sell any patented invention that may in any way be related thereto.

Trade names cited in this report do not constitute an official endorsement or approval of the use of such commercial hardware or software.

DISPOSITION INSTRUCTIONS

Destroy this report when no longer needed. Do not return it to the originator.

Unclassified

Security Classification

DOCUMENT CONTROL DATA - R & D

Security classification of title body of abstract and indexing annotation must be entered when the overall report is classified)

1. ORIGINATING ACTIVITY (Corporate author) United Aircraft Corporation Research Laboratories East Hartford, Connecticut	2a. REPORT SECURITY CLASSIFICATION Unclassified 2b. GROUP

3. REPORT TITLE

AN INVESTIGATION OF THE QUANTITATIVE APPLICABILITY OF MODEL HELICOPTER ROTOR WAKE PATTERNS OBTAINED FROM A WATER TUNNEL

4. DESCRIPTIVE NOTES (Type of report and inclusive dates)

Final Report

5. AUTHOR(S) (First name, middle initial, last name)

Anton J. Landgrebe
Elton D. Bellinger

6. REPORT DATE December 1971	7a. TOTAL NO. OF PAGES 140	7b. NO. OF REFS 24

8a. CONTRACT OR GRANT NO. DAAJ02-70-C-0009 b. PROJECT NO. c. Task 1F162204A14232 d.	9a. ORIGINATOR'S REPORT NUMBER(S) USAAMRDL Technical Report 71-69 9b. OTHER REPORT NO(S) (Any other numbers that may be assigned this report) UARL Report K910917-23

10. DISTRIBUTION STATEMENT

Approved for public release; distribution unlimited.

11. SUPPLEMENTARY NOTES	12. SPONSORING MILITARY ACTIVITY Eustis Directorate U.S. Army Air Mobility R&D Laboratory Fort Eustis, Virginia

13. ABSTRACT

An analytical investigation was conducted to evaluate quantitative applications of available model rotor tip vortex patterns from a water tunnel. This evaluation consisted of reducing selected photographic wake data to coordinate form, and comparing the resulting wake geometries with both theoretical results and available experimental data taken in air. Additionally, the study included an examination of the sensitivity of water tunnel wake geometry to the water tunnel test parameters which did not duplicate full-scale rotor values and the applicability of a water tunnel wake geometry to determine the airloads of a full-scale rotor. Finally, the possibility of developing simplified wake documentation and generalization procedures and improved water tunnel test techniques was assessed.

It was found that the usefulness of the available photographic wake data for quantitative purposes is limited. Many of the limitations could be eliminated in future tests through the improved test procedures recommended herein. The capability of a theoretical analysis to predict the water tunnel wake features in forward flight was also demonstrated. The analysis was used (1) to determine that the primary parameters influencing tip vortex geometry in moderate to high-speed forward flight ($\mu > 0.15$) are number of blades, rotor advance ratio, thrust coefficient, and tip-path plane angle, and (2) to show that tip vortex geometry is insensitive to differences in the azimuth variation of blade loading produced by variations of blade flexibility, cyclic pitch, Reynolds number, and Mach number. Thus the fact that the full-scale values of the latter parameters were not accurately simulated in the water tunnel does not appear to significantly compromise the representation of the full-scale rotor wake by the wake of the model rotor, providing the primary parameters are duplicated. The analysis was also used to show that for typical high-speed flight, wake distortions generally have a negligible effect on blade airloads except at local points where the tip vortices pass close to the blades. Procedures for simplifying wake documentation, generalizing forward-flight wake geometry, and improving water tunnel test techniques are also presented along with a discussion of the advantages and disadvantages of testing in water and air.

DD FORM 1 NOV 65 1473 REPLACES DD FORM 1473, 1 JAN 64, WHICH IS OBSOLETE FOR ARMY USE.

Unclassified

Security Classification

Unclassified

Security Classification

14. KEY WORDS	LINK A ROLE	LINK A WT	LINK B ROLE	LINK B WT	LINK C ROLE	LINK C WT
Helicopter Rotors						
Helicopter Rotor Wake						
Wake Geometry						
Vortices						
Flow Visualization						
Rotor Flow Patterns						
Helicopter Rotor Aerodynamics						
Helicopter Rotor Airloads						
Distorted Wake						
Model Helicopter Rotor Tests						
Water Tunnel Tests						
Rotor Wake Theory						

Unclassified

Security Classification

DEPARTMENT OF THE ARMY
U S ARMY AIR MOBILITY RESEARCH & DEVELOPMENT LABORATORY
EUSTIS DIRECTORATE
FORT EUSTIS, VIRGINIA 23604

This report has been reviewed by the Eustis Directorate, U. S. Army Air Mobility Research and Development Laboratory and is considered to be technically sound.

The purpose of the program was to conduct an analytical investigation to evaluate qualitative applications of model rotor tip vortex patterns obtained in a water tunnel. This included developing and applying procedures for transforming photographic wake data to coordinate form, comparing the resulting wake geometries with available theoretical and experimental results, examining the sensitivity of wake geometry to nonsimulated parameters, and investigating procedures for simplifying the documentation and generalization of rotor wake geometry data and for improving water tunnel testing techniques.

This report is published for the exchange of information and the stimulation of ideas. The program was conducted under the technical management of Mr. John L. Shipley and Mr. Paul H. Mirick of the Aeromechanics Division of the Directorate.

Task 1F162204A14232
Contract DAAJ02-70-C-0009
USAAMRDL Technical Report 71-69
December 1971

AN INVESTIGATION OF THE QUANTITATIVE APPLICABILITY OF MODEL HELICOPTER ROTOR WAKE PATTERNS OBTAINED FROM A WATER TUNNEL

UARL K910917-23

by

Anton J. Landgrebe
Elton D. Bellinger

Prepared by

United Aircraft Corporation
Research Laboratories
East Hartford, Connecticut

for

EUSTIS DIRECTORATE
U. S. ARMY AIR MOBILITY RESEARCH AND DEVELOPMENT LABORATORY
FORT EUSTIS, VIRGINIA

Approved for public release;
distribution unlimited.

SUMMARY

An analytical investigation was conducted to evaluate quantitative applications of available model rotor tip vortex patterns from a water tunnel. This evaluation consisted of reducing selected photographic wake data to coordinate form, and comparing the resulting wake geometries with both theoretical results and available experimental data taken in air. Additionally, the study included an examination of the sensitivity of water tunnel wake geometry to the water tunnel test parameters which did not duplicate full-scale rotor values and the applicability of a water tunnel wake geometry to determine the airloads of a full-scale rotor. Finally, the possibility of developing simplified wake documentation and generalization procedures and improved water tunnel test techniques was assessed.

It was found that the usefulness of the available photographic wake data for quantitative purposes is limited. Many of the limitations could be eliminated in future tests through the improved test procedures recommended herein. The capability of a theoretical analysis to predict the water tunnel wake features in forward flight was also demonstrated. The analysis was used (1) to determine that the primary parameters influencing tip vortex geometry in moderate to high-speed forward flight ($\mu > 0.15$) are number of blades, rotor advance ratio, thrust coefficient, and tip-path plane angle, and (2) to show that tip vortex geometry is insensitive to differences in the azimuth variation of blade loading produced by variations of blade flexibility, cyclic pitch, Reynolds number, and Mach number. Thus the fact that the full-scale values of the latter parameters were not accurately simulated in the water tunnel does not appear to significantly compromise the representation of the full-scale rotor wake by the wake of the model rotor, providing the primary parameters are duplicated. The analysis was also used to show that for typical high-speed flight, wake distortions generally have a negligible effect on blade airloads except at local points where the tip vortices pass close to the blades. Procedures for simplifying wake documentation, generalizing forward-flight wake geometry, and improving water tunnel test techniques are also presented along with a discussion of the advantages and disadvantages of testing in water and air.

Preceding page blank

FOREWORD

This investigation was sponsored by the U. S. Army Aviation Materiel Laboratories (now the Eustis Directorate, U. S. Army Air Mobility Research and Development Laboratory) under Contract DAAJ02-70-C-0009, Task 1F162204A14232. Efforts under this contract were initiated in September 1969 and completed in July 1971. The assistance provided to this investigation by Mr. Peter J. Arcidiacono, Chief, Aerodynamics (UARL) and Mr. M. C. Cheney, Supervisor, Rotary Wing Technology (UARL) is gratefully acknowledged. The technical representatives of the Contracting Officer for this contract were John L. Shipley and Paul H. Mirick of USAAMRDL.

Preceding page blank

TABLE OF CONTENTS

	Page
SUMMARY	iii
FOREWORD	v
LIST OF ILLUSTRATIONS	ix
LIST OF TABLES	xiii
LIST OF SYMBOLS	xiv
INTRODUCTION	1
EXPERIMENTAL AND THEORETICAL METHODS	3
DESCRIPTION OF THE OCEANICS WATER TUNNEL TEST	3
DESCRIPTION OF THEORETICAL METHODS	5
MODEL BLADE CHARACTERISTICS AND ROTOR OPERATING CONDITIONS	11
MODEL BLADE DIMENSIONAL, STRUCTURAL, AND AIRFOIL CHARACTERISTICS	11
INFLUENCE OF WATER ON BLADE RESPONSE CHARACTERISTICS	12
ROTOR OPERATING CONDITIONS	14
REDUCTION OF WATER TUNNEL WAKE DATA TO COORDINATE FORM	18
LIMITATIONS OF THE WATER TUNNEL FLOW VISUALIZATION DATA	18
PROCEDURES FOR FLOW VISUALIZATION DATA REDUCTION	20
DATA CORRECTIONS AND ACCURACY	22
WATER TUNNEL WAKE COORDINATES AND COMPARISON WITH OTHER SOURCES	23
HOVER -- WATER TUNNEL WAKE VERSUS EXPERIMENTAL WAKE IN AIR	23
FORWARD FLIGHT -- WATER TUNNEL WAKE VERSUS THEORETICAL WAKE	27
SENSITIVITY OF WAKE GEOMETRY TO NONSIMULATED PARAMETERS	30
SENSITIVITY OF WAKE GEOMETRY TO BLADE FLEXIBILITY, PRECONING, AND ROTOR TIP-PATH PLANE ANGLE	30
SENSITIVITY OF WAKE GEOMETRY TO CYCLIC PITCH	32
SENSITIVITY OF WAKE GEOMETRY TO REYNOLDS NUMBER AND MACH NUMBER	33

 Preceding page blank

Page

SENSITIVITY OF WAKE GEOMETRY TO THRUST COEFFICIENT. 33
COMPARISON OF THEORETICAL MODEL AND FULL-SCALE ROTOR WAKES. . . 35
SUMMARY OF WAKE GEOMETRY SENSITIVITY RESULTS. 35

APPLICATION OF WATER TUNNEL AND THEORETICAL WAKE GEOMETRY TO DETERMINE FULL-SCALE ROTOR AIRLOADS 37

SENSITIVITY OF FULL-SCALE ROTOR AIRLOADS TO WAKE DEVIATIONS CAUSED BY NONSIMULATED PARAMETERS. 37
COMPARISON OF THEORETICAL FULL-SCALE AIRLOADS WITH FLIGHT TEST DATA 38
SENSITIVITY OF FULL-SCALE ROTOR AIRLOADS TO WAKE POSITION . . . 39
GENERAL DISCUSSION OF WAKE EFFECTS ON ROTOR AIRLOADING. 43

SUGGESTED PROCEDURES FOR FUTURE WATER TUNNEL FLOW VISUALIZATION TESTS 46

IMPROVED TEST PROCEDURES. 46
PROCEDURES FOR DOCUMENTING AND GENERALIZING WAKE GEOMETRY DATA. 49
TUNNEL WALL CORRECTIONS 55

MODEL ROTOR TESTING IN WATER VERSUS AIR. 58

POTENTIAL ADVANTAGES OF WATER TUNNEL TESTING. 59
POTENTIAL DISADVANTAGES OF WATER TUNNEL TESTING 59

CONCLUSIONS. 62

RECOMMENDATIONS. 64

LITERATURE CITED 121

DISTRIBUTION 124

LIST OF ILLUSTRATIONS

Figure		Page
1	Photographs of Model Rotor and Wake In Water Tunnel -- Two Blades, Simulated 10,000-Lb Lift, Zero Forward Velocity. . . .	66
2	Photographs of Model Rotor and Wake In Water Tunnel -- Two Blades, Simulated 6,000-Lb Lift, Zero Forward Velocity	67
3	Photographs of Model Rotor and Wake In Water Tunnel -- Two Blades, Simulated 10,000-Lb Lift and 35-Kt Forward Velocity. .	68
4	Photographs of Model Rotor and Wake In Water Tunnel -- Two Blades, Simulated 10,000-Lb Lift and 90-Kt Forward Velocity. .	69
5	Components of the UARL Rotor Analysis.	70
6	Rotor-Wake Coordinate System	71
7	Blade and Wake Azimuth Coordinate System	72
8	Three-View Drawing of Oceanics Model Rotor Blade	73
9	NACA 0012 Airfoil Data Used for Model Blade in UARL Rotor Analysis -- Mach Number = 0.13, Reynolds Number = 110,000. . .	74
10	Model Blade Static Calibration Rig	75
11	Comparison of Measured and Predicted Bending Deflections of Model Blade in Water -- Simulated 90 Kt, 10,000-Lb Lift. . . .	76
12	Water Tunnel Tip Vortex Pattern From Blade 1 -- Model Rotor, Hover, Simulated 10,000-Lb Lift, $\psi_{b_{0,1}} = 0$ deg	77
13	Water Tunnel Tip Vortex Pattern From Blade 2 -- Model Rotor, Hover, Simulated 10,000-Lb Lift, $\psi_{b_{0,1}} = 180$ deg	78
14	Comparison of Water Tunnel Tip Vortex Coordinates With UARL Test Results -- Hover, Simulated 10,000-Lb Lift.	79
15	Comparison of Water Tunnel Tip Vortex Coordinates With UARL Test Results -- Hover, Simulated 6,000-Lb Lift	80

Figure		Page
16	Photograph of Wake Instability of a Hovering Model Rotor in Air.	81
17	Water Tunnel Tip Vortex Patterns -- Model Rotor, Simulated 35 Kt, 10,000-Lb Lift	82
18	Comparison of Experimental and Undistorted Wake Patterns -- Model Rotor, Simulated 35 Kt, 10,000-Lb Lift.	83
19	Comparison of Experimental and Undistorted Wake Boundaries -- Model Rotor, Simulated 35 Kt, 10,000-Lb Lift.	84
20	Comparison of Experimental and Theoretical Wake Patterns -- Model Rotor, Simulated 35 Kt, 10,000-Lb Lift.	85
21	Comparison of Experimental and Theoretical Wake Axial Coordinates -- Model Rotor, Simulated 35 Kt, 10,000-Lb Lift .	86
22	Schematic of Rotor and Fixed-Wing Wakes	90
23	Water Tunnel Tip Vortex Patterns -- Model Rotor, Simulated 90 Kt, 10,000-Lb Lift	91
24	Comparison of Experimental and Undistorted Wake Patterns -- Model Rotor, Simulated 90 Kt, 10,000-Lb Lift.	92
25	Comparison of Experimental and Undistorted Wake Boundaries -- Model Rotor, Simulated 90 Kt, 10,000-Lb Lift.	93
26	Comparison of Experimental and Theoretical Wake Patterns -- Model Rotor, Simulated 90 Kt, 10,000-Lb Lift.	94
27	Comparison of Experimental and Theoretical Wake Axial Coordinates -- Model Rotor, Simulated 90 Kt, 10,000-Lb Lift .	95
28	Effect of Blade Flexibility on Model Rotor Loading and Wake Geometry for Constant Rotor Tip-Path Plane Angle.	99
29	Effect of Blade Coning on Model Rotor Wake Geometry	100
30	Effect of Rotor Tip-Path Plane Angle on Model Rotor Loading and Wake Geometry	101

Figure		Page
31	Effect of Rotor Tip-Path Plane Angle on Model Rotor Wake Distortions	102
32	Effect of Cyclic Pitch on Model Rotor Loading and Wake Geometry	104
33	Effect of Reynolds Number and Mach Number on Model Rotor Loading and Wake Geometry	105
34	Effect of Thrust Coefficient on Model Rotor Loading and Wake Geometry	106
35	Comparison of Predicted Loading and Wake Geometry of the Full-Scale UH-1D Rotor and Water Tunnel Model Rotor	107
36	Predicted Wake Geometry Sensitivity Results at Blade-Vortex Intersections -- $\mu = 0.19$, $C_T = 0.0033$	108
37	Top View of Undistorted Wake Patterns -- b = 2, $\mu = 0.19$	109
38	Sensitivity of Predicted Full-Scale Rotor Airloads to Wake Geometry -- UH-1D Rotor, V = 90 Kt, $\mu = 0.19$, $C_T = 0.0033$	110
39	Theoretical Wake Pattern From One Blade of the UH-1A Rotor, V = 89 Kt, $\mu = 0.21$, $C_T = 0.0037$	111
40	Comparison of Predicted Full-Scale Rotor Airloads Based on Experimental and Theoretical Wake Coordinates With Flight Test Data -- UH-1A Rotor	112
41	Comparison of Predicted Full-Scale Rotor Airloads Based on Various Theoretical Inflow Sources With Flight Test Data -- UH-1A Rotor, $\mu = 0.21$, $C_T = 0.0037$, $\alpha_{TPP} = 3.6$ deg	113
42	Tip Vortex Positions Relative to the 85 Percent Radial Station of the Following Blade, $\psi_b = 90$ deg	114
43	Radial Airloading Distributions at the 90-deg Azimuth Position	115
44	Sensitivity of UH-1A Airloads to Deviations of the Inboard Wake Coordinates, V = 89 Kt, $\mu = 0.21$, $C_T = 0.0037$	116

Figure		Page
45	Radial and Azimuthal Coordinates Associated With Blade-Vortex Intersections -- b = 2, μ = 0.19.	117
46	Axial Coordinates of Experimental Wake Boundaries Versus Wake Azimuth Position -- Model Rotor, Simulated 90 Kt, 10,000-Lb Lift	118
47	Sample Photograph of Wake Flow Visualization for a Model Rotor Operating in Air	119
48	Sample Shadowgraph of Wake of a Model Propeller Obtained Using Laser Holography Techniques.	120

LIST OF TABLES

Table		Page
I	Model Blade Dimensional and Structural Characteristics	11
II	Model Blade Natural Frequency Ratios	13
III	Comparison of Experimental and Theoretical Rotor Parameters. .	14
IV	Test Conditions for This Investigation	14
V	Rotor Operating and Control Parameters	
	Part I - Hover Conditions.	16
	Part II - Forward Flight Conditions	17
VI	Comparison of Oceanics and UARL Model Rotor Design Characteristics	23
VII	Test Conditions and Rotor Parameters for Comparing Blade Airloads.	38

LIST OF SYMBOLS

a_o	blade coning or precone angle, deg
a_{1_s}	longitudinal flapping angle for the first harmonic; coefficient of $-\cos\psi$ term in Fourier series expansion of blade flap angle with respect to plane normal to the rotor shaft axis, deg
AR	blade aspect ratio, AR = R/c
A_{1_s}	cosine component of first harmonic cyclic pitch; coefficient of $-\cos\psi$ term in Fourier series expansion of the blade pitch angle with respect to the plane normal to the rotor shaft, deg
b	number of blades
B_{1_s}	sine component of first harmonic cyclic pitch; coefficient of $-\sin\psi$ term in Fourier series expansion of blade pitch angle with respect to the plane normal to the rotor shaft, deg
c	blade chord, in.
C_L	rotor lift coefficient, $L/\rho\pi R^2(\Omega R)^2$
$C_{L_{INC,MODEL}}$	lift coefficient for model rotor in water (incompressible) obtained from full-scale rotor lift coefficient (compressible); see Equation (1)
$C_{L_{COMP,F.S.}}$	lift coefficient of full-scale rotor in air (compressible)
C_T	rotor thrust coefficient, directed along shaft, $T/\rho\pi R^2(\Omega R)^2$
GC	geometric influence coefficient for induced velocity; see Equation (3)
I_F	flapwise section area moment of inertia, in.^{4}
ℓ	blade spanwise loading, lift/unit span, lb/in.
ℓ_o	steady value of blade spanwise loading at a specific blade station, lb/in.

L	rotor lift, lb
M	local blade section Mach number
$M_r=0.7$	Mach number at $r = 0.7$
r	radial coordinate from rotor axis of rotation to blade section or point on tip vortex, nondimensionalized by R
$r_{b_{0,0}}$	radial position at which vortex shed from blade (normally 1 for tip vortex)
$r_{b_{1,1}}$	radial position of blade vortex intersection
R	rotor radius, ft or in.
Re	Reynolds number at blade tip, $Re = c(\Omega R)/\nu$ (value at $\psi_b = 0$ for forward flight conditions)
t	time, sec
T	rotor thrust, lb
V	forward velocity or tunnel flow velocity, kt
V_i	induced velocity, fps
$V_{i_{MOM}}$	momentum value of axial induced velocity, positive down, fps; see Equation (2)
w	blade weight per unit spanwise length, lb/in.
x	longitudinal coordinate measured from center of rotor disc in tip-path plane, nondimensionalized by R, positive as shown in Figure 6
y	lateral coordinate measured from center of rotor disc in tip-path plane, nondimensionalized by R, positive as shown in Figure 6
z	axial coordinate measured from center of rotor disc and normal to tip-path plane, nondimensionalized by R, positive up as shown in Figure 6

α_s	rotor shaft angle of attack (mast angle). Angle between forward velocity and plane normal to shaft axis, positive nose up, deg
α_{TPP}	rotor tip-path plane angle of attack. Angle between forward velocity and tip-path plane (see Figure 6), positive nose up, deg
Γ	local blade circulation or circulation of a vortex element, ft^2/sec
θ_0	blade collective pitch angle at center of rotation relative to plane of rotation, deg
θ_1	rate of change of local blade pitch angle due to built-in linear twist with respect to blade spanwise direction, positive when tip section is twisted leading-edge up relative to root section, deg
θ_{75}	blade collective pitch angle as measured at r = 0.75, deg
λ	rotor inflow ratio; see Equation (11)
μ	rotor advance ratio, $\mu = V\cos\alpha_{TPP}/\Omega R$
ν	kinematic viscosity, $(ft^2/sec)^{-1}$
ρ	water or air density, $lb\text{-}sec^2/ft^4$
σ	rotor solidity ratio, $\sigma = bc/\pi R$
χ_{TPP}	undistorted wake deflection angle based on momentum induced velocity, angle between wake streamlines and tip-path plane, positive when wake is below tip-path plane, deg; see Equations (9), (10), and (13)
ψ_b	blade azimuth angle measured from positive x axis (downstream direction) to blade in direction of blade rotation, deg or rad; see Figure 6
$\psi_{b_{0,0}}$	blade azimuth angle of blade that originated (shed) vortex element -- at the time of origination, deg or rad; see Figure 7

$\psi_{b_{0,1}}$	blade azimuth angle of blade that originated (shed) vortex element -- at the current time of interest, deg or rad; see Figure 7
$\psi_{b_{1,1}}$	blade azimuth angle of intersecting blade at blade-vortex "intersection" -- at the current time of interest, deg or rad
ψ_W	wake azimuth position, azimuth angle of vortex element (point) relative to the blade from which it originated, measured from the blade in a moving coordinate system that rotates with the blade and translates with the rotor center in flight or with the flow velocity in the tunnel, deg or rad; see Figure 7
ω	natural bending or torsional frequency ratio of blade, natural frequency/Ω
Ω	rotational frequency of blade, rad/sec

INTRODUCTION

Water tunnel testing to visualize tip vortex trails of a model rotor has recently been presented as a method for determining wake characteristics representative of full-scale rotors. Water tunnel tests conducted at Oceanics, Inc., under USAAMRDL sponsorship have provided a large quantity of wake visualization photographic data for model rotors simulating both hover and forward flight. A description of these tests and sample photographs of the wake patterns are presented in References 1 through 3. Potential applications of wake visualization data obtained in a water tunnel are:

1. To provide a fundamental understanding of rotor wake characteristics

2. To provide experimental wake geometry data for comparison with wake geometries predicted by theoretical methods

3. To provide quantitative wake geometry information for use in theoretical analyses for computing the instantaneous rotor flow field and associated blade airloads, rotor performance, stress, vibration and acoustic characteristics

Water tunnel data acquired at Oceanics, Inc. were primarily obtained to define qualitative rotor wake features. Qualitative observations which are of value in clarifying many physical characteristics of the rotor wake are included in Reference 1. However, it remained to be determined the degree to which the available data are applicable, in a quantitative sense, to full-scale rotors operating in air.

For the past several years the United Aircraft Research Laboratories (UARL) have been engaged in experimental and analytical studies pertaining to both the visualization and prediction of rotor wake geometries, and the development of helicopter aerodynamic analyses which include provisions for both distorted and undistorted wake geometries. These studies, described in References 4 through 8, have provided valuable data and analytical methods for determining rotor wake characteristics. The objectives of the investigation reported herein were to apply the results of these studies with those of the Oceanics' experiments to:

1. Develop and apply procedures for transforming photographic wake data to quantitative form using water tunnel wake measurements

2. Evaluate and demonstrate procedures for using water tunnel wake data to determine full-scale rotor wake patterns and blade airloads

3. Review and recommend methods for simplifying the documentation and generalization of rotor wake geometry data and improving water tunnel testing techniques

This report contains sample results from the water tunnel experiments along with a brief description of the test procedures used. Also included are: (1) a description of the techniques used to reduce the wake data to coordinate form, (2) comparisons of the data with theory and other experimental wake data, (3) a sensitivity study to evaluate the effect of nonsimulated parameters in the water tunnel tests, and (4) a discussion of the applicability of model water tunnel wake geometry data to determine full-scale airloads. Finally, procedures for documenting and generalizing wake geometry data, suggestions for improving test procedures, and a discussion of the relative merits of testing in water and air are presented.

EXPERIMENTAL AND THEORETICAL METHODS

DESCRIPTION OF THE OCEANICS WATER TUNNEL TEST

The experimental program conducted in the Oceanics water tunnel is described in detail in Reference 1. Briefly, the experimental program, conducted in 1967, consisted of testing single model rotor configurations designed to simulate teetering rotor flight conditions from hover to 120 kt. The Oceanics water tunnel is a recirculating, closed-jet type tunnel with a test section having a square cross section 20 in. on a side and a length of approximately 7 ft. The model helicopter rotor blades were geometrically scaled from the blades of the UH-1D main rotor. A scale factor of 48 was used to simulate the full-scale rotor having a 24-ft radius with the model rotor having a radius of 6 in. Although the UH-1D rotor is a two-bladed teetering rotor, the model was tested with one, two, and three blades rigidly attached to the hub (i.e., hingeless). The test conditions consisted of simulated 4000-, 6000-, 8000-, and 10,000-lb lift values for the two-bladed configuration, and the same control settings (i.e., collective pitch and shaft tilt) were used for the one- and three-bladed configurations. In addition to hover, simulated forward velocities of 10, 20, 25, 35, 50, 60, 70, 90, 110, and 120 kt were investigated.

In order to observe and document the tip vortex patterns created by the model rotors, the tip vortices were made visible by emitting air bubbles from the tip of each blade. These bubbles remained trapped in the core of the tip vortices, thereby making the vortex trails visible. The tip vortex trails were recorded in 16 mm high-speed movies and stop-action and time-exposure photographs. Sample photographs showing the top and side views of the wake of the two-bladed rotor operating at the simulated 10,000-lb and 6000-lb lift conditions and zero forward velocity (hover) are presented in Figures 1 and 2. Photographs for the same rotor operating at the simulated 10,000-lb lift condition and 35 kt and 90 kt forward velocity are presented in Figures 3 and 4. In addition to the flow visualization data, rotor lift, rotational speed, shaft angle of attack (or mast tilt as referred to in Reference 1), blade collective pitch, and tunnel velocity were recorded.

The test procedures consisted of the following. The collective pitch (for the two-bladed rotor) was initially set to the full-scale flight test value. The model shaft angle of attack was set equal to the angle between the full-scale rotor tip-path plane and the free stream (tip-path plane angle of attack). Neither a teetering hinge nor cyclic pitch was incorporated in the model rotor, so the airload distribution and blade

response of the test rotor were not truly representative of the full-scale helicopter operation. The model advance ratio was set equal to the full-scale advance ratio by equating the ratio of the water tunnel velocity and model tip speed (25.21 fps) to the ratio of the full-scale velocity and full-scale tip speed (800 fps). The rotational velocity of the model rotor was maintained at 8 rps in a direction opposite to conventional full-scale operation (i.e., the model rotated clockwise when viewed from above). Operating under these conditions, the rotor thrust along the shaft was measured and converted to rotor lift (normal to the free-stream direction). If the lift coefficient value obtained in the water tunnel was not within 3 percent of the desired full-scale value (corrected through the use of the Prandtl-Glauert factor at the 0.7 radius), the collective pitch angle was changed and the test was repeated until the measured lift coefficient was within the specified tolerance range. In this manner, collective pitch values were established for the two-bladed rotor conditions. These same values of collective pitch were then employed for investigations involving the one- and three-bladed rotor configurations. To account for the difference in the compressibility characteristics between the test medium for the model (water) and the operating medium for the full-scale rotor (air), the Prandtl-Glauert compressibility correction was applied to the full-scale lift coefficient, $C_{L_{COMP,F.S.}}$, to obtain the corresponding incompressible model lift coefficient, $C_{L_{INC,MODEL}}$, applicable to operation in water. The following Prandtl-Glauert compressibility correction was used:

$$C_{L_{INC,MODEL}} = \sqrt{1 - (M_{0.7})^2}\; C_{L_{COMP,F.S.}} \tag{1}$$

The Mach number, $M_{0.7}$, was taken as the mean value at the 0.7 radius of the full-scale rotor ($M_{0.7} = 0.49$), which results in a Prandtl-Glauert correction factor of 0.87. As discussed in a later section of this report, this compressibility correction is applicable when the correlation of model and full-scale collective pitch values are of interest. However, when it is desired to simulate the wake geometry of a full-scale rotor in a water tunnel, the full-scale lift coefficient should be duplicated directly without the application of the compressibility correction.

No corrections were included for differences in viscous effects between the model and full-scale rotors. The Reynolds number, $Re = c\Omega R/\nu$, based on the rotor chord length and tip speed, was approximately 7.9×10^6 for the UH-1D rotor and 9.3×10^4 for the model rotor operating in the water tunnel. It was assumed that the Reynolds number effect on the total rotor lift coefficient is negligible. The effect of Reynolds number on

the drag characteristics was recognized, and thus rotor torque was not measured.

Corrections were not included for tunnel wall interference. However, for the hover and transitional velocity conditions, the lift and photographic data were recorded after the rotor reached a constant rotational speed but prior to the establishment of substantial recirculation from the impingement of the wake on the tunnel floor and walls.

DESCRIPTION OF THEORETICAL METHODS

Several theoretical methods developed at the United Aircraft Research Laboratories in recent years were used during the course of this investigation to evaluate and apply water tunnel data. The following background information is presented to acquaint the reader with the theoretical methods used and the procedures for their application.

The theoretical methods used in this study are depicted schematically in Figure 5. The Blade Response Analysis, Circulation Analysis, and Wake Geometry Analysis are used in sequence to compute blade response, rotor and wake circulations, wake geometry, blade inflow, and airload distributions. Provisions for the calculation of integrated rotor performance, blade stresses and vibrations based on the calculated airload distributions are also included. The combination of the component theoretical methods, shown in Figure 5, makes up what will be referred to as the UARL Rotor Analysis. Iterations between the component methods are required to insure compatibility between the input and output items. A brief description of each of the component methods making up the UARL Rotor Analysis follows.

Blade Response Analysis

The Blade Response Analysis is used to determine the performance, flapping and fully-coupled elastic blade response based on predetermined airfoil data and inflow distributions. The blade response can be represented by up to five flapwise, two chordwise, and two torsional elastic modes. Blade rigid body modes -- flapping and lagging -- are also considered for articulated rotors. If blade flexibility is not desired, rotor performance and airloads are calculated using rigid blade motions only. When flexibility is desired, a normal mode technique (Reference 9, p. 125) is used to determine the elastic blade deflections. Reference 10 contains the basic differential equations of motion which are solved in the computerized Blade Response Analysis by a numerical integration technique that consists of a finite difference, step-by-step temporal integration of the equations.

A given distribution of blade induced velocities (inflow) over the rotor disc is required for the analysis. The source of these velocities, which are normal to the plane of the rotor, may simply be the "constant inflow" based on the momentum value of induced velocity (Reference 11),

$$V_{i_{MOM}} = \frac{\Omega R C_T}{2\sqrt{\mu^2 + \lambda^2}} \tag{2}$$

or it may be the more complex "variable inflow" determined from the computation of the induced effects of the rotor wake pattern at the blades.

The rotor operating parameters and blade structural characteristics are required as input to the analysis. The operating parameters consist of such items as the rotor velocity, tip speed, air density, cyclic pitch, and a specified combination of rotor lift and propulsive force, or collective pitch and inflow ratio, or rotor lift and angle of attack. The blade dimensional and structural characteristics include blade planform dimensions, airfoil shape, and distributions of twist, mass, and stiffness. In addition, airfoil section aerodynamic data and blade natural vibration characteristics are required for the Blade Response Analysis. Two options for the aerodynamic data are available. The first option is based on steady-state, two-dimensional airfoil data. The second replaces the steady-state airfoil data, where possible, by unsteady data derived from available data for two-dimensional airfoils executing forced, pure sinusoidal pitching motion. For the applications of the analysis described herein (which involve largely unstalled conditions), steady-state, two-dimensional airfoil data were used. The required natural vibration characteristics of the blade are derived from a separate computer analysis in the form of blade natural frequencies and mode shapes.

Circulation Analysis

If variable inflow and/or wake geometry is to be computed, the Circulation Analysis is used to calculate the time-varying bound circulation distributions on the blade and the associated trailing vortex circulation distributions. The circulation distributions are calculated given the rotor blade motions and control settings and a specified geometry of the rotor wake. The technical approach used in the Circulation Analysis is basically similar to that described in Reference 12, and the analysis generally represents a rotary-wing equivalent of the classical lifting-line approach used successfully for fixed wings.

Once the circulations are computed, the variable inflow velocities induced at the blade by the bound and trailing vorticity of the rotor can be determined through application of the Biot-Savart law which can be expressed simply in the following form:

$$V_i = f(\Gamma, \text{Wake Geometry}) = \frac{1}{4\pi} \sum (\Gamma)(GC) \tag{3}$$

Here the induced velocity at a point on the blade, V_i, is a function of the circulations and wake geometry and is proportional to the summation of the products of the circulation strength, Γ, and the geometric influence coefficient, GC, of each element of vorticity in the rotor-wake system. The geometric coefficient is related only to the distance between a wake element and the point at which the induced velocity is being computed.

Wake Geometry Analysis

The Circulation Analysis requires that the rotor wake geometry be specified in order for circulations and induced velocities to be determined. Either an undistorted or distorted wake geometry may be used.

Undistorted Wake

In earlier variable inflow methods (e.g., Reference 12), the wake was assumed to be a classical undistorted skewed helical sheet of vorticity defined from momentum considerations (hereafter referred to as the undistorted wake). The equations for the undistorted wake coordinates are presented below.

$$x = \cos(\psi_{b_{0,1}} - \psi_w) + \mu\psi_w \tag{4}$$

$$y = \sin(\psi_{b_{0,1}} - \psi_w) \tag{5}$$

$$z = -(\tan \chi_{TPP})\mu\psi_w - \lambda\psi_w \tag{6}$$

A diagram of the rotor-wake coordinate system in the water tunnel is presented in Figure 6. The origin of the coordinate system is defined as

the center of the rotor disc in the tip-path plane. The rectilinear coordinates x, y, and z are nondimensionalized by the rotor radius, R. The azimuthal wake coordinate, ψ_W, hereafter referred to as the wake azimuth position, is the azimuth angle in the rotating coordinate system of a point on the vortex filament relative to the blade from which it originated. As shown in Figure 7, it is equivalent to the blade azimuth travel from the time it shed the vortex point to the current time of interest:

$$\psi_W = \psi_{b_{0,1}} - \psi_{b_{0,0}} \quad (\psi_{b_{0,1}} > \psi_{b_{0,0}}) \tag{7}$$

ψ_b is defined as the blade azimuth in the fixed coordinate system relative to the downstream blade position (see Figure 6). $\psi_{b_{0,0}}$ is the particular azimuth position of the blade from which the vortex was originated at the time the vortex point was shed (see Figure 7). $\psi_{b_{0,1}}$ is the azimuth position of the originating blade at the current time of interest (see Figure 7). In Equation (7), $\psi_{b_{0,1}}$ must be greater than $\psi_{b_{0,0}}$ and can be greater than 360 deg, depending upon the number of times the originating blade passed the $\psi_b = 0$ position since the vortex point was shed.

The coordinates of the undistorted wake representation are obtained from the rotor advance ratio, μ, thrust coefficient, C_T, and angle of attack relative to the tip-path plane, α_{TPP}. For example, the top view of the tip vortex filaments is obtained directly from the helicoidal path of the blade tip as it translates at the velocity $V\cos\alpha_{TPP}$ and rotates at the velocity ΩR. These two velocity components are contained in the advance ratio, μ, that appears in Equation (4). The side view is dependent on the wake deflection angle, χ_{TPP} (angle between the rotor disc and wake streamlines), which is defined in the following manner:

$$\tan \chi_{TPP} = \frac{\text{MEAN ROTOR FLOW VELOCITY}}{\text{ROTOR TRANSLATIONAL VELOCITY}} \tag{8}$$

or

$$\chi_{TPP} = \tan^{-1} \left\{ - \frac{V \sin\alpha_{TPP} - V_i}{V \cos \alpha_{TPP}} \right\} \tag{9}$$

If the momentum value of induced velocity from Equation (2) is used for V_i, the wake deflection angle relation is

$$\chi_{TPP} = \tan^{-1}\left(-\frac{\lambda}{\mu}\right) \tag{10}$$

in which λ is the rotor inflow ratio,

$$\lambda = \frac{V \sin \alpha_{TPP} - V_i}{\Omega R} \tag{11}$$

For moderate to high-speed flight conditions (typically, $\mu > 0.15$),

$$V_i \sim \frac{\Omega R\ C_T}{2\mu} \tag{12}$$

and the wake deflection angle relation is

$$\chi_{TPP} = \tan^{-1}\left\{\tan(-\alpha_{TPP}) + \frac{C_T}{2\mu^2}\right\} \tag{13}$$

Distorted Wake

To eliminate the necessity for prescribing an undistorted wake geometry, an analytical method for computing more realistic wake geometries was developed at UARL. The basic approach of this method, entitled the Wake Geometry Analysis, involves the following. First, an undistorted wake model is defined along with the distribution of circulation strengths of the various vortex elements comprising the wake. The classical Biot-Savart law is then applied to determine the velocities induced by each vortex wake element at numerous points in the wake. These distorting velocities are then numerically integrated over a small time increment to obtain new wake element positions. The process of alternately computing new velocities and positions is continued until a converged, periodic distorted wake geometry is attained. By dividing the

wake into near and far wake elements, an approximate analysis which eliminates the potentially massive computing cost requirements has been developed without significantly compromising the accuracy of the technical results. Further details of the procedures used to compute wake geometries are given in References 4 and 5.

MODEL BLADE CHARACTERISTICS AND ROTOR OPERATING CONDITIONS

MODEL BLADE DIMENSIONAL, STRUCTURAL, AND AIRFOIL CHARACTERISTICS

The dimensional and structural characteristics of the Oceanics model rotor, required as input information for the theoretical analyses, are given in Table I. A three-view drawing of the Oceanics model blade is presented in Figure 8.

TABLE I. MODEL BLADE DIMENSIONAL AND STRUCTURAL CHARACTERISTICS

Rotor radius, R, in.	6.0
Blade aerodynamic length, in.	5.42
Blade chord, c, in.	0.437
Number of blades, b	2
Blade linear twist, θ_1, deg	-10.9
Rotor solidity, σ	0.0464
Blade root constraint	hingeless
Airfoil section	NACA 0012
Precone angle, a_o, deg	4.0
Material	stainless steel
Blade weight per unit length, w, lb/in.	0.000367*
Blade flapwise area moment of inertia, I_F, in.^{4}	2.35×10^{-6}*

*Applies to uniform thickness portion of blade.

The blade centroidal and elastic axes were calculated to be aft of the aerodynamic center (1/4 chord) by 17 and 12 percent, respectively. In the computation of the blade characteristics, a solid steel blade was assumed;

i.e., the influence of a small slot containing the stainless steel tube to provide airflow to the blade tip (shown in Figure 8) was assumed to be negligible.

Available UARL incompressible two-dimensional NACA 0012 airfoil data in the general Reynolds number range of the Oceanics test program (110,000 vs. 93,000 at the model blade tip in hover) were incorporated in the analyses. The airfoil data are presented in Figure 9. Since the maximum lift coefficient for a given airfoil is highly dependent on Reynolds number, ideally, the lift characteristics of the rotor as a function of the local Reynolds number at each radial station should be included. However, airfoil data covering the Reynolds number range from 0 to 100,000 were not available. The use of the 110,000 Reynolds number data is believed reasonable considering the relatively small contributions of the inboard sections of the blade to the total lift and assuming the blade tip regions were unstalled for the conditions investigated.

INFLUENCE OF WATER ON BLADE RESPONSE CHARACTERISTICS

The use of water instead of air as the fluid medium for the model rotor test program influenced the dynamic response characteristics of the blades. The properties of water and their effect on the blade characteristics must therefore be accounted for in the theoretical analyses. For example, the density of water (1.939 slugs/ft^3) is greater, by a factor of 815, than that of air (0.0022 slugs/ft^3 for full-scale UH-1D rotor conditions reported herein). Also, the analysis was modified to incorporate the influence of the virtual mass of water on the blade response. This was accomplished by including the virtual mass terms (derived from p. 263 of Reference 9) in the differential equations of motion of the blade. The influence of the virtual mass on the blade response characteristics was found to be very significant. For example, the virtual mass per unit blade length, which is equivalent to the mass of water enclosed in a unit length cylinder with a diameter of one chord-length, was calculated to be 1.23 times the blade mass per unit length. The virtual mass, when included in the linear acceleration term in the flapwise equation of motion in Reference 10 (it is not included in the centrifugal term), increases this term by a factor of 2.23.

The blade mass and stiffness distributions, rotor rotational speed, and virtual mass effects were used to determine the natural frequencies and mode shapes of the model blade. Table II shows a comparison of the uncoupled model blade bending and torsional frequencies in air and water nondimensionalized by the model rotational frequency of 50.4 rad/sec (25.2 ft/sec tip speed).

TABLE II. MODEL BLADE NATURAL FREQUENCY RATIOS		
	Frequency Ratio in Air	Frequency Ratio in Water
1st Mode Flapwise	6.24	4.18
2nd Mode Flapwise	38.1	25.5
3rd Mode Flapwise	105.1	70.4
1st Mode Chordwise	51.0	34.1
1st Mode Torsion	164.3	116.0

The high model blade frequency ratios reflect the low rotational frequency of the test. In addition, the chordwise frequency ratios are higher than those of conventional full-scale blades because of the increased chordwise stiffness to mass ratio of the solid stainless-steel model blades. The lower frequency ratios for operation in water relative to operation in air result from the virtual mass effects of the water. Also, due to the low rotational frequency, the centrifugal stiffening effects are small compared to typical full-scale rotors; for example, the rotational contribution to the first flapwise frequency in water is only 2 percent of the total.

As a result of the high bending frequencies, the effects of the third flapwise and first chordwise bending modes on the blade response were negligible. The effect of structural coupling between the first torsional mode and the flapwise modes was determined through the use of an experimental static calibration rig shown in Figure 10. This rig was used to determine the static torsional deflection of the model blade under load. Weights were hung from various chordwise positions at the tip of the blade, and the torsional deflection angles were measured. For representative torsional moments, negligible torsional deflections were measured, indicating that the contribution of the torsional modes to the total blade response was negligible. Thus, the model rotor theoretical cases, to be described in following sections, were based on the inclusion of only two flapwise bending modes to simulate the blade flexibility.

The general ability of the theoretical analysis to predict the blade dynamic response is demonstrated in Figure 11, in which a comparison of the measured and predicted blade bending displacements from the preconed position is presented. A two-bladed rotor operating at a simulated 90-kt condition was selected for the comparison. The nondimensional deflections of the blades at several azimuth positions were scaled from the photographic data for the selected flight condition and compared with the predicted deflections. The full-scale rotor parameters and the model rotor parameters are listed in Table III and compared with the analytical results based on a calculated distorted wake.

TABLE III. COMPARISON OF EXPERIMENTAL AND THEORETICAL ROTOR PARAMETERS

	Full-Scale Rotor	Oceanics Test	UARL Rotor Analysis
Velocity, kt	90	2.83	2.83
Rotor lift, lb	10,000	3.1	3.1
Shaft tilt, deg	-8.9	-8.9	-8.9
Collective pitch, deg (at grip on hub)	14.7	14.9	14.9

ROTOR OPERATING CONDITIONS

The investigation described herein was limited to the reduction of the wake for four water tunnel test conditions to coordinate form. The selected conditions are shown in Table IV and represent a typical range of full-scale operating conditions.

TABLE IV. TEST CONDITIONS FOR THIS INVESTIGATION

Condition No.	No. of Blades	Simulated Forward Velocity (kt)	Simulated Lift (lb)
1	2	0	10,000
2	2	0	6,000
3	2	35	10,000
4	2	90	10,000

From a choice of the one-, two-, and three-bladed rotors tested in the water tunnel, a two-bladed rotor was selected since full-scale rotor performance and airload data were available for two-bladed rotors. Two hover conditions were selected to show the effect of thrust level on the wake geometry of a hovering rotor and to compare with available model rotor data from tests in air. The simulated 35-kt condition was selected as a representative condition for the transition speed range. The 90-kt condition was selected as being representative of a cruise speed condition and was approximately the condition for which full-scale airloads data are available.

The operating and control parameters for the four model rotor conditions are presented in Table V. The corresponding operating and control parameters of the full-scale UH-1D are also tabulated for comparison on the following two pages.

TABLE V. ROTOR OPERATING AND CONTROL PARAMETERS
PART I: HOVER CONDITIONS
(Model and Flight Test Values)

FORWARD VELOCITY	0 (Hover)		0(Hover)	
ROTOR LIFT[a]	10,000 lb		6000 lb	
ROTOR	Model	UH-1D	Model	UH-1D
Actual forward velocity, V, kt	0	0	0	0
Tip speed, ΩR, fps	25.2	800	25.2	800
Rotational speed, rev/sec	8.0	5.31	8.0	5.31
Shaft angle of attack, α_s, deg	0	0	0	0
Tip-path plane angle, ν_{TPP}, deg	0	0	0	0
Advance ratio, μ	0	0	0	0
Collective pitch, θ_o, deg[b]	17.0	17.0	14.1	14.2
Collective pitch, θ_{75}, deg	8.8	8.8	5.9	6.0
Cyclic pitch, cosine component, A_{1_s}, deg	0.0	~0.0	0.0	~0.0
Cyclic pitch, sine component, B_{1_s}, deg	0.0	~0.0	0.0	~0.0
Rotor lift, lb	3.28	~10,000	1.93	~6000
Rotor lift coefficient, C_L[c]	0.0034	0.0039	0.0020	0.0024
Fluid medium	Water	Air	Water	Air
Fluid density, slugs/ft^3	1.939	0.0022	1.939	0.0022
Reynolds number[d]	9.3×10^4	7.9×10^6	9.3×10^4	7.9×10^6
Mach number	0	0.69	0	0.69

[a]Simulated values for model rotor.
[b]Collective pitch at center of rotation; 0.8 deg has been added to Reference 1 values which are at grip.
[c]Model C_L is actual incompressible C_L. Model $C_L \approx$ UH-1D C_L when compressibility correction (Equation (1)) applied.
[d]Average value at tip of blade.

TABLE V. - Continued
PART II: FORWARD FLIGHT CONDITIONS
(Model and Flight Test Values)

FORWARD VELOCITY[a]	35 kt		90 kt	
ROTOR LIFT[a]	10,000 lb		10,000 lb	
ROTOR	Model	UH-1D	Model	UH-1D
Actual forward velocity, V, kt	1.10	35	2.83	90
Tip speed, ΩR, fps	25.2	800	25.2	800
Rotational speed, rev/sec	8.0	5.31	8.0	5.31
Shaft angle of attack, α_s, deg	-3.9	g	-8.9	g
Tip-path plane angle, α_{TPP}, deg[e]	-2.8	-3.9	-6.3	-8.9
Advance ratio, μ	0.074	0.074	0.19	0.19
Collective pitch, θ_o, deg[b]	15.5	14.7	15.7	15.5
Collective pitch, θ_{75}, deg	7.3	6.5	7.5	7.3
Cyclic pitch, cosine component, A_{1_s}, deg	0.0	g	0.0	g
Cyclic pitch, sine component, B_{1_s}, deg	0.0	g	0.0	g
Rotor lift, lb	3.27	~10,000	3.16	~10,000
Rotor lift coefficient, C_L[c]	0.0034	0.0039	0.0033	0.0038
Fluid medium	Water	Air	Water	Air
Fluid density, slugs/ft^3	1.939	0.0022	1.939	0.0022
Reynolds number[d]	9.3×10^4	7.9×10^6	9.3×10^4	7.9×10^6
Mach number[f]	0	0.74	0	0.82

[a-d]Footnoted on previous page.
[e]Accounts for blade flexibility.
[f]Advancing tip Mach number (at ψ_b = 90 deg).
[g]Unavailable flight test data.

REDUCTION OF WATER TUNNEL WAKE DATA TO COORDINATE FORM

To apply or compare flow visualization data from the water tunnel test, the data must first be transformed to detailed quantitative form. Procedures were thus developed for transforming the photographic wake data to three-dimensional coordinate form. The accuracy of the coordinates obtained were limited by the test techniques used. These limitations are discussed below.

LIMITATIONS OF THE WATER TUNNEL FLOW VISUALIZATION DATA

Since the objectives of the Reference 1 investigation were mainly to determine the qualitative nature of the rotor wake, the techniques used for recording the wake data resulted in several limitations for quantitative applications. Some of the more significant limitations of the water tunnel flow visualization data as recorded on movie film in the experimental program of Reference 1 are:

1. The lack of visibility of the air bubble vortex traces in some regions of the wake

2. The difficulties involved in locating corresponding points of a three-dimensional wake pattern from two-dimensional photographic data

3. The difficulty involved in determining the azimuth positions of the blade and the associated wake azimuth positions in the side view of the photographic data

4. The lack of sufficient water tunnel reference points and recorded camera positions

5. Photographic parallax and water refraction

6. The absence of flow visualization of the inboard wake

The visibility of the filmed air bubble vortex trails is completely diminished in some regions of the still photographs and movie frames. Some of the contributing factors are the physical interference of the blades, hub, shaft housing, and nearer bubble traces, particularly for the retreating side of the rotor (the camera was always located on the advancing side of the rotor for the side view). Some visibility is also lost in the top view, in which the lateral edges of the rotor and lateral vortex trails are hidden by the window frame of the test section.

This lateral edge limitation was more severe in the movie film data than in the still photographs shown in Figures 1 through 4. The white grid lines on the back wall of the tunnel also decrease the clarity of the white vortex trails. In addition, some clarity is lost in the projection of the single movie frames. For two- and three-bladed rotors, visibility is especially important for identifying the specific blade from which a vortex trail originated. The overlapping and close spacing of the bubble traces from various blades make this difficult for many test conditions and, obviously, the problem worsens with increasing number of blades.

The tip vortex trails are distorted and at low advance ratios dissipated by the interference with the rotor hub. Although this occurs on full-scale rotors, the model hub, which is oversized both in planform (0.2 rotor radius) and depth (0.12 rotor radius), overaccentuates this phenomenon.

The side and top views of the wake were not photographed simultaneously and thus were neither synchronized nor necessarily photographed at the same camera distance and angle. As a result, it is difficult to accurately cross reference the longitudinal coordinate, x, between the two views in order to obtain corresponding lateral and axial coordinates. Also, it is difficult to cross reference rotor azimuth position between top and side views. In order to associate the position of a vortex element with its circulation strength, it is necessary to establish a correspondence between an element in the wake (i.e., bubble) and the azimuth position of the blade at the time it was shed ($\psi_{b0,0}$). The desirable procedure for this would be to follow a specific bubble in the top view, for a specified blade rotation angle, from the time of its emission from the blade and then locate the corresponding bubble in the side view. The lack of synchronization of the two views makes this procedure impossible. This was further complicated by the fact that the film speed was not constant during filming.

Reference marks were inadequate for simplifying data reduction. The grid system located on the back wall of the water tunnel was not useful because of parallax and the fact that the grid line spacing was not conveniently related to the rotor size. Also, reference marks were not present in the top view.

Photographic parallax, defined as the apparent displacement of a point in the water tunnel as seen from two different viewing points, and the refraction of the wake points due to the difference in density between water and air, also complicated the data reduction. Corrections for these factors could only be approximated due to the nonstationary position and viewing angle of the camera during the test and the lack of precise information concerning the camera location.

PROCEDURES FOR FLOW VISUALIZATION DATA REDUCTION

General Data Reduction Procedures

Considering the above limitations, special data reduction procedures were developed to enhance the extent and accuracy of the wake coordinate transformation from the existing flow visualization data. Although single frames of the projected movie film data are not as clear as the existing still photographs, analysis of the movie data was decided upon since such data were available for all blade azimuth positions, whereas still photographs were taken at only one azimuth position. This is a particularly limiting factor for forward velocity conditions for which the wake geometry varies with azimuth position. Also, a sequence of photographs showing the wake for different blade azimuth locations is desirable in hover to aid in determining the complete wake time history.

Procedures were first developed for calibrating the rotor radius in order to nondimensionalize the wake coordinates by the radius. The width of the shaft housing (48.5 percent R) was used as a reference scaling dimension. The origin of the coordinate system was defined as the center of the rotor disc in the tip path plane (see Figure 6). Procedures were developed for calibrating the rotor azimuth position from which the wake azimuth coordinates could be determined. This calibration was accomplished by starting with a blade at a known azimuth position and advancing the film to count the number of frames per revolution from which the angle of blade rotation per frame was calculated. Variations in the frame speed and camera position (due to vibration) lead to the necessity of recalibrating for each half-revolution of the rotor.

Data Reduction Procedures for Hovering Conditions

For the hovering conditions analyzed, Telereadex equipment was used to project single movie frames onto a screen, and tip vortex coordinates were automatically recorded by positioning the intersection of two digitized cross-wires at the desired wake points. The accuracy of this procedure (approximately ±0.2 percent R) is well within the accuracy of the visibility and repeatability of the photographic data. Transformation of the tip vortex patterns to coordinate form was limited to approximately two wake revolutions. This was due to the difficulty in accurately distinguishing the remaining wake because of interference of the recirculated wake from the tunnel floor. Also, it was difficult to clearly visualize an individual tip vortex trail as a continuous filament on single movie frames due to the visual interference of the second vortex trail and the hub and shaft housing. Thus, procedures were employed which consisted of determining the coordinates from the left and right sides of

the wake from a series of frames of the side view. To initiate the procedures, a frame of the side view was selected such that the blades were located in the 0 and 180 deg azimuth position (ψ_b = 0 and 180 deg) as shown in the side view in Figure 2. Alternate points located on the extreme right of each wake revolution and shed from the blade located at ψ_b = 0 correspond to 360-deg increments in the wake azimuth angle, ψ_W, starting with ψ_W = 0 at the blade tip. Similarly, alternate points on the extreme left of each wake revolution from the same blade correspond to 360-deg increments in ψ_W starting with ψ_W = 180 deg. The remaining alternate points on each side correspond to the extreme right or left points of the wake revolutions generated by the second blade, which is shown at ψ_b = 180 deg. Knowing the wake azimuth coordinate, and measuring the radial and axial coordinates for such points, the three-dimensional coordinates were recorded. By proceeding to other frames for which the increment in blade azimuth travel was known, the complete set of wake coordinates was obtained. This technique is similar to that used for determining vortex patterns from flow visualization tests in which smoke is emitted externally from the blades as described in Reference 5. For conditions in which the wake is symmetrical (independent of blade azimuth position) and repeatable, the coordinates obtained by the above procedure (i.e., from the streamlines on the right and left sides of the rotor) are representative of each blade azimuth position, and the three-dimensional helical tip vortex pattern may be reconstructed.

Data Reduction Procedures for Forward Velocity Conditions

Since vortex trail visibility was a major concern for the forward velocity conditions, a Photo-Optical Data Analyzer was used to obtain the wake coordinates for these conditions instead of the previously described Telereadex equipment. The Photo-Optical Data Analyzer permitted the projection of the film data at specified slow frame speeds in addition to the projection of a single frame. The primary procedure for obtaining the tip vortex coordinates consisted of projecting single frames with the blades in predetermined azimuth positions, tracing the projected vortex trails on paper, and measuring the coordinates (automatic coordinate acquisition is not a feature of the Photo-Optical Data Analyzer). However, since the tip vortex filaments could not be visualized as complete continuous filaments in single movie frames of the side view of the wake, advantage was taken of the slow frame speed feature. In order to determine the tip vortex patterns and their time histories with respect to rotor rotation, a second procedure was developed in which the trajectory of small groupings of bubbles was viewed while the film was in motion. The film was started at a specific blade azimuth angle and advanced for specific intervals of blade rotation during which the bubbles shed from the starting position of the blade were tracked. The trajectories of the

groupings of bubbles were then traced on the projection paper. By cross referencing azimuth intervals between tip vortex bubble trajectories, the helicoidal wake pattern from a blade at each azimuth position was reconstructed in coordinate form. Since portions of the wake were difficult to visualize, a significant amount of repetition was required.

DATA CORRECTIONS AND ACCURACY

A photogrammetric procedure was developed to estimate the errors in the uncorrected coordinates due to camera parallax and refraction of the water. For example, in the vicinity of the rotor plane (within 0.2 R) the resulting corrections produce a downward displacement of 2 percent of the radius at a lateral distance of one radius from the longitudinal centerline of the rotor on the retreating side, and an equivalent upward displacement at the same distance on the advancing side. The parallax errors are greater at the downstream end of the wake. However, emphasis in this investigation was primarily directed toward the near-wake region since it is the near wake that most significantly influences the induced effects at the rotor.

Considering the data reduction procedures and limitations, it is estimated that the accuracy of the rectilinear wake coordinates (x, y, z) is within approximately ±3 percent R in the visible wake regions. The estimated accuracy of the blade azimuth angle, ψ_b, and wake azimuth angle, ψ_W, is within ±4 deg and ±8 deg, respectively. Investigation of the influence of inaccuracies in the wake coordinates on the results of the theoretical applications will be discussed in a later section.

WATER TUNNEL WAKE COORDINATES AND COMPARISON WITH OTHER SOURCES

Using the procedures described above, coordinates of the tip vortex patterns from the filmed flow visualization data were obtained for the four test conditions listed in Table IV. These coordinates were compared with theoretical results and experimental results from tests of model rotors in air, as described below.

HOVER -- WATER TUNNEL WAKE VERSUS EXPERIMENTAL WAKE IN AIR

The tip vortex coordinates for the model rotor simulating a hovering UH-1D rotor with a lift of 10,000 and 6000 lb were obtained from the water tunnel data and compared with tip vortex coordinates from model rotor tests conducted in air at UARL. The wake geometry results of the UARL hover tests are presented in Reference 5 in the form of generalized wake equations based on the systematic experimental variation of number of blades, thrust level, blade twist, aspect ratio, and tip speed. A comparison of the design characteristics of the Oceanics rotor and the most similar UARL rotors is presented in Table VI.

TABLE VI. COMPARISON OF OCEANICS AND UARL MODEL ROTOR DESIGN CHARACTERISTICS

	Oceanics Rotor	UARL Rotor
Number of Blades	2	2
Aspect Ratio, AR	13.7	13.6
Rotor Solidity, σ	0.046	0.045
Linear Twist, θ_1	-10.9 deg	-8, -16 deg
Root Constraint	hingeless	articulated
Airfoil Section	NACA 0012	NACA 0012

The data from Reference 5 were interpolated to the thrust coefficient and twist of the Oceanics rotor using the generalized wake equations. The model rotor thrust coefficients (incompressible) for the two hovering conditions are:

Simulated Lift	Thrust Coefficient, C_T	Thrust Coefficient/ Solidity, C_T/σ
10,000 lb	0.0034	0.073
6,000 lb	0.0020	0.043

Simulated 10,000-lb Thrust Condition

The top and side views of the tip vortex patterns from each blade of the two-bladed Oceanics rotor simulating the 10,000-lb thrust condition are shown in Figures 12 and 13. Analysis of the tip vortex patterns was limited to two and one-half revolutions because of the difficulty in accurately distinguishing the remaining wake as a result of interference of the recirculated wake from the tunnel floor. The flagged versus unflagged symbols in Figure 12 indicate the difference between coordinates obtained from the top and side views, respectively. Photographs of the top and side views for this condition are shown in Figure 1. Note that in the photographs the blades are at different azimuth positions than in Figures 12 and 13. Comparison of corresponding points (at equal wake azimuth intervals from the blade) on the tip vortex from each blade shows that the wake patterns from the two blades are not equivalent. This is more clearly shown in Figure 14, where the radial and axial coordinates of the tip vortex from each blade at one instant of time are plotted versus the tip vortex azimuthal coordinate, ψ_W. As mentioned previously, the wake azimuth position, ψ_W, is the azimuth of a point on the tip vortex relative to the blade from which the tip vortex originates, and is equivalent to the blade azimuth travel from the time it generated the vorticity of that point. The differences in the wake coordinates of the two blades are evident, particularly beyond one wake revolution ($\psi_W > 360$ deg). It is noted that beyond this azimuth the wake coordinates of each blade are also unsteady with time. The generalized wake coordinates from the UARL model rotor operating in air are included in Figure 14. The coordinates of the Oceanics and UARL rotors are similar up to approximately one wake revolution, at which point differences in the wake coordinates of the two Oceanics blades appear.

Simulated 6000-lb Thrust Condition

The tip vortex coordinates for the two-bladed Oceanics rotor simulating the 6000-lb thrust condition are shown in Figure 15. As with the 10,000-lb condition, appreciable differences are observed in the vortex coordinates from the two different blades. In addition to the dependence on the particular blade from which the vortex is shed, the coordinates were found to vary with the azimuth position of the originating blade. That is, different coordinates resulted when a blade was on

opposite sides of the rotor. For example, in Figure 15 the difference in the two axial coordinate positions (Point A and Point B) of the vortex from Blade 1 at ψ_W = 360 deg is attributable to data points taken when Blade 1 was on opposite sides of the rotor (on the right and left sides of the movie frames). Significant differences in the right and left sides of the wake are clearly evident in the side view of the wake in Figure 2.

Interpretation of Hover Results

A common feature of the two hover conditions analyzed was the pairing of successive revolutions of the tip vortices. For the two-bladed rotor, successive revolutions originate from opposite blades. The pairing was most evident for the 6000-lb condition, where rotation of one vortex trail about another occurred. For example, points A' and B' in the photograph in Figure 2 indicate a point on the tip vortex from each blade. Point A' was emitted from the blade on the left in the photograph (Blade 1) and is shown following one and one-half revolutions of rotation (ψ_W = 540 deg), and Point B' was emitted from the blade on the right (Blade 2) and is shown following two revolutions of rotation (ψ_W = 720 deg). Although Point B' would normally be expected to lie farther downstream in the wake than Point A', just the opposite is true. In fact, Point A' has actually passed inside of Point B' and is located below it in the photograph. These two points are also indicated as A' and B' in Figure 15. This rolling up of successive revolutions of two vortex trails has also been observed in the wakes of both model and full-scale rotors operating in air (Reference 5), and has been predicted using the hover version of the UARL Wake Geometry Analysis (Reference 5). A sample photograph showing the interaction of the cross sections of two vortex trails from a model rotor in air is presented in Figure 16. Although the same phenomenon occurs in air, it occurred sooner (i.e., closer to the rotor) in the water tunnel data analyzed. For example, for a two-bladed rotor in air, the tip vortex from the model rotors was found to roll up following approximately one and one-half to two revolutions in contrast to approximately one revolution in water.

The more rapid roll-up of the pairs of vortices noted in the water tunnel appears to correlate with the observation of the increased unsteadiness of the water tunnel wake described earlier for the two conditions analyzed. The exact cause of this increased unsteadiness is not known, although several possibilities have been identified. These are listed below.

1. The increased bending of the water tunnel blades results in the contracted tip vortex trails passing closer to the following blades. In fact, for the simulated 6000-lb thrust condition,

the vortex trails passed above the following blade. It is possible that the interference with the blades could have triggered the unsteadiness of the wake earlier than in air.

2. The wake unsteadiness could have been increased by the recirculation effects of the vortex trails due to the presence of the tunnel floor and side walls.

3. Small differences in collective pitch setting between the two blades in the water tunnel may have been a factor.

4. Increased wake unsteadiness could have resulted from a slight skew angle in the wake resulting from the existence of a slight forward velocity in the tunnel or a slight inclination of the drive shaft.*

From a discussion with Oceanics personnel, it was learned that the pairing of the vortex trails (at hover) was clearly evident in most test runs performed during the original (Reference 1) and subsequent test programs. To determine if this pairing was a result of an error in the collective pitch setting between the two blades (as well as to determine the floor and ceiling influence), the rotor was positioned during a subsequent test program so that it operated as a propeller; i.e., the wake was directed along the tunnel axis with no flow in the tunnel. With that arrangement, it was not possible to obtain a wake in which pairing of adjacent vortex trails did not occur. A determination as to whether the unsteadiness was delayed was not made.

Comparison of the water tunnel wake coordinates in Figures 14 and 15 with the coordinates from the UARL generalized wake in air shows that the tip vortex coordinates in air lie between the bounds of the coordinates in water. Also, the characteristic trend of the axial coordinates to increase with increasing thrust level is also evident in the water tunnel wake. The major difference between the results in air and the results in water, for the two conditions evaluated, is the degree of unsteadiness of the wake. In order to determine if this increased unsteadiness is generally representative of water tunnel testing, an extensive range of hovering conditions should be analyzed. This was beyond the scope of this investigation which was limited to two hovering conditions.

---

*This appears to be a particular possibility for the 6000-lb condition. The wake appears slightly skewed in the photograph shown in Figure 2. (However, the skew angle was less evident in the movie data used which was taken at a different time.)

FORWARD FLIGHT -- WATER TUNNEL WAKE VERSUS THEORETICAL WAKE

The tip vortex coordinates for the Oceanics model rotor simulating a UH-1D rotor operating at 35 and 90 kt with a lift of 10,000 lb were obtained from the water tunnel data. Figures 3 and 4 contain sample photographs of the wake for these two conditions. Attempts to compare these coordinates with experimental data from other sources were unsuccessful due to the lack of available wake geometry data consistent with the water tunnel conditions analyzed. Of the available sources of forward-flight flow visualization data (References 13 through 16, and unpublished UARL data), several did not indicate essential parameters such as thrust coefficient, and only one (Reference 13) contained data reduced to coordinate form. Reference 13 contains forward flight data for a single-bladed rotor reduced to coordinate form and generalized over a range of thrust coefficient, angle of attack, and advance ratio. However, following initial analysis of some of the single-bladed water tunnel data, it was found that unacceptable extrapolations of the Reference 13 data were required to permit comparisons of the wake geometries at similar thrust conditions.

In lieu of comparable experimental wake coordinates, the water tunnel wake geometries were compared with the theoretical wake geometries predicted by the UARL Wake Geometry Analysis. Comparisons with the theoretical distorted wake coordinates and with the theoretical undistorted wake coordinates will be presented below.

Simulated 35-kt Condition

The top and side views of the tip vortex patterns from each blade of the two-bladed Oceanics rotor simulating the 10,000-lb, 35-kt condition are shown in Figure 17 for the blades in the upstream (ψ_b = 180 deg) and downstream (ψ_b = 0 deg) positions. In forward flight, the tip vortex coordinates relative to the originating blade vary with the azimuth position of the blade. Figure 17 shows a sampling of the wake patterns for two azimuth positions. The upstream side of each wake revolution is dispersed following its impingement on the rotor hub. In addition, portions of the wake were obscured for reasons discussed earlier.

In Figure 18, the experimental wake coordinates are compared with the undistorted wake coordinates for the wake from the blade in the upstream azimuth position (ψ_b = 180 deg). The most striking distortions of the experimental wake from the undistorted wake representation exist in the axial coordinates as shown in the side view. Following a given air bubble with time allows one to map the streamline trajectory corresponding to the blade azimuth position at the instant of emission of the air bubble. The

streamlines generated when the blade is in the 180- and 0-deg azimuth positions define the fore and aft wake boundaries. A comparison of the experimental wake boundaries with the undistorted wake boundaries is shown in Figure 19. The angle of the undistorted wake boundaries relative to the tip-path plane is the wake deflection angle, χ_{TPP}. The contraction of the experimental wake boundaries from the undistorted wake boundaries is evident in Figure 19.

A comparison of the experimental wake and theoretical distorted wake (uncorrected for wall effects) for the upstream blade position is presented in Figure 20. Agreement is good in the top view. In the side view, the theoretical wake has distortion characteristics similar to the experimental wake. For example, the raised vertical position of the lateral region (Points A in Figure 20) is common to both the analytical and experimental vortex patterns. Comparison of the side views also demonstrates the characteristic dip (Points B and D) over the aft region of the tip vortex. A more detailed comparison of the axial positions of the theoretical and experimental tip vortices is presented in Figure 21 (Points A through D from Figure 20 are indicated in Figure 21(c)). The axial coordinates are shown versus wake azimuth position, ψ_W, for the wake patterns associated with four blade azimuth positions ($\psi_{b0,1}$ = 0, 90, 180, and 270 deg). Also, indicated as the secondary horizontal scale is the azimuth position of the blade at the time the tip vortex element was generated ($\psi_{b0,0}$). This scale is presented to indicate the fore ($\psi_{b0,0}$ = 180 deg), aft ($\psi_{b0,0}$ = 0 deg), and lateral sides of the wake ($\psi_{b0,0}$ = 90 and 270 deg). The greater distortions (relative to the undistorted wake) in a direction toward the rotor occur consistently on the lateral sides of the wake, and the greater distortions away from the rotor occur consistently in the aft region of the wake. The forward wake region is consistently distorted toward the rotor. Although the theoretical distortions are greater than experiment, the ability of the theoretical analysis to predict the basic distortion characteristics is clearly demonstrated.

The distorted wake characteristics just described have been analyzed in Reference 4, where it is shown that they are indicative of a gross rolling up of the undistorted skewed helical wake. It is also shown in Reference 4 that this process may be more easily visualized in terms of the rolling up of an imaginary cylinder traced out by the helical vortex filaments as they travel downstream. This is shown in Figure 22. The basic mechanism of the rolling-up process is identified in Reference 4 and is similar to that causing the well-known roll-up of a fixed-wing wake.

Simulated 90-kt Condition

The top and side views of the tip vortex patterns from each blade of the two-bladed water tunnel model rotor simulating the 10,000-lb, 90-kt condition are shown in Figure 23 for the blades in the upstream (ψ_b = 180 deg) and downstream (ψ_b = 0 deg) positions. As with the 35-kt condition, the upstream side of each wake revolution is dispersed following its impingement on the rotor hub.

A comparison of the experimental wake pattern with the undistorted wake pattern is shown in Figure 24 for the tip vortex when the blade is in the upstream azimuth position. In the top view, the experimental vortex pattern is in close agreement with the undistorted tip vortex, indicating only minor distortions of the longitudinal, x, and lateral, y, wake coordinates. However, greater distortions exist in the side view which are similar to but not as extreme as those of the simulated 35-kt condition. A comparison of the fore and aft experimental and undistorted wake boundaries is presented in Figure 25. Contraction of the experimental boundaries relative to the undistorted wake boundaries is evident, although not as great as for the 35-kt condition.

A comparison of the experimental and theoretical tip vortex coordinates for a blade in the upstream position is presented in Figure 26. Again, agreement is reasonable in the top view (lateral and longitudinal coordinates). The axial coordinates are directly compared in Figure 27 for four blade azimuth angles, and the capability of the theory to predict the major distortion characteristics is again demonstrated.

SENSITIVITY OF WAKE GEOMETRY TO NONSIMULATED PARAMETERS

A fundamental question regarding model rotor wake geometry data acquired in a water tunnel concerns the applicability of the data to full-scale rotors. Specifically, are the water tunnel wake patterns sufficiently representative of full-scale rotor wakes such that they may be used to determine full-scale rotor airloads and dependent characteristics such as stresses, vibrations, and noise? In an attempt to answer this question, an analytical study was conducted to evaluate the sensitivity of wake geometry to full-scale rotor design and operational parameters which were not accurately simulated in the water tunnel test. These include:

1. Blade flexibility effects
2. Rotor tip-path plane angle
3. Blade cyclic pitch
4. Viscous effects (Reynolds number)
5. Compressibility effects (Mach number)
6. Rotor thrust coefficient

The sensitivity of the model rotor wake geometry to the nonsimulated parameters was determined by varying the parameters independently in the theoretical analysis. The study was limited to one flight condition -- the simulated 90-kt, 10,000-lb case for the two-bladed rotor -- and thus the results strictly apply only to similar high-speed conditions.

SENSITIVITY OF WAKE GEOMETRY TO BLADE FLEXIBILITY, PRECONING, AND ROTOR TIP-PATH PLANE ANGLE

The elastic response of the blade in the flapwise direction is determined primarily by the mass, stiffness, rotational speed, fluid medium, and type of blade root restraint employed. All of these factors were significantly different between the water tunnel model rotor and the full-scale UH-1D rotor. The rotational speed of the model rotor was of such a low value that the centrifugal stiffening was almost a negligible contributor to the total blade stiffness, therefore requiring a hingeless rotor to be used in place of a teetering rotor. Also, as mentioned earlier, the model blade bending displacement was influenced in water by virtual mass effects, which are negligible in air.

The flexibility of the rotor influences the wake geometry in three ways. First, the flexible blade dynamic response alters the rotor air-loading distribution which, in turn, influences the wake circulation distribution and wake geometry. Second, blade flexibility influences the positioning of the wake relative to the blades. Third, through differential fore and aft bending, it affects the rotor tip-path plane angle of attack associated with a given shaft tilt. The latter influences the component of forward velocity normal to the rotor disc ($V \sin \alpha_{TPP}$) which, in turn, affects the wake deflection angle. These three effects were investigated using the UARL Rotor Analysis.

The influence of blade flexibility on water tunnel wake geometry, blade loading, and relative blade-wake positioning was initially determined by comparing the analytical results using flexible blades (two flapwise bending modes) with those assuming infinitely rigid blades. Considering the high stiffness of the model blades, it was found that the significant flexibility effects were limited to the first and second flapwise bending modes and that chordwise and torsional deflections were negligible. Advance ratio and thrust coefficient were maintained constant. Also, tip path plane angle was maintained constant by changing shaft angle. In Figure 28, a typical comparison of the axial tip vortex coordinates for blades with and without flexibility is presented for one blade azimuth position ($\psi_{b_{0,1}} = 0$ deg) along with the azimuthal loading distributions for one representative blade station ($r = 0.75$). The axial coordinates are compared because they consistently exhibit the greatest sensitivity to changes in rotor design or operating parameters. It is shown in Figure 28 that only minor changes occur in wake geometry even though significant changes in the loading distribution due to flexibility are indicated.

The independent effect of relative blade-wake positioning was examined by calculating the wake geometries corresponding to the model rotor with 0 deg and 4 deg preconing and without flexibility. Variations in coning influence the blade-wake positioning by changing the axial positions of the inboard sections of the blades relative to the tip and thus also relative to the tip vortices. The effects of preconing on wake geometry are minor as shown in Figure 29.

The sensitivity of the model rotor wake geometry to tip-path plane angle variations produced by blade flexibility was determined analytically by duplicating the test procedure. The test procedure used in the Oceanics water tunnel test consisted of setting the model rotor shaft angle equal to the full-scale rotor tip-path plane angle. Assuming no model blade flexibility, the model rotor tip-path plane would also be at the same angle. However, as has been shown (Figure 11), substantial differential

blade bending between the fore and aft blade positions occurred during testing of the model rotor. This bending significantly affected the rotor tip-path plane angle. To duplicate the actual and assumed test conditions, the model shaft angle was set equal to the UH-1D value (α_s = -8.9 deg) in the analysis and two conditions, with and without flexibility, were compared. For the condition without flexibility, the tip-path plane angle remained equivalent to the shaft angle as was assumed in the Oceanics test procedure. However, when flexibility was added, the calculated tip-path plane angle increased to α_{TPP} = -6.7 deg, which was representative of the angle measured from the photographic data (α_{TPP} = -6.3 deg) as shown in Figure 11. The effect of tip-path plane variations due to blade flexibility on loading distribution and wake geometry is shown in Figure 30. Although significant loading variations are indicated, it was concluded that since comparable loading variations produced little change in wake geometry with the tip-path plane angle held constant (Figure 28), the relatively large wake coordinate variations shown in Figure 30 were produced from another source. This source is the inflow component of the forward velocity ($V_{\sin\alpha_{TPP}}$) which changes the undistorted wake deflection angle (see Equation (9)). The change in wake deflection angle influences the axial positioning of the undistorted wake relative to the rotor disc as shown in Figure 30. However, it was found that the tip vortex distortions relative to the undistorted wake position are not significantly influenced by tip-path plane angle variations (Figure 31). This appears logical inasmuch as the axial distortions for a given rotor thrust are principally determined by the projection of the wake geometry on the rotor plane. This projection remains relatively constant as long as the deflection angle is small. It was thus concluded that tip-path plane angle is an important parameter for simulating wake geometry. However, its influence appears to be mainly on the basic undistorted wake position and not the distortions of the wake from that position. This finding may be important for future wake generalization considerations and will be discussed further in a later section of this report.

SENSITIVITY OF WAKE GEOMETRY TO CYCLIC PITCH

A conventional rotor feature not included in the model rotor design is cyclic pitch control. The independent influence of cyclic pitch on model rotor wake geometry was investigated by analytically incorporating cyclic pitch control in the hingeless model rotor system and comparing the wake results with those for the system operating without cyclic pitch. The cyclic pitch values (A_{1_s} = -1.3 deg, B_{1_s} = 3.9 deg) were selected to simulate a typical trimmed flight condition where the rotor rolling and pitching moments are essentially zero. The advance ratio, tip-path plane angle, and thrust coefficient were held constant. In Figure 32, the results of the trimmed condition are compared to those of the zero-cyclic-

pitch, high-rotor-moment condition tested in the water tunnel, and it is shown that the tip vortex coordinates exhibit more sensitivity to cyclic pitch variations than to the parameters previously considered. However, it will be shown that the tip vortex coordinates are particularly insensitive to cyclic pitch variations at the points of importance near the rotor (where the vortices pass close to the blades).

SENSITIVITY OF WAKE GEOMETRY TO REYNOLDS NUMBER AND MACH NUMBER

The effects of viscosity and compressibility on rotor airloading were accounted for in the analysis by use of airfoil data corresponding to the appropriate Reynolds number and Mach number combinations of the airfoil sections. Airfoil data closely corresponding to the average tip Reynolds number of the model test (Re = 110,000 vs. 93,000) and approximating incompressible flow (M = 0.13) were used to represent the model rotor airfoil characteristics (Figure 9). Also available were high Reynolds number ($Re = 12 \times 10^6 \times M$) airfoil data representative of full-scale blade conditions with varying Mach number. These airfoil data are presented in Reference 17.

The independent influence of Reynolds number is shown in Figure 33, in which air loading and wake geometry for the model rotor with incompressible model Reynolds number airfoil data are compared with the model rotor results with incompressible, full-scale Reynolds number data. The combined influence of Reynolds number and Mach number is also shown in Figure 33, in which the loading and wake geometry are compared for the model rotor with incompressible, model Reynolds number airfoil data and compressible, full-scale Reynolds number data. Again, rotor advance ratio, thrust coefficient, and tip-path plane angle were unchanged for these comparisons, and the effects of the relatively small changes in loading on wake geometry are shown to be negligible.

SENSITIVITY OF WAKE GEOMETRY TO THRUST COEFFICIENT

In the previous figures where the predicted wake geometries are essentially equivalent (Figures 28, 29, 32, and 33), the model rotor thrust coefficient was constant ($C_T = 0.0033$). The sensitivity of blade loading and wake geometry to a 15 percent increase in thrust coefficient (to 0.0038) is shown in Figure 34. To show the independent effect of thrust coefficient, the advance ratio, tip-path plane angle, Reynolds number, and Mach number were held constant. Since thrust coefficient affects the wake deflection angle, the axial coordinates of the undistorted wake change. Generally, the axial tip vortex distortions relative to the appropriate undistorted coordinates are shown to increase in magnitude by approximately 15 percent. The equivalence of the percentage change in wake

distortions and that in the thrust coefficient seems reasonable when the direct relations between wake distortion velocities, circulations, loading, and thrust coefficient are considered. Thus, it may be hypothesized that tip vortex distortions are proportional to thrust coefficient. This means that the change in the tip vortex coordinates would have been proportionately greater than that shown in Figure 34 if a larger thrust coefficient increment had been selected.

The 15 percent increment in thrust coefficient, selected for the sensitivity study, corresponds to the difference between the value for the model rotor operation in water and that for the UH-1D rotor condition in air. This difference resulted from a compressibility correction applied by Oceanics in selecting their test conditions. In the preceding section, in which the effect of compressibility on wake geometry was discussed, the rotor thrust coefficient was held constant. This is not consistent with the test procedure employed in the Oceanics water tunnel test program. As previously discussed, one of the main objectives of the water tunnel test reported in Reference 1 was to investigate the correlation of model and full-scale rotor collective pitch settings for the rotor set at appropriate shaft angles and scaled thrust coefficient values. For this correlation, the compressibility correction presented in Equation (1) (Prandtl-Glauert correction = 0.87) was introduced to account for compressibility as it affects the relation between local lift coefficients and angle of attack values at the blade sections. Thus, in simulating a given full-scale thrust coefficient, the model rotor was operated at a lower thrust coefficient. For example, for the 90-kt flight condition under consideration, the model rotor was operated at a thrust coefficient, C_T, of 0.0033 compared to a full-scale thrust coefficient of 0.0038. Although this is the correct procedure to correlate blade angle settings, the resulting model wake geometry obtained is not strictly representative of the full-scale rotor wake geometry. The wake circulation strengths which influence the wake geometry are dependent on the actual lift at each section, which is integrated into the total thrust coefficient, and are not directly dependent on the blade angles which produced the section lift values. In Figure 34, the wake variations due to thrust coefficient increments associated with the compressibility correction are shown to be fairly small. However, it is concluded that in order to most correctly simulate the wake geometry of a full-scale rotor in the water tunnel, the full-scale thrust coefficient should be duplicated directly without the application of the compressibility correction.

COMPARISON OF THEORETICAL MODEL AND FULL-SCALE ROTOR WAKES

The wake geometry of the full-scale UH-1D rotor operating at 90 kt was computed using the UARL Rotor Analysis. In Figure 35, the predicted full-scale wake coordinates are compared with the predicted coordinates for the model rotor operated in the water tunnel at a thrust coefficient, C_T, of 0.0033 and a tip-path plane angle, α_{TPP}, of -8.9 degrees. The similarity of the theoretical wake of the full-scale rotor operating in air and the theoretical wake of the model rotor operating in water at the same tip-path plane angle, thrust coefficient, and advance ratio, as shown in Figure 35, is of major significance in that it indicates that, although many parameters are not accurately simulated in water tunnel testing, the experimental wakes obtained therefrom may still be representative of the wakes of full-scale rotors as long as certain essential parameters are simulated properly.

SUMMARY OF WAKE GEOMETRY SENSITIVITY RESULTS

The wake geometry results of the sensitivity study are summarized in Figure 36, in which the axial distance of the tip vortices relative to the rotor tip-path plane at points where the vortices pass beneath the blades (blade-vortex "intersections" in the top view) are plotted versus blade azimuth angle, ψ_b, for the various rotor conditions analyzed. A sample diagram showing the blade-vortex "intersections" when the rotor blades are at ψ_b = 90 deg and 270 deg is included in Figure 36. The approximate location of the blade-vortex "intersections" for other rotor azimuth positions may be obtained from Figure 37, in which the top view of the undistorted tip vortex patterns is presented. Since the wake is most influential on blade airloading at the blade-vortex "intersections", the intersection points may be used as the primary indicators of wake sensitivity to particular parameters, although greater wake geometry differences exist for other less critical points in the wake, particularly downstream of the rotor. Presented in Figure 36 are: (1) the sensitivity at constant thrust coefficient of the predicted model rotor wake geometry to independent variations in the nonsimulated parameters (blade flexibility, tip-path plane angle, cyclic pitch, Mach number and Reynolds number), (2) a comparison of the predicted model and full-scale rotor wake geometries, and (3) the undistorted wake positions for the model and full-scale rotors. It is shown in Figure 36 that at the blade-vortex "intersections", the model rotor wake is insensitive to blade flexibility, cyclic pitch, Reynolds number and Mach number variations, but sensitive to tip-path plane angle. It is also shown that at the "intersections", the model rotor wake is equivalent to the full-scale rotor wake for the same tip-path plane angle. In addition, the distortions from the undistorted wake positions are consistently in a direction toward the rotor at the "intersections".

A major conclusion drawn from this wake geometry sensitivity study is that, in addition to number of blades, the primary parameters that determine wake geometry for typical, high-speed rotor operating conditions are those that establish the undistorted wake deflection angle. As defined previously, the wake deflection angle is the angle between the undistorted wake streamlines and the rotor tip-path plane. These primary wake parameters for a given blade design are:

1. Number of blades, b
2. Rotor advance ratio, μ
3. Rotor thrust coefficient, C_T
4. Rotor tip-path plane angle, α_{TPP}

As shown in Figure 36, for constant values of these parameters, wake geometry was found to be relatively insensitive to variations in azimuthal (time-varying) distributions of blade airloading. This was true even though rather extreme variations in blade airloading distribution resulted from the incorporation of cyclic pitch and the elimination of flexibility in the model rotor as shown in Figure 32. The blade airloading variations due to Reynolds number and Mach number differences were shown in Figure 33 to be relatively small. Also, the wake predicted for the model rotor operating in water, shown in Figure 35, was found to correlate well with the wake predicted for the full-scale rotor (UH-1D) operating in air, even though large differences in blade airloading azimuthal distributions existed for the two cases. For the selected flight condition for which μ and C_T were held constant, significant changes in wake geometry resulted only when α_{TPP} was varied. The α_{TPP} variation of primary interest for improving water tunnel test procedures corresponds to the differences between the values for the full-scale and model rotors which resulted from the fact that blade flexibility was not accounted for when setting the model rotor shaft angle in the water tunnel (full-scale α_{TPP} = -8.9 deg vs. model value of -6.7 deg*). The sensitivity of wake geometry to blade design parameters influencing the radial (spanwise) distribution of airloading (twist, taper, tip design, etc.) remains to be investigated.

The earlier discussed findings that the axial distortions of the tip vortex from the undistorted coordinates may be insensitive to tip-path plane angle and proportional to thrust coefficient are important for wake generalization considerations. The ability to simplify the representation of the effects on the wake of these two primary wake parameters would greatly facilitate future attempts to generalize wake geometry. Since the basis for these findings is limited to the conditions described herein, it is recommended that further checks at other conditions be made.

*Theoretical α_{TPP} = -6.7 deg, test α_{TPP} = -6.3 deg (for model rotor).

APPLICATION OF WATER TUNNEL AND THEORETICAL WAKE GEOMETRY TO DETERMINE FULL-SCALE ROTOR AIRLOADS

To determine the sensitivity of full-scale rotor airloads to wake geometry, the theoretical wake geometries presented in the previous section were used in the analysis to calculate the airloads of the full-scale UH-1D rotor. In addition, to demonstrate the application of the water tunnel wake coordinates to represent the full-scale wake in the computation of full-scale rotor airloads, the experimental model rotor wake for the 90-kt condition was used to compute the airloads for a full-scale UH-1A rotor condition for which flight test airloads data were available. These forward flight airloading results are presented in this section along with a general discussion of the influence of wake geometry on the airloads of a hovering rotor.

SENSITIVITY OF FULL-SCALE ROTOR AIRLOADS TO WAKE DEVIATIONS CAUSED BY NONSIMULATED PARAMETERS

To determine the sensitivity of predicted full-scale rotor airloads to differences in the predicted model rotor wake geometries due to the nonsimulated parameters, the following computations were made. The full-scale UH-1D rotor wake geometry was calculated and used to predict the full-scale rotor airloading distribution. The theoretical model rotor wake geometries, discussed above, were then used in dimensionally scaled form to represent the full-scale rotor wake, and the resulting airloads were compared with the airloads based on the full-scale rotor wake. These airloading comparisons are presented in Figure 38. For a constant α_{TPP} and C_T, the predicted model wake was shown in the previous section to correlate well with the predicted full-scale rotor wake due to the insensitivity of the wake to the other nonsimulated parameters. Thus the full-scale airloads are also insensitive to the other nonsimulated model rotor parameters. The results indicate that virtually identical airloads are computed regardless of whether the wake used is the one computed for the UH-1D rotor or whether it is a wake computed for a model rotor operating in water. However, this is true only if the primary parameters influencing the wake (μ, C_T, α_{TPP}, b) are held constant. The dashed curve shown in Figure 38 indicates the differences in airloads that would result if the model rotor wake were computed for the α_{TPP} that actually existed in the water tunnel due to the blade flexibility effects. The local differences in airloading for the two α_{TPP} values (e.g., at r = 0.35, ψ_b = 180 deg, and at r = 0.85, ψ_b = 90 deg) are due to the closer position of the tip vortex to the rotor for the α_{TPP} = -6.7 deg condition. This sensitivity of airloading to tip vortex position will be discussed further below (in particular, the sensitivity at r = 0.85, ψ_b = 90 deg indicated by Points A, B, and C in Figure 38).

COMPARISON OF THEORETICAL FULL-SCALE AIRLOADS WITH FLIGHT TEST DATA

Since experimental airloads data for the UH-1D rotor were unavailable, the flight test airloads data from Reference 18 for the UH-1A rotor operating at 88.5 kt were selected as the basis for the airloads correlation study. The values of the primary wake parameters for the selected UH-1A test condition are compared in Table VII with the values for the water tunnel rotor. Although it is recognized that the primary wake parameters are not equal, the UH-1A test condition most similar to the water tunnel rotor condition was selected.

TABLE VII. TEST CONDITIONS AND ROTOR PARAMETERS FOR COMPARING BLADE AIRLOADS

	UH-1A Full-Scale Rotor	Water Tunnel Model Rotor
Number of blades, b	2	2
Rotor advance ratio, μ	0.21	0.19
Thrust coefficient, C_T	0.0037	0.0033
Rotor tip-path plane angle, α_{TPP}	-3.6 deg	-6.3 deg
Rotor solidity, σ	0.0369	0.0464
Blade twist, θ_1	-12 deg	-10.9 deg
Blade taper	None	None
Blade aspect ratio, AR	17.3	13.7
Airfoil section	NACA 0015	NACA 0012
Root constraint	Teetering	Hingeless

The theoretical tip vortex pattern for the UH-1A flight test condition is presented in Figure 39 for a sample rotor position. The distortions in the top view are shown to be small, particularly in the region of the rotor. The wake distortion features characteristic of those observed experimentally in the water tunnel are present in the calculated

distorted wake pattern. These consist of the contraction of the tip vortex toward the tip-path plane at the forward points of each revolution (ψ_W = 180 deg and 540 deg), the lower positions of the aft wake points (ψ_W = 360 deg and 720 deg), and the higher positions of the lateral sides of the wake (ψ_W = 90 deg, 270 deg, etc.).

Although the differences in rotor design and flight conditions are recognized, the experimental wake coordinates presented earlier for the model rotor operating in water at the simulated 90-kt condition were used to represent the UH-1A rotor wake. Using this wake, the airloads were computed and are compared with the flight test data in Figure 40. The predicted airloads based on the theoretical wake for the UH-1A are also presented in this figure. As shown, the predicted airloads based on both the experimental model rotor wake and the theoretical full-scale wake are in good agreement with the flight test data except at certain local positions on the rotor disc. It will now be shown that the local differences in airloading may be attributed to the extreme sensitivity of the predicted airloads to tip vortex position where the tip vortex passes close to a blade.

SENSITIVITY OF FULL-SCALE ROTOR AIRLOADS TO WAKE POSITION

High-Speed Flight

The sensitivity of the UH-1A rotor airloading distributions in high-speed flight ($\mu > 0.15$) to various theoretical inflow representations is shown in Figure 41. The inflow representations were based on (1) variable inflow from a distorted wake, (2) variable inflow from an undistorted wake, and (3) constant inflow. At the 0.95 R radial station the calculated airloads from the variable inflow methods, which account for wake effects, are greatly improved over the constant inflow results. For the inboard stations, the inclusion of wake effects, distorted or undistorted, generally resulted in little effect on the airloads except at certain local positions on the rotor disc. It was found that these positions coincide with points where a tip vortex passes beneath the blade (blade-vortex "intersections"). Such intersections are generally evident as high-frequency oscillations in the airload distributions. For example, in Figure 40, a high-frequency disturbance is indicated at the 0.4 R station in the blade azimuth region between 120 deg and 200 deg. The source of this oscillation is shown in Figure 39, in which the tip vortex from the preceding blade (Blade 1) is shown to be in close proximity to the point on the blade under consideration (Point A′ of Blade 2). For the blade in the azimuth position shown in this figure (ψ_b = 180 deg), the vortex is inboard of Point A′ and thereby induces an upflow at that point which is reflected as an increase in the airloading at that position (see Figure

40). However, when the blade was at ψ_b = 140 deg, the tip vortex passed beneath Blade 2 on the outer side of Point A', resulting in an induced downflow at that point.

Another blade-vortex "intersection" occurs near the 0.85 R station at the blade azimuth position of 90 deg. In Figure 41, the predicted wake distortion is shown to result in an increase in airloading (Point D) relative to both the test data and the airloading based on the undistorted wake. In Figure 38, the influence of the predicted UH-1D wake distortion is shown to be just the opposite: a decrease in airloading, at 0.85 R, due to the blade-vortex "intersection" in this region as shown in Figure 37 at ψ_b = 90 deg. This can be explained by examining the locations of the tip vortex relative to the point on the blade at the blade-vortex intersections as shown in Figure 42. The tip vortex of the UH-1D rotor is located outboard of the 0.85 R radial station (Points B and C) and thus induces a downflow at that point which decreases the airloading. However, due to the change in advance ratio between the UH-1A and the UH-1D conditions (μ = 0.21 vs. 0.19), the tip vortex of the UH-1A rotor is located inboard of the 0.85 R radial station (Points D and E) and thus induces an upflow which increases the airloading. Although the loading variations are also influenced by distortions of other regions of the wake, by slight radial distortions of the tip vortex near the blade, and by coupling effects between loading and blade response, an estimate of the sensitivity of airloading to the axial position of the tip vortex may be obtained by noting the airloading values at r = 0.85, ψ_b = 90 deg in Figures 38, 40, and 41 that correspond to the tip vortex positions indicated in Figure 42 (Points A through E). For example, the axial distortion of the tip vortex for the UH-1D rotor at α_{TPP} = -8.9 deg of 0.04 R, which displaced the vortex from 0.08 R to 0.04 R from the blade (C to B), produced only a 10 percent change in loading, whereas the 0.035 R distortion of the tip vortex of the UH-1A rotor from 0.04 R to 0.005 R from the blade (E to D) resulted in a 35 percent change in loading. The induced effects of the tip vortex distortions are also evident in the radial airloading distributions of the two rotors as shown in Figure 43.

Rotor airloads are dependent on the vorticity shed from the inboard portion of the blades in addition to the tip vorticity. Since the water tunnel wake data is limited to tip vortex data, the inboard wake geometry must be assumed in an airload analysis. In the UARL Rotor Analysis, the inboard wake was assumed to be undistorted and at the momentum skew angle. In order to demonstrate the sensitivity of the predicted airloads to this assumption, the inboard wake coordinates were arbitrarily shifted toward the rotor. The shift in the inboard wake coordinates was selected by assuming that the wake-induced inflow was zero at the rotor ($V_{i_{MOM}}$ = 0) and thereby setting the inboard wake skew angle of the UH-1A equal to

the flight test tip-path plane angle ($\chi_{TPP_{inboard}} = \alpha_{TPP} = -3.6$ deg) which results in the wake being parallel to the free-stream velocity. The water tunnel tip vortex coordinates were not changed. The resulting airloads are shown in Figure 44* to be insensitive to this large change in the inboard wake geometry.

In general, for the conditions investigated, it was found that when the tip vortex is located within 0.05 R from the blade, the sensitivity of airloads to relatively small deviations in vortex position is appreciable and increases with decreasing vortex distance from the blade. This is in accord with the Biot-Savart law, which states that the velocity induced at a point by a vortex varies inversely with distance between the point and the vortex. This sensitivity indicates the importance of obtaining accurate wake coordinates in such regions. The local high harmonic airload ocillations which are predicted for the UH-1A rotor based upon both the theoretical and water tunnel wake geometry and which do not appear in the measured flight test data in Figure 40 are apparently due to the placement of the tip vortex too close to the blades at certain blade-vortex "intersections". It is noted that the axial tip vortex displacement from the blade near r = 0.85 R, $\psi_b = 90$ deg was the same from the water tunnel data as that predicted by the analysis (0.005 R), which resulted in equivalent airloading values at that point (see Figure 40). The fact that the predicted and experimental tip vortex displacements at that point are identical is coincidental, considering the differences in the primary wake parameters. However, it is important to note that agreement with the test data could be produced by displacing both wake geometries by approximately 0.03 R in this region. This displacement is equivalent to the estimated accuracy of the reduced water tunnel wake coordinates. Also, when a tip vortex is positioned within approximately 0.01 R from a blade (approximately 0.2 chord length), an accurate representation of the vortex core in size and structure is required in the analysis. However, vortex core data applicable to full-scale rotors are extremely limited. A vortex core radius of 0.1 chord was assumed in the analysis.

*The predicted UH-1A airloads presented in Figure 44 based on the unmodified distorted wake coordinates differ from those presented in Figures 40 and 41 due to the use of a different rotor disc angle in the analysis during the early period of the investigation. However, the differences between the airloads corresponding to the modified and unmodified wake coordinates are representative.

It has been shown that, for the flight condition investigated, wake distortions generally have only a small effect on rotor airloads. This implies that, for such conditions (moderate to high speed and appreciable wake deflection angle), the use of an undistorted wake would generally be acceptable for predicting rotor performance and estimating blade bending stresses. However, the increased amplitude of specific higher harmonics of loading due to local wake distortions near the blades could be significant in determining accurate stress distributions and rotor vibration and noise characteristics. These harmonic amplitudes increase as the flight condition is varied in a manner such that the wake approaches the rotor blades. For example, low α_{TPP} and associated low wake deflection angle conditions occur particularly for helicopters with auxiliary propulsion as well as for helicopters in maneuvers. The existence of significant vibrations caused by tip-vortex-induced forces on the blade is discussed in Reference 19.

Low Flight Speeds and Hover

At low flight speeds ($\mu < 0.15$), the rotor airloads are more sensitive to wake geometry. Investigation of the airload sensitivity in the low-speed region, which encompasses the hover and transition flight regimes, was beyond the scope of this study. Furthermore, the applicability of the existing water tunnel wake data to predict airloads for the transition speed conditions is hindered by the limitations mentioned previously for transforming the wake data to coordinate form.

The sensitivity of rotor airloads to wake geometry for hovering conditions has been determined previously based on wake coordinates from model rotor tests in air and the UARL Prescribed Wake Hover Performance Analysis, and the results are reported in Reference 5. It is shown in Reference 5 that rotor hovering performance (thrust-power) and the radial distribution of blade airloading are very sensitive to small changes in wake geometry. For example, an axial movement of the tip vortex beneath the following blade of 0.01 R changed the integrated thrust coefficient by as much as 3 percent for a two-bladed rotor and 10 percent for a six-bladed rotor. The increased sensitivity with increasing number of blades is attributed to the closer position of the tip vortex to the following blades. Predicted airload distributions and integrated performance would be very sensitive to the variations in the water tunnel tip vortex coordinates noted in Figures 14 and 15. Even assuming the wake to be steady prior to the passage of the following blade ($\psi_W = 180$ deg), the change in integrated thrust based on the extreme axial coordinates for the simulated 6000-lb condition shown in Figure 15 was estimated to be ±15 percent of the measured thrust value. Thus, if the occurrence of the unsteady wake behavior in the water tunnel at a closer position to the

rotor than in air is generally representative of water tunnel testing, the water tunnel wake data should not be used to calculate hover performance of rotors in air. However, even without unsteady effects, due to the extreme sensitivity of hovering performance to small changes in tip vortex position, it is questionable whether water tunnel wake data would be of sufficient accuracy (within 0.01 R) for quantitative performance calculations for rotors in air. It is thus recommended that, until the unsteadiness problem is resolved and the accuracy is determined, future experimental programs to accurately determine the wake geometry of rotors hovering in air be restricted to tests in air.

GENERAL DISCUSSION OF WAKE EFFECTS ON ROTOR AIRLOADING

The study of wake distortion effects on rotor airloading has, until recently, been a neglected area in the field of helicopter technology. This is mainly attributable to the lack of sufficient wake geometry test data and theoretical wake methods. With the recent completion of flow visualization tests and the development and incorporation of the Wake Geometry Analysis in the UARL Rotor Analysis, the application of realistic distorted wake geometries to the rotor airloads problem became feasible. Prior to the investigation reported herein, efforts at United Aircraft concerning wake distortion effects on airloading were mainly directed toward the hover condition. The influence of wake geometry on hovering rotor performance and airloads is discussed in detail in Reference 5, and thus the following discussion will pertain mainly to forward flight conditions. In the course of evaluating the water tunnel test procedures and data, this investigation provided an opportunity to apply the theoretical analysis and thereby obtain an understanding of some of the fundamentals of the forward-flight airloads problem. Although the investigation of a wide range of rotor conditions remains to be conducted, the following hypotheses regarding forward-flight wake geometry and wake effects have been deduced from conditions analyzed to date.

1. Wake geometry in forward flight for a given blade design is primarily determined by number of blades and the following parameters which determine the wake deflection angle (see Equation (13)): advance ratio, μ, rotor tip path plane angle of attack, α_{TPP}, and thrust coefficient, C_T.

2. Rotor wake effects on blade airloading generally decrease with increasing advance ratio, increasing rotor angle of attack, and decreasing number of blades. Increasing the advance ratio reduces the number of blade-vortex "intersections" by displacing the wake downstream from the rotor. Increasing the rotor angle of attack increases the axial spacing between the wake and the

rotor by providing an additional component, $V\sin\alpha_{TPP}$, to the wake axial transport velocity relative to the rotor disc. Decreasing the number of blades reduces the number of blade-vortex "intersections" by reducing the number of tip vortices in the wake. In addition, for rotors with fewer blades, the vortices from the previous blades have more time to move further beneath a blade due to the increased blade spacing. The effect of rotor thrust level is more complex in that it tends to increase wake effects at the rotor by increasing the strength of the tip vortices, but at the same time it tends to decrease wake effects by increasing the rotor-wake axial spacing. In addition to the reduction of wake effects due to these blade-wake geometry considerations, advance ratio and angle of attack influence the proportion of the wake-induced velocities to the total induced velocities at the blades. An increase in either of these parameters leads to an increase in the axial velocity component, $V\sin\alpha_{TPP}$, which contributes to the total rotor inflow. An increase in this inflow component decreases the significance of the wake-induced velocities. At moderate to high flight speeds ($\mu > 0.15$), this component is typically greater than half of the total inflow.

3. For moderate to high-speed flight ($\mu > 0.15$) the wake deflection angle is the predominant factor in determining the significance of wake effects. For most conventional helicopter conditions where the rotor supports the total gross weight and provides the total propulsive force, the rotor is normally tilted over at an angle of attack which results in a wake deflection angle of sufficient magnitude to reduce the sensitivity of the airloads to wake effect . However, wake effects can be anticipated as being very significant for helicopters with auxiliary propulsion or for helicopters in a maneuvering condition for which the wake deflection angle may approach zero, or for which the rotor may be rolling into its wake.

4. For low-speed flight ($\mu < 0.15$), the sensitivity of airloads to wake effects is greater because of the lower magnitude of the flight velocity components, $V\cos\alpha_{TPP}$ and $V\sin\alpha_{TPP}$. This limits the extent to which the wake is transported away and results in a greater number of blade-vortex "intersections" closer to the rotor. In fact, tip vortices pass above the blades for some low-speed flight conditions. The typical "roughness" experienced by aircraft flying in this low-speed range is attributable to wake effects on the vibratory response of the rotor blades.

5. In addition to the factors mentioned above, wake effects on rotor forward-flight performance are less than wake effects on hover performance since in forward flight the tip vortices do not continuously pass beneath the tip region of the following blades. As shown in Reference 5, the hovering rotor generates as much as one-third of its lift over the outer 10 percent of the blades. The passage of a tip vortex close to the blade in this tip region has been shown to significantly influence the tip airloading, and thus the integrated rotor performance. In forward flight, the vortices do not continuously pass under the blades in the predominant loading regions. In fact, for rotors with low numbers of blades flying at high advance ratios, there are no blade-vortex "interactions" for a large extent of the blade azimuth travel.

6. In forward flight, the inclusion of wake distortions is important in the regions in which the vortices pass close to the blades. Although the more prominent distortions occur downstream of the rotor where wake roll-up occurs, leading to large excursions of the wake relative to the undistorted wake, these are of less significance at the rotor. Since the blade airloading is very sensitive to small changes in the axial position of the vortex beneath the blade when the vortex is in close proximity, the prediction (or measurement) of the distortion to a high degree of accuracy is required.

7. Refinements in the analyses to include improved vortex core information, interference effects of the rotor hub and fuselage, and vortex breakdown and decay characteristics appear to be warranted.

SUGGESTED PROCEDURES FOR FUTURE WATER TUNNEL FLOW VISUALIZATION TESTS

From the results of this investigation, methods for improving water tunnel testing and wake documentation procedures for future tests have become evident. These, along with a method for generalizing wake geometry in forward flight, are discussed below.

IMPROVED TEST PROCEDURES

The test techniques used during the water tunnel experimental program were reviewed to determine improved test procedures for acquiring rotor wake data to be used for quantitative applications. A series of suggested improvements for future water tunnel tests were formulated based on the results of the data reduction and sensitivity phases of this investigation. The suggested test procedures have been categorized under (1) general test techniques, (2) selection of model rotor operating conditions for full-scale rotor simulation, (3) photographic data recording, (4) wake dimension acquisition and scaling, and (5) selection of future test parameters. These are discussed below.

General Test Techniques

1. Emit bubbles from only one blade at a time. Bubble emission from all blades was judged to be the most significant hindrance in interpreting photographs of three-dimensional wake patterns from multi-blade configurations. However, provision should also be included for multi-blade bubble emissions for qualitative study of the vortex interaction characteristics.

2. Release bubbles at specified time intervals. Starting and stopping bubble emission would result in bubble groupings with easily identifiable end points. Streamlines could be traced by following the end bubbles. Also, association of the end bubbles with the blade azimuth position at the time of emission ($\psi_{b_{0,0}}$) would facilitate the determination of the wake azimuth coordinate (ψ_W) using Equation (7).

3. Reverse thrust direction and rotor shaft angle setting so that the wake is shed above, rather than below, the rotor. The objectives of this procedure would be threefold. First, the far side of the wake would not be visually blocked by the hub and shaft housing. Second, by comparing the wake data with the results of the reverse mode of operation, the effect of buoyancy on the tip vortex coordinates could be checked experimentally. Third, wake impingement on the hub and the associated distortion and dissipation would be eliminated. This would be of

particular merit when correlating with theoretical results for an isolated rotor. However, it is recognized that hub interference on the flow over the aft portion of the rotor would exist for a full-scale rotor operating at conventional shaft tilt. The effect of this could also be evaluated by comparison with results of the opposite mode of operation.

4. If hovering rotor wake data must be taken in a water tunnel, position the rotor so that the wake is directed along the tunnel axis rather than toward the tunnel floor as was done in the test program reported in Reference 3. This will eliminate floor and ceiling effects on wake recirculation. However, there still may be some effects of the walls, and it will be necessary to limit the duration of the test period in the closed-circuit tunnel to insure quiescent flow upstream of the rotor.

5. Emit dye externally from the rotor to visualize cross sections of the wake as was done in the test program reported in Reference 3. In addition to observing the wake recirculation, the use of the dye patterns to visualize the cross sections of the vortex sheet shed from the inboard region of the blade could be explored.

6. Rotate the rotor blades in the conventional direction relative to the camera position to facilitate comparisons with photographic wake data from other sources.

Selection of Model Rotor Operating Conditions
for Full-Scale Rotor Simulation

1. Operate the model rotor at the same advance ratio, μ, and with the same number of blades, b, as the full-scale rotor condition being simulated.

2. Set the model rotor shaft angle, accounting for blade bending, such that the resulting tip-path plane angle is equivalent to the full-scale rotor value.

3. When wake data are of interest, operate the rotor at the full-scale rotor lift coefficient (or thrust coefficient). Do not include a Prandtl-Glauert compressibility correction as was done in Reference 1.

4. If possible, use model blades with higher effective stiffness (i.e., higher structural stiffness, and/or lower rotational speeds) to reduce spanwise bending and thereby more accurately simulate the coning, flapping, and bending of the full-scale rotor blades. This would improve the simulation of the relative blade-wake geometry, and would reduce the occurrence of some unrealistic blade-vortex encounters as well as the passage of the model rotor tip vortex trails above the blades.

Photographic Data Recording

1. Take photographs of the top view and both the advancing and retreating sides of the rotor. However, if the camera position must be limited to one side of the rotor, place the camera on the advancing side since the more significant blade-vortex intersections occur on that side.

2. Take photographs of different views of the flow field at the same time. This would greatly facilitate the data reduction efforts and would eliminate possible differences in the wake coordinates obtained from different views due to any unsteadiness in the wake.

3. Include a rotor blade azimuth indicator in each view of the wake.

4. Record the camera distances and viewing angle to a fixed reference point in the tunnel, and do not change the position of the camera during the test.

5. If still photographs are to be used to obtain quantitative wake data, (a) measure and record the rotor azimuth position corresponding to each photograph, and (b) take a sequence of photographs at varying azimuth positions.

Wake Dimension Acquisition and Scaling

1. Mark the rotor hub center for use as a reference point, and mark a reference length on the top and side of the shaft housing (e.g., 0.04 R with division markings at each 0.01 R).

2. Use a black background for contrast with the white bubbles. Since the white grid lines previously used interfere with the visibility of the bubbles, do not include grid markings in the background region behind the wake. However, include grid markings or reference marks outside of the wake region in all views. If grid markings are used, space them at even increments of the rotor radius and, if possible, corrected for parallax, camera lens distortion, and water refraction.

3. To evaluate corrections to account for parallax, camera lens distortion, and water refraction, prior to testing place a reference grid in the water tunnel at various distances from the camera and record on film.

Selection of Future Test Parameters

1. To determine the sensitivity of wake geometry to the primary rotor operating parameters, systematically vary the parameters μ, C_T, and α_{TPP}.

2. Include rotors having more than three blades and varying blade designs (i.e., designs which vary the radial distribution of loading).

PROCEDURES FOR DOCUMENTING AND GENERALIZING WAKE GEOMETRY DATA

Wake Documentation

The detail to which wake geometry test data must be reduced is dependent on its proposed application. Several possible applications are:

1. To compare the general wake characteristics of various test conditions and configurations

2. To compare the wake data with the results of other test programs

3. To compare the wake data with predicted wake coordinates to evaluate theoretical wake methods

4. To determine the wake interference with objects located downstream of the rotor

5. To incorporate the experimental wake geometry in analyses for determining the rotor-induced flow field, blade response, and airloads, and associated characteristics such as blade stress, vibrations, and noise

Several alternative methods, each representing a different level of detail and accuracy, are available for documenting wake coordinates. The selection of the particular method to be used will depend on the specific application and the accuracy required for that application. At one extreme, a complete set of experimental wake coordinates may be required; at the other extreme, no data reduction is required if known undistorted wake coordinates are considered adequate. The fact that the data reduction can be a very time-consuming process leads one to select the simplest method with sufficient accuracy for his application. Also, comparisons of the wake patterns may be presented in a more easily understood format using simplified coordinate representations which are more readily adaptable to theoretical analyses.

Obviously, the most accurate and straightforward but also the most extensive and time-consuming wake documentation procedure would be to obtain three-dimensional coordinates of the entire vortex trail system for all blade azimuth positions. This was accomplished for the four test conditions reported herein and may be necessary in the future for applications in which local effects are of interest or a high degree of accuracy is required. The most accurate wake documentation procedure, other than tabulating and plotting all of the wake coordinates, is to develop curve-fit equations in which the wake coordinates are expressed in terms of constants describing certain wake features. For example, curve-fitting techniques used to represent the wake for a hovering rotor were applied in the investigation reported in Reference 5. It was found that the steady portion of the hovering rotor wake (near the rotor) could be expressed in terms of relatively simple equations which facilitate the rapid estimation of contracted wake geometries for a wide range of rotor designs and operating conditions. Although the wake of a rotor in forward flight is more complex than the hovering rotor wake due to the variation of the entire wake pattern with time, it may still be possible to develop simplified curve-fit equations to represent it. In fact, this has already been attempted for a single-bladed rotor as reported by Gray in Reference 13. A review of Gray's procedure was encouraging. However, considering the wake features apparent from the current investigation, certain assumptions in Reference 13, such as the representation of each wake revolution by a circle, are questionable. The development of a curve-fitting method for the water tunnel data was beyond the scope of this investigation due to the limited number of flight conditions reduced. Future effort toward evaluating the applicability of curve-fit techniques to forward flight wake geometries is recommended. It is noted, however, that unless the curve-fit constants can be generalized for various rotor designs and operating conditions, the curve-fitting technique only results in a simpler method for presenting the data, since the entire set of wake data must still be reduced to coordinate form in order to determine the appropriate curve-fit equations and constants.

In order to obtain a less complex coordinate representation of the wake which would enable one to document the major wake features, several intermediate approaches were considered. One suggested intermediate method of wake documentation which appears to have promise will now be discussed. This method was developed as a reasonable compromise for applications in which the wake in the immediate vicinity of the rotor is of primary interest. In its most simple form, the method takes advantage of the absence of significant wake distortions in the top view in the vicinity of the rotor for moderate and high-speed conditions. The validity of an assumed undistorted wake increases with increasing advance ratio. Using the undistorted wake coordinates in the top view for the x and y

coordinates, the wake documentation is reduced to applying techniques for determining the axial coordinate, z. The suggested technique to accomplish this is to document the axial coordinates of the tip vortex at the blade-vortex "intersections" in combination with the axial coordinates for the fore, aft, and lateral wake boundaries. This results in an accurate documentation of the tip vortex near the blades and a description of the general wake features (in the axial direction) downstream of the rotor.

A sample plot of the axial coordinates, z, at the blade-vortex "intersections", obtained from the theoretical wake results, was presented in Figure 36. Similar plots could be developed from experimental wake data. The manner in which one may obtain the other two wake coordinates, x and y corresponding to the blade-vortex "intersections" based on the undistorted wake representation, will now be presented.

The radial location at which the blade-vortex "intersection" (in the top view) occurs is presented in Figure 45. A new value "1" of the first subscript for ψ_b is introduced to identify the blade at which the vortex intersection occurs. It is noted that the blade originating the vortex and the blade intersecting the vortex may be the same. It is shown in Figure 45 that, for a two-bladed rotor at a μ of 0.19, "intersections" with the tip vortex of the intersecting blade occur only over one-fourth of the azimuth range ($\psi_{b_{1,1}}$ = 60 to 120 deg, and 345 to 15 deg). Intersections with the preceding blade occur over a larger azimuth region but not the entire azimuth range. In fact, blade-vortex "intersections" over the outer half of the blade ($r_{b_{1,1}} > 0.5$) are limited to the lateral sides of the rotor. Also included in Figure 45 is the azimuth position of the blade which shed the intersecting vortex at the time the intersection point of the vortex was shed ($\psi_{b_{0,0}}$). The values of this azimuth coordinate are never less than 90 deg nor greater than 270 deg, for it is only the wake from the upstream side of the rotor that intersects with the blades. The wake from the aft side of the rotor is swept downstream. This azimuth coordinate, $\psi_{b_{0,0}}$, is of importance in determining the wake azimuth coordinate, ψ_W, which in turn is important for determining the undistorted wake coordinates, x and y, from Equations (4) and (5). The wake azimuth coordinate, ψ_W, may be obtained from the following equations:

If the originating blade is also the intersecting blade,

$$\psi_W = \psi_{b_{1,1}} - \psi_{b_{1,0}} + 360^\circ \tag{14}$$

If the originating blade is the preceding blade,

$$\psi_W = \psi_{b_{0,1}} - \psi_{b_{0,0}} \tag{15}$$

in which

$$\psi_{b_{0,1}} = \psi_{b_{1,1}} + 360^\circ/b \tag{16}$$

It is noted that for configurations in which blades other than the originating or preceding blades are involved in the blade-vortex "intersections", increments of 360 deg/b must be added to $\psi_{b_{1,1}}$. For other advance ratios in which more wake revolutions are involved in the blade-vortex intersections, increments of 360 deg must be added to ψ_W.

The blade-vortex "intersection" coordinates presented in Figure 45 may be obtained for other combinations of number of blades and advance ratio from the following equations:

$$r = r_{b_{0,0}} \sin \psi_{b_{0,0}} / \sin \psi_{b_{0,1}} \tag{17}$$

$$0 = r_{b_{0,0}} \cot \psi_{b_{1,1}} - r_{b_{0,0}} \cot \psi_{b_{0,0}} - \mu \ (\psi_{b_{0,1}} - \psi_{b_{0,0}}) / \sin \psi_{b_{0,0}} \tag{18}$$

Equation (18) is a transcendental equation which may be solved for $\psi_{b_{0,0}}$ using iterative techniques.

In addition to the wake coordinates at the blade-vortex intersections, it is suggested that the axial coordinates for the fore, aft, and lateral wake boundaries be documented. These boundaries are equivalent to the streamlines of a point on the tip vortex shed when the blade azimuth, $\psi_{b_{0,0}}$, is 0 deg (aft boundary), 90 deg (advancing side boundary), 180 deg (forward boundary), and 270 deg (retreating side boundary). The fore and aft boundaries were presented for the model rotor in Figures 19 and 25 for

the simulated 35-kt and 90-kt conditions, respectively. If, as suggested, the x coordinate is to be based on the undistorted wake, the data reduction is simplified by measuring only the axial coordinates and plotting the results as shown in Figure 46. In this figure, curves for the four boundaries are presented for the model rotor operating at the simulated 90-kt condition. The axial coordinates, z, are plotted versus ψ_W, which is representative of the time that has passed since a particular vortex point on the streamline was shed from the blade. It is equivalent to the azimuth travel of the blade from the time it shed the point of vorticity. If, for a given vortex point on the streamline, the blade that originated the point is at the azimuth position ψ_b in the fixed coordinate system, then the wake azimuth position, ψ_W, of the vortex point relative to the blade at ψ_b may be obtained from Equation (7). The azimuth coordinate, ψ_W, can be used in the undistorted wake equations, Equations (4) and (5), to obtain the x and y coordinates corresponding to the measured axial coordinates, z, of the wake boundaries.

The above wake documentation method, in addition to simplifying the presentation of the wake data to a set of simple equations and plots of the axial coordinates at the blade-vortex "intersections" and wake boundaries, reduces the data reduction efforts significantly. The axial coordinates at the blade-vortex "intersections" may be readily obtained by selecting a frame of the movie film showing the side view of the wake at a given blade azimuth position, $\psi_{b1,1}$, measuring the axial distance between the vortex and the tip-path plane at the few intersection points that usually exist, and repeating the process for other azimuth positions. The axial coordinates at the boundaries may be readily obtained by selecting the frame of the movie film in which a blade is at the azimuth position equivalent to the boundary azimuth position ($\psi_{b0,0}$ = 0 deg, 90 deg, 180 deg, or 270 deg), advancing the film frame by frame at known azimuth intervals relative to the first frame (ψ_W), and measuring the axial distances to the tip-path plane of a point on the vortex which left the blade at $\psi_{b0,0}$. For the water tunnel film data, a particular air bubble trapped in the tip vortex may be used to identify a vortex point.

Although the above suggested method is based on the documentation of only a limited number of points in the wake, it is possible to connect them and obtain a reasonable reconstruction of the entire wake pattern, particularly near the rotor. The approximate x and y coordinates of all points in the wake are known from the assumed applicability of the undistorted wake equations. From these and the measured axial coordinates associated with the wake boundaries, four points on each revolution of each tip vortex are available for each rotor position. From the coordinates associated with the blade-vortex "intersections", several additional points near the rotor are available for each rotor position.

Reasonable fairing, based on knowledge of the realistic wake features, through the available vortex points should result in a reconstructed wake which is sufficient for most applications.

The accuracy resulting from applications of the above simplified wake documentation remains to be determined. It is expected that the accuracy will be greatest near the rotor and for moderate and high-flight speeds due to the assumption of the undistorted top view. Variations from this approach may be developed to improve the accuracy for certain applications. For example, if even greater accuracy is required near the rotor, several more streamlines of vortex points emitted from the forward half of the rotor ($\psi_{b_{0,0}}$ = 90 deg to 270 deg) may be reduced. Additional streamlines from the rearward half of the rotor ($\psi_{b_{0,0}}$ = 270 deg to 90 deg) would not be required because they are located downstream of the rotor. Another refinement to this procedure that could be considered would replace the undistorted x and y coordinates by actual measurements for the blade vortex "intersections". This would still involve less work than reducing data for the entire wake. Finally, it may be desirable to include modifications to account for hub interference on the wake distortions and dissipation downstream from the hub.

Wake Generalization

Further simplification of wake documentation, which would also permit the rapid determination of wake geometry for untested configurations and flight conditions, may be possible through generalization of the wake coordinates. This has been substantially accomplished for the hovering flight condition as reported in Reference 5 in which experimental wake coordinates are generalized in terms of simple equations for a wide range of the following rotor design and operating parameters: number of blades, rotor solidity, rotor thrust level, tip speed, blade twist, and aspect ratio. Similar generalization techniques may be possible for forward-flight conditions. However, the problem is complicated by the introduction of additional variables such as flight speed, rotor tilt, and time (blade azimuth position).

One form of generalization is the potential representation of the top view of the wake by the undistorted wake coordinates for a certain range of conditions. This generalizes the x and y coordinates in terms of advance ratio, μ, and number of blades, b. It also provides a rapid means for determining the blade radial locations for blade-vortex "intersections". That is, generalized charts of the form shown in Figure 45 could be developed to cover the complete range of number of blades and advance ratio. The determination of the primary rotor operating parameters which affect the wake (b, μ, C_T, α_{TPP}) represents another step

toward generalization since it reduces the number of variables to be considered. From the results for the limited conditions reported herein, the possibility of generalizing the variation of wake geometry with these parameters appears encouraging. For example, from the results presented in Figure 31, it appears that the tip vortex distortions relative to the undistorted wake position are not significantly influenced by α_{TPP} variations, and thus the influence of α_{TPP} is mainly on the undistorted wake position (wake deflection angle). If this holds true at other conditions, then α_{TPP} could be eliminated as a variable influencing wake distortions. A second example concerns the possible generalization of the effect of thrust coefficient, C_T, on wake geometry. Since the tip vortex circulation strength is proportional to C_T, it might be anticipated that, if the other variables are held constant, the tip vortex distortions relative to the undistorted wake position are proportional to C_T. An example of this was shown in Figure 34. A third example concerns number of blades. For the hovering condition, it is reported in Reference 5 that the influence of number of blades on the wake geometry was mainly restricted to determining the wake azimuth position, ψ_W, at which the magnitude of the axial wake transport velocities are changed. A similar generalization for forward-flight conditions remains to be investigated. Also, an investigation to determine if blade design parameters influencing radial load distributions affect the forward-flight wake remains to be conducted. However, inasmuch as these may be expected to influence the details of the wake circulation, based on the results of the sensitivity studies presented previously, these parameters may also prove to be unimportant.

An investigation directed toward the generalization of the wake geometry characteristics of rotors in forward flight should consist of determining the sensitivity of wake geometry to the rotor design and operating parameters over a wide range of designs and conditions, generalizing the results, and developing a set of generalized wake charts (and/or equations). Considering the cost of an experimental program and the experimental limitations cited herein, it is recommended that this wake generalization study be conducted, at least initially, using the analytical tools available. Following the development of improved test techniques, the analytical results could be checked and/or expanded upon experimentally.

TUNNEL WALL CORRECTIONS

The presence of the tunnel walls implies that the rotor wake geometries observed in the water tunnel (or any tunnel) will not be exactly the same as those observed in unconstrained flow. Considerable progress has been made in developing procedures for determining the influence of wind tunnel walls on model flow fields for low-speed

conditions where the wake is deflected sharply from the free-stream direction (e.g., References 20 and 21). This work has principally been concerned with evaluation of tunnel-induced velocities in the vicinity of the model lifting device (the rotor in this case), and results along the longitudinal and lateral axes of a model centered in a tunnel are given in Reference 20. Limited graphical results for the plane of symmetry of the entire flow field are also given in Reference 21; however, these results are for a rotor located 30 percent above the center line of the tunnel. This contrasts with the Oceanics model location, which was on the center line of the tunnel. The application of detailed tunnel wall corrections to the water tunnel wake geometry data was beyond the scope of this study. The intent here is to give some indication of the magnitude of the corrections that are likely to exist for the two forward-flight conditions analyzed in this study (V = 35 and 90 kt).

A primary indicator of the potential severity of the tunnel wall corrections is the wake deflection angle (χ_{TPP}). The corrections are smallest in high-speed flight, where the wake deflection angle is close to 0 deg and becomes most severe as the deflection angle approaches 90 deg for the hover condition. For the 35- and 90-kt conditions, the wake deflection angles in free air without tunnel wall effects are approximately 19 deg and 9 deg, respectively. These are relatively low values and, as a result, the wall corrections near the rotor are also fairly small. Thus, from Reference 20, the walls cause the wake deflection angle (as defined by the velocities at the rotor center) for the 35-kt condition to be reduced by only about 2 deg. This means that the measured water tunnel wake would be closer to the rotor than would be the case in unconstrained flow. For the 90-kt condition, a reduction of only about 0.5 deg in deflection angle at the center of the rotor would result.

The tunnel wall effects are, of course, different throughout the flow field. The results presented in Reference 21 can be used to estimate the effects of the walls at different points in the vertical plane of symmetry. At the leading edge of the rotor disc, the error between the deflection angles with and without wall effects is only about two-thirds that at the center of the rotor. On the other hand, the errors become larger at points downstream of and below the rotor center (e.g., at a point located 1 radius aft and below the trailing edge, the deflection angle error is about twice as big as the rotor center error). Far downstream, of course, the wall effects must reduce the deflection angle to zero if the wake in the tunnel is to end up flowing parallel to the tunnel walls. Reference 20 shows that for the deflection angles being considered here, the wall corrections to axial velocities over the lateral axis of the rotor are approximately equal to those at the center line.

If emphasis is to be placed on the effect of wake distortions on rotor loads, the above-mentioned flow regions where the tunnel wall effects are the largest are of little consequence because of their distance from the rotor. The wake from the forward half of the rotor passes closest to the rotor blades. Therefore, a logical method for correcting water tunnel wake data would be to increase the measured axial displacements of the wake from the rotor tip-path plane by the average correction in wake deflection angle for this region of the flow. The average deflection angle corrections for the 35-kt and 90-kt conditions would be, then, about 1.6 deg and 0.4 deg, respectively.

It should be noted that following the initiation of this study, References 3 and 22 were published. In these references, it is inferred by the authors from recent water tunnel data that tunnel wall corrections of the type considered in this section (i.e., those for wind tunnels) may not be applicable to water tunnel data. This was attributed to different "wake energy dissipation scaling" in water and in air. It is also inferred that, due to the increased viscous dissipation in water, water tunnel wall effects are less than wind tunnel wall effects for the same model to tunnel size ratio. The data presented in Reference 3 do not appear to fully support the statements made. A plot of the "mass flow wake deflection angle" as a function of forward velocity (Reference 3, Figure 21) for different test section sizes shows measured wake angle changes of approximately 5 deg with varying test sections at both the 35- and 90-kt conditions. These wake angle deflections are greater than the above-mentioned deflections (less than 2 deg) predicted for a wind tunnel.

MODEL ROTOR TESTING IN WATER VERSUS AIR

The following discussion compares the advantages and disadvantages of testing in water with those of testing in air. Primary emphasis is placed on flow visualization tests to obtain wake data.

A sample flow visualization photograph of the wake of a model rotor in air was presented in Figure 16 for a hovering condition. The test techniques used to obtain such photographs and the results obtained therefrom are presented in Reference 5. A sample photograph of the wake in air for a model rotor operating in the UARL wind tunnel is presented in Figure 47. Flow visualization photographs taken in air showing the wake in the rotating system (smoke emitted from the blades) are presented in References 14 and 23. In addition to the use of smoke as a flow visualization technique in air, several new approaches are currently under development which do not require the introduction of an external agent (e.g., smoke). A Schlieren system for photographing the wake is discussed in Reference 24. Another technique using laser-holography to obtain three-dimensional holograms of the wake is under development at UARL. A sample shadowgraph of the wake of a model propeller obtained from a hologram is shown in Figure 48.

The following is a listing of the advantages and disadvantages of water tunnel testing relative to testing in air. In reviewing the statements made, it should be remembered that a major question in selecting a water tunnel as opposed to a wind tunnel for any future wake geometry tests is "Do the details of the rotor airloading azimuthal distribution have to be simulated?". If the answer is yes, then the potential disadvantages discussed below become very real and a water tunnel may not be appropriate. The theoretical sensitivity results presented in this report indicate that at moderate speeds, the details of the airloading were not important in determining wake geometry. Hence, the water tunnel can be considered for further, improved testing in this speed regime. However, similar sensitivity calculations should be conducted for low-forward-speed conditions before any further water tunnel testing in this regime is attempted.

POTENTIAL ADVANTAGES OF WATER TUNNEL TESTING

1. Clarity of Tip Vortex Patterns

The water tunnel flow visualization technique provides an extremely clear qualitative demonstration of the tip vortex pattern. The retention of the air bubbles in the core of the vortex far downstream of the rotor makes this a useful technique for studies which require knowledge of the far wake.

2. Viewing Range

The small test section size permits a viewer and/or a camera to observe the entire wake pattern from one viewing point.

3. Tunnel Wall Effects

It is claimed in References 3 and 22, for the same relative size of the model rotor and tunnel, that the tunnel wall effects in water are less than those in air due to differences in wake dissipation. However, as mentioned in the preceding section, it is believed that more work is required to substantiate this.

4. Cost of Testing

Because of their relatively small sizes, water tunnels provide a relatively inexpensive means of conducting rotor flow visualization tests. In particular, if it is required to test in air in a large wind tunnel facility to reduce wall effects, the costs of testing in water would be less. This advantage does not necessarily apply to hover tests, for which tests in air are not conducted in a wind tunnel.

POTENTIAL DISADVANTAGES OF WATER TUNNEL TESTING

1. Size Limitations

The model size is restricted by tunnel size limitations, which are significantly greater for existing water tunnels than for wind tunnels. Size limitations are of particular importance for testing models with small dimensional refinements in blade design such as the incorporation of cambered airfoil sections and new tip designs. Also, the design of blades which are dynamically scaled to full-scale blades would be impossible.

2. Reynolds Number Limitations

The size limitations coupled with the increased loads in water (due to the increased fluid density) limit the rotational speeds to extremely low values to avoid structural problems. The low rotational speed and model size compromise the Reynolds numbers in water to values less than those typical of testing in air, even though the density of water is almost three orders of magnitude greater. This is particularly true for hover tests, in which the model rotor tip speed in air is not compromised by tunnel speed limitations to attain higher advance ratios. For example, in the model rotor tests in air, reported in Reference 5, the tip Reynolds number was 52×10^4 compared to 9.4×10^4 in the water test of Reference 1. Reynolds number effects on airfoil characteristics are mainly of significance in the stall region, where they determine the maximum section lift coefficient. Thus the maximum rotor thrust coefficient of the water tunnel model may be less than that of the model rotor in air.

In addition to the above, there are other viscous limitations. Rotor drag characteristics in water are not scalable and thus rotor torque data would not be meaningful. Also, vortex core sizes may differ due to viscous effects.

3. Compressibility Limitations

Tests in which compressibility effects are important would obviously be severely compromised in an incompressible fluid such as water. However, thus far, no serious compromises of water tunnel wake geometry patterns caused by lack of compressibility effects have become evident. Also, in the test results reported in Reference 5, wake geometry was insensitive to tip Mach number variations over the range of tests (0.46 to 0.61).

4. Similarity With Full-Scale Blades

Due to the size limitations, virtual mass effects, and the absence of centrifugal stiffening, flapping hinges and cyclic pitch control may not be incorporated in the water tunnel model. This leads to unreasonable bending deflections. Size and structural limitations make dynamic similarity impossible. Also, blade mass balance and elastic axis position are not scaled. Although these limitations might be expected to severely compromise the simulation of full-scale wake geometry, their influence on the wake for moderate and high-speed conditions was predicted to be generally small as reported herein.

5. Inboard Vortex Sheet

The inability to obtain realistic results from external emission of air bubbles due to the buoyancy problem discussed in Reference 1 implies that the location of the inboard vortex sheet may not be obtained in the manner previously used in smoke testing (Reference 5). However, the external emission of dye as shown in Reference 3 should be explored for this purpose.

6. Other Test Measurements

Measurements of blade stresses and blade and slipstream dynamic pressures are impractical in water.

CONCLUSIONS

Conclusions pertaining specifically to the usefulness of existing water tunnel wake geometry data for quantitative purposes should be considered in the light that the data evaluated were primarily obtained to define qualitative rotor wake features. That objective was achieved, and the water tunnel flow visualization technique provides an excellent qualitative demonstration of tip vortex patterns.

1. From the two hover conditions analyzed, the existing wake geometry data obtained in the water tunnel for the hover conditions do not appear useful for quantitative purposes. The data differ significantly from those obtained in air, particularly with regard to the steadiness of the wake near the rotor. However, further substantiation of the generality of this conclusion is required through analysis of more test conditions.

2. Based on comparisons with theoretical results, the existing forward-flight wake geometry data obtained in the water tunnel appear reasonable. However, major portions of the tip vortex filaments comprising the wake cannot be accurately defined from the available photographs due to the test techniques used. This problem becomes more severe as rotor advance ratio is decreased.

3. Improved test procedures are required to improve the quality of the wake data for quantitative applications and to facilitate the accuracy and efficiency of data reduction. A list of suggested test procedures for future water tunnel tests of rotor wake geometry has been formulated

4. Simplified, cost-effective procedures for reducing and documenting photographic wake geometry data appear possible. Suggested in this report is a method which emphasizes the documentation of blade-vortex "intersection" points and the fore, aft, and lateral boundaries of the wake.

5. The theoretical results indicate that, for forward flight conditions, the primary parameters influencing wake geometry for a given blade design are number of blades, rotor advance ratio, thrust coefficient, and tip-path plane angle. Any attempt to apply available water tunnel data to specific full-scale rotor flight conditions should insure that these parameters are duplicated.

6. The theoretical results indicate that tip vortex geometry for moderate to high-flight speed ($\mu > 0.15$) is insensitive to parameters which influence the azimuthal variation of blade airloading such as blade flexibility, cyclic pitch, Reynolds number, and Mach number. Thus the fact that the full-scale values of these parameters were not accurately simulated in the water tunnel does not appear to compromise the data significantly, at least for two-bladed rotors. However, viscous and compressibility effects on the structure of the vortex core and its influence on the wake geometry in both water and air remain to be determined.

7. The relative insensitivity of rotor wake geometry to many parameters heretofore considered potentially important leads to the definite possibility that rotor wake distortions may be generalized in terms of only a few variables. This result should provide a framework within which future wake geometry tests and theoretical computations should be conducted.

8. Rotor wake distortions can be expected to have a significant effect on blade loadings at those forward-flight conditions where the tip vortex lies within about 5 percent of the rotor radius from the blade. For such conditions, the airloads are very sensitive to small changes in vortex position, and thus a very accurate experimental determination or theoretical prediction of this position is required.

RECOMMENDATIONS

1. The suggestions made herein for improving water tunnel test procedures should be incorporated in any future testing having as its objective the measurement of rotor wake geometries.

2. Additional sensitivity studies similar to those discussed in this report should be made for the lower flight speed regime. Thro the use of available rotor wake geometry analyses, the degree to which wake geometry can be affected by conventional rotor parameters which cannot be simulated in a water tunnel should be determined.

3. Following the incorporation of improved test procedures, a check of the analytical wake sensitivity results should be conducted in the water tunnel. This could be done by scaling the blade design and duplicating the number of blades, advance ratio, thrust coefficient, and tip-path plane angle of a small model rotor operating in a large wind tunnel for which flow visualization data would also be taken. In addition, it is recommended that several full-scale rotor conditions, for which airloads data are available, be accurately simulated in the water tunnel to provide experimental wake geometries that directly correspond to the full-scale rotor conditions. These wake geometries should be used in theoretical analyses to predict and compare airloads.

4. The sensitivity of wake geometry to blade design parameters influencing the radial distribution of loading (e.g., twist, aspect ratio, taper, and tip design) for forward-flight conditions should be determined analytically and experimentally. Also, the variation of wake geometry in forward flight with number of blades (two through eight) should be investigated.

5. A wide range of hover conditions should be analyzed to determine the comparative extent of the unsteadiness of the water tunnel wake relative to the rotor wake in air. Until this is completed, it is recommended that future experimental programs to accurately determine the wake geometry of rotors hovering in air be restricted to tests in air. Investigations should also be undertaken to examine in detail the stability characteristics of the wake of a hovering rotor.

6. It is recommended that the suggested simplified procedures for wake documentation, described herein, be used in future wake studies to provide data for identifying the significant wake features and to provide a

common basis for comparison. The use of the simplified wake data to determine rotor airloads should also be evaluated.

7. An investigation to generalize the wake geometry characteristics of rotors in forward flight is recommended. This should consist of determining the sensitivity of wake geometry to the rotor design and operating parameters over a wide range of designs and conditions, generalizing the results, and developing a set of generalized wake charts (and/or equations). Considering the cost of an experimental program and the experimental limitations cited herein, it is recommended that this wake generalization study be conducted, at least initially, using the analytical tools available. Following the development of improved test techniques, the analytical results could be checked and/or expanded upon experimentally.

8. In view of the predicted sensitivity of rotor airloads to small variations in tip vortex position when the vortex lies close to a blade, and the observation of the wake instabilities, investigations of the structure and decay of the vortex core appear warranted.

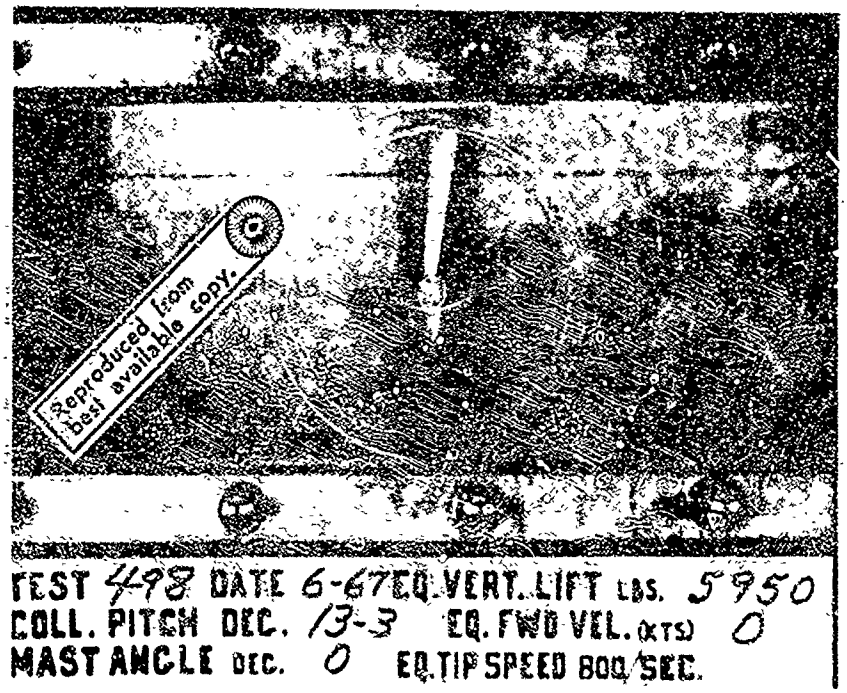

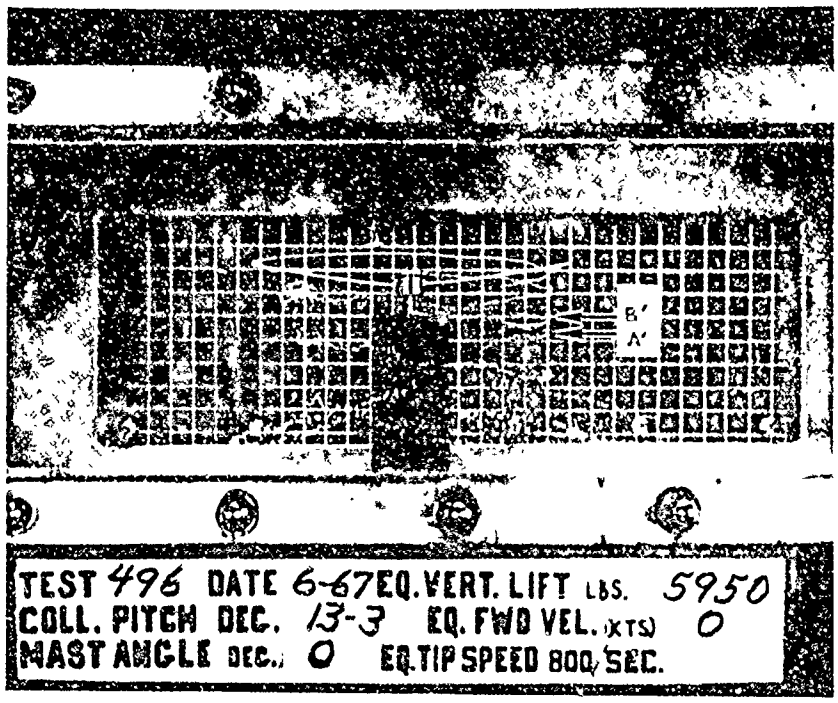

Figure 1. Photographs of Model Rotor and Wake In Water Tunnel -- Two Blades, Simulated 10,000-Lb Lift, Zero Forward Velocity.

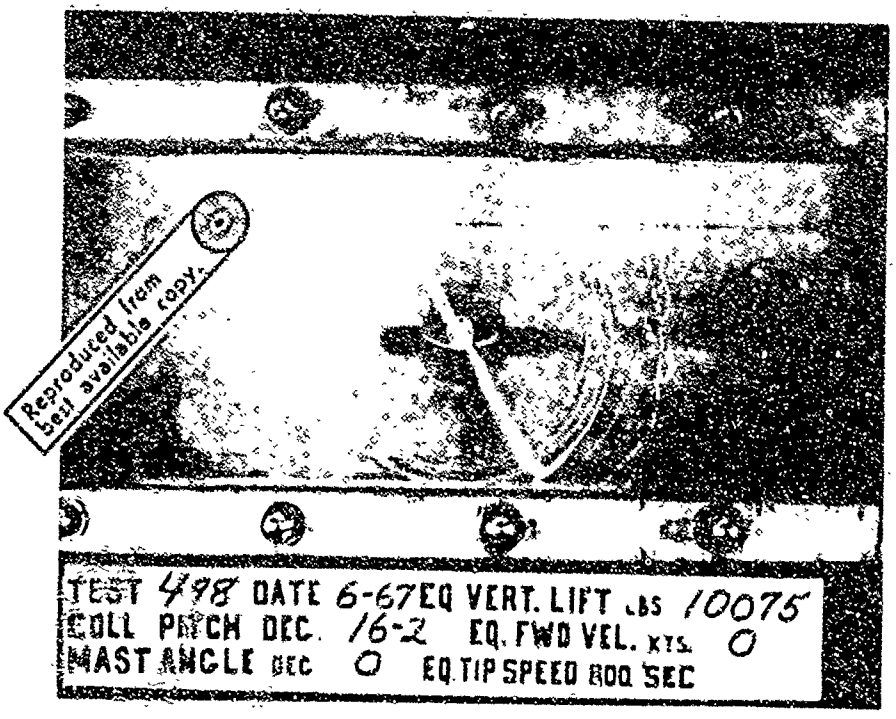

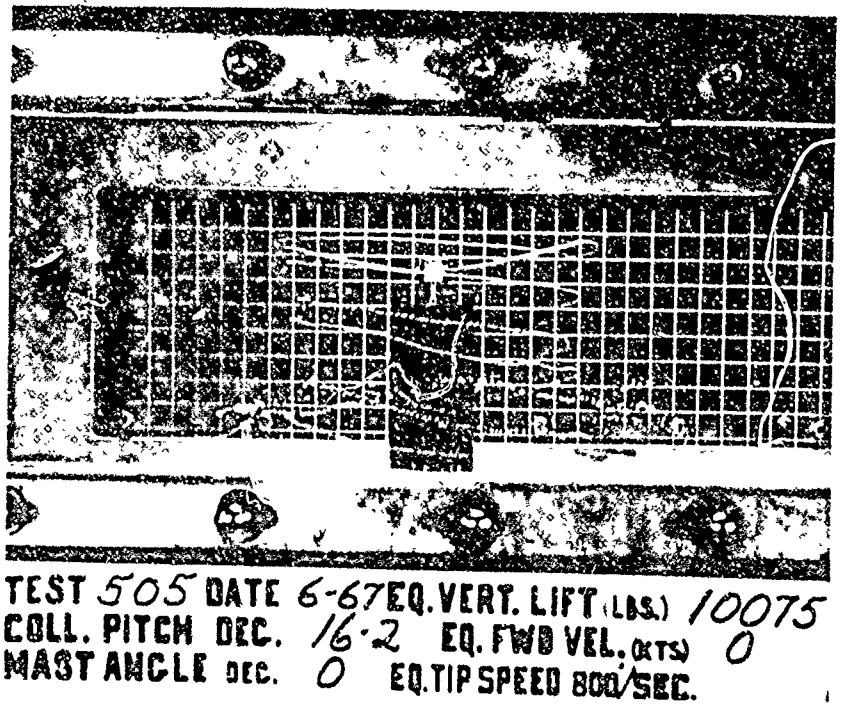

Figure 2. Photographs of Model Rotor and Wake In Water Tunnel -- Two Blades, Simulated 6,000-Lb Lift, Zero Forward Velocity.

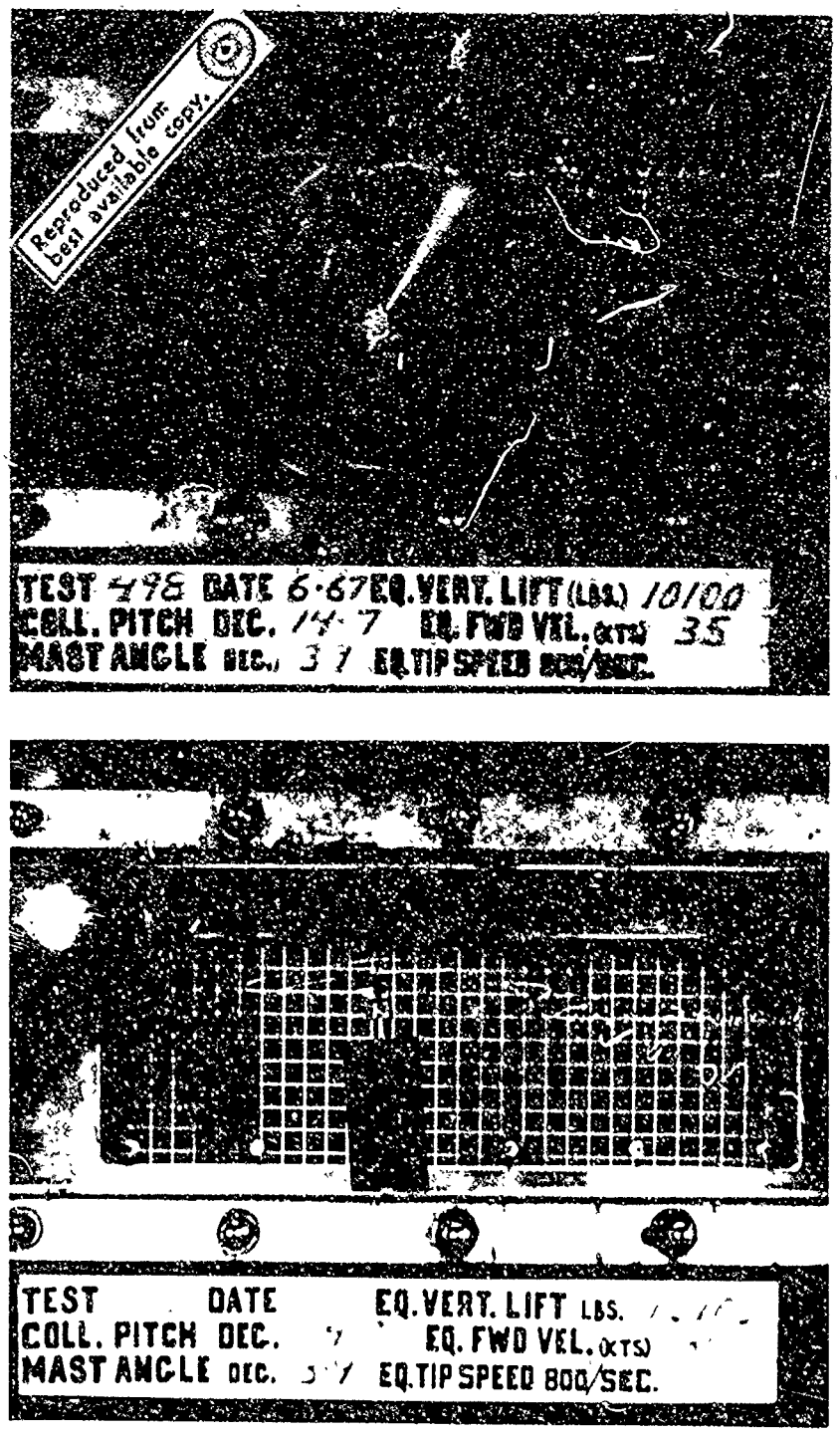

Figure 3. Photographs of Model Rotor and Wake In Water Tunnel -- Two Blades, Simulated 10,000-Lb Lift and 35-Kt Forward Velocity.

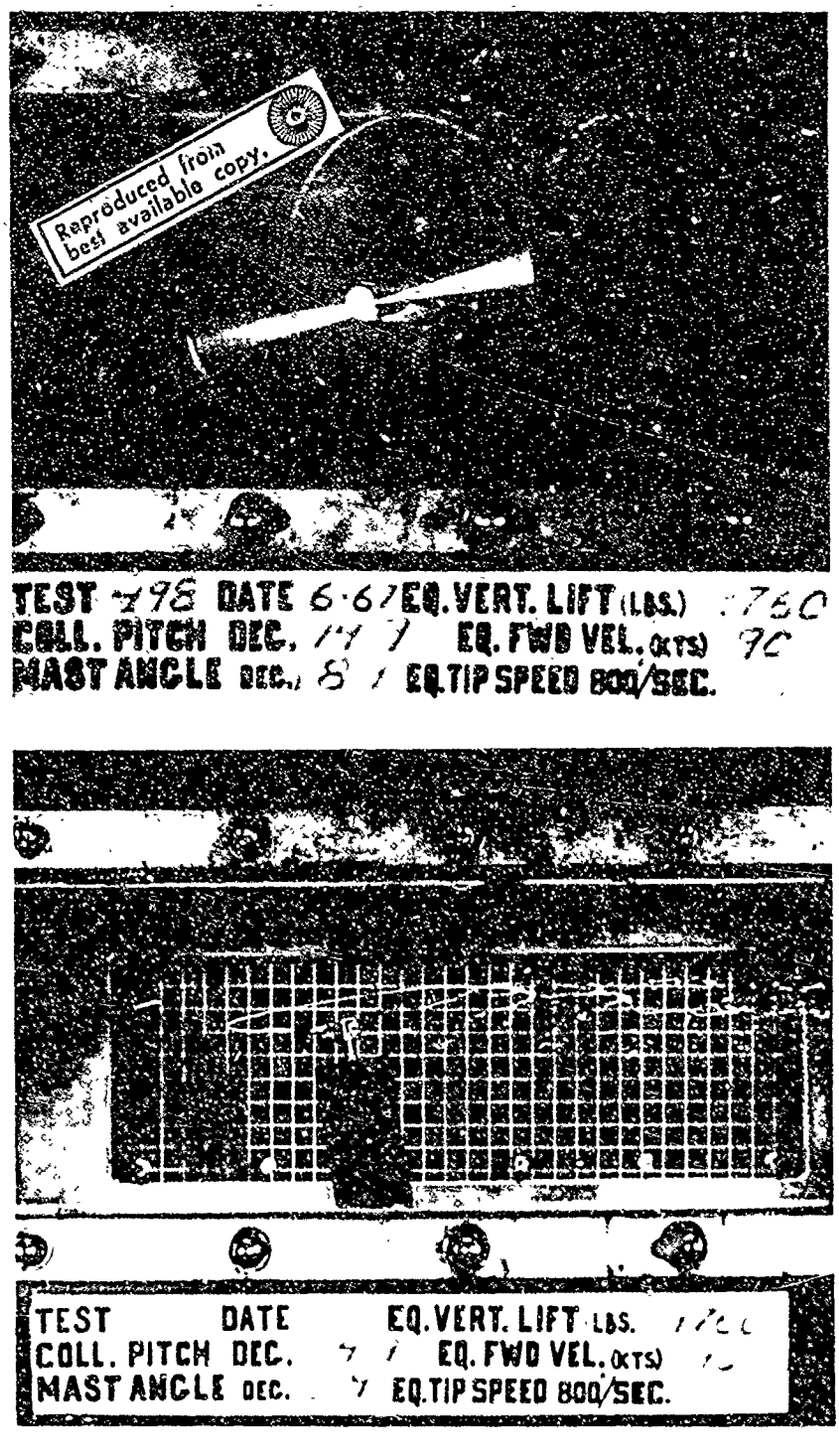

Figure 4. Photographs of Model Rotor and Wake In Water Tunnel -- Two Blades, Simulated 10,000-Lb Lift and 90-Kt Forward Velocity.

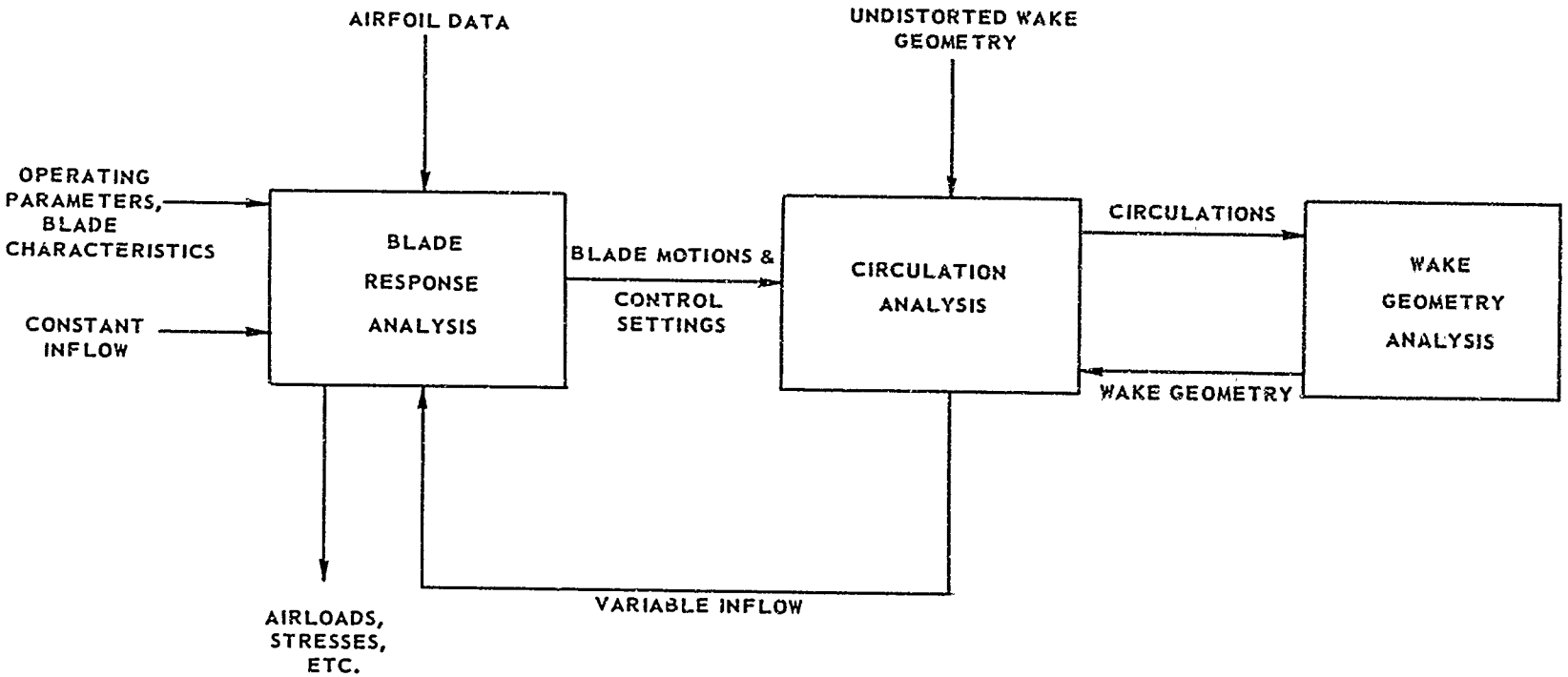

Figure 5. Components of the UARL Rotor Analysis.

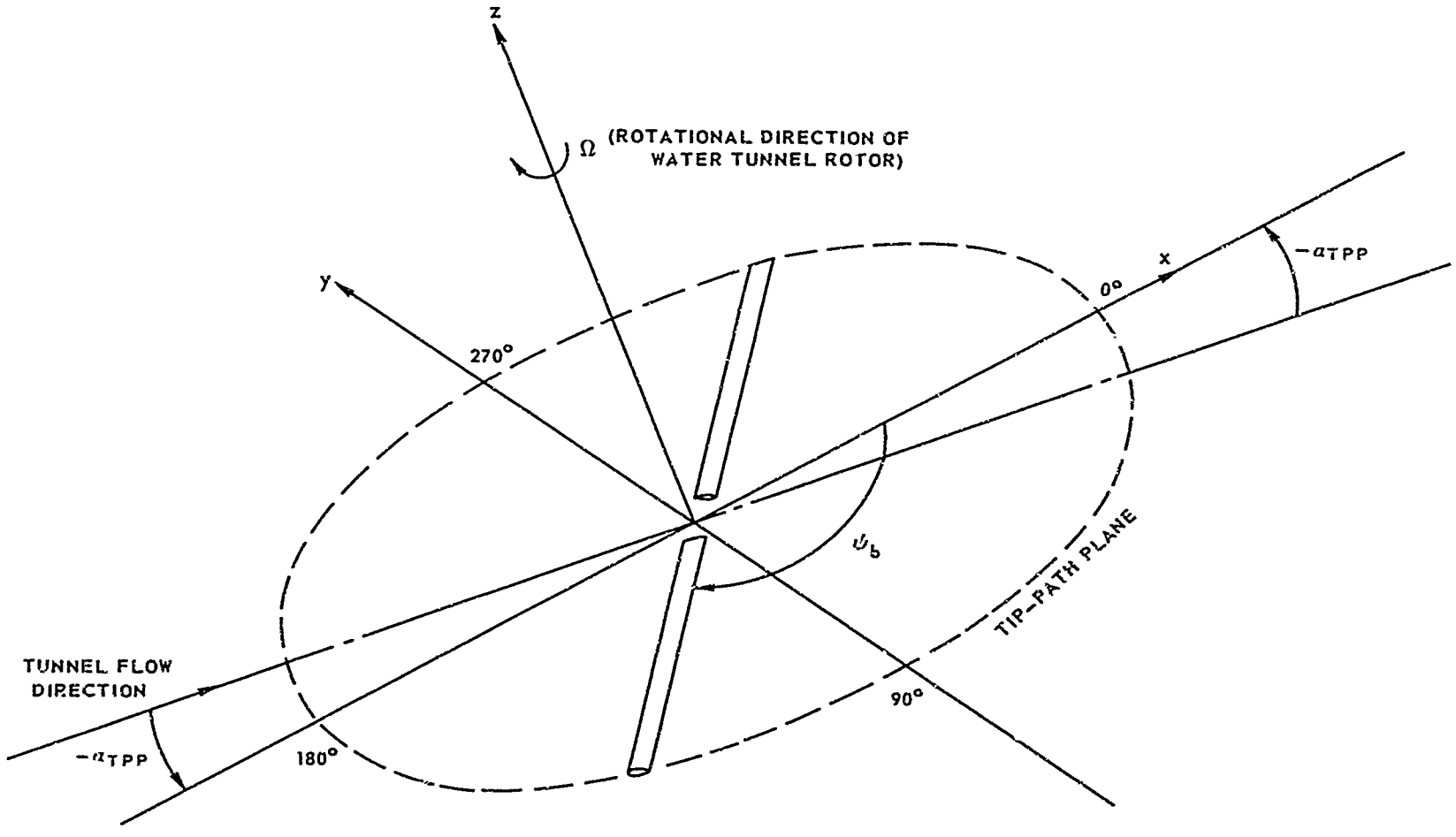

Figure 6. Rotor-Wake Coordinate System.

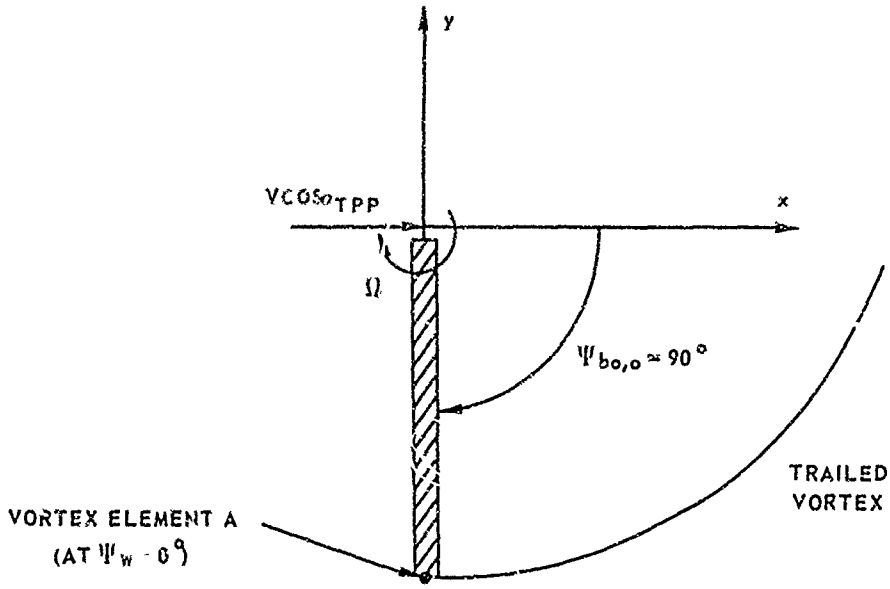

ROTOR-WAKE GEOMETRY AT TIME VORTEX ELEMENT IS SHED

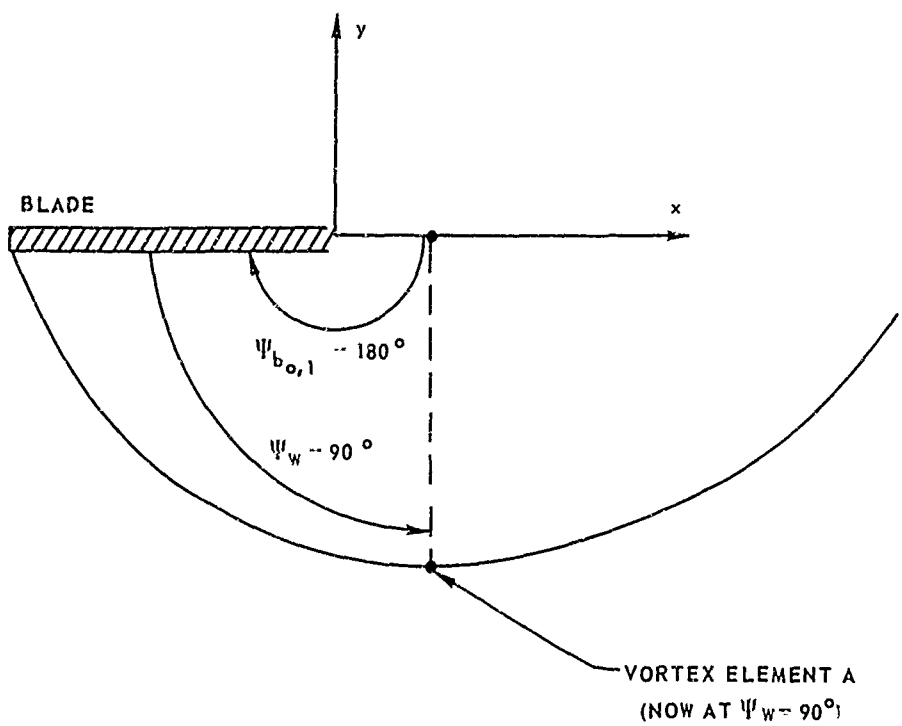

ROTOR-WAKE GEOMETRY AT SOME LATER INSTANCE OF TIME

Figure 7. Blade and Wake Azimuth Coordinate System.

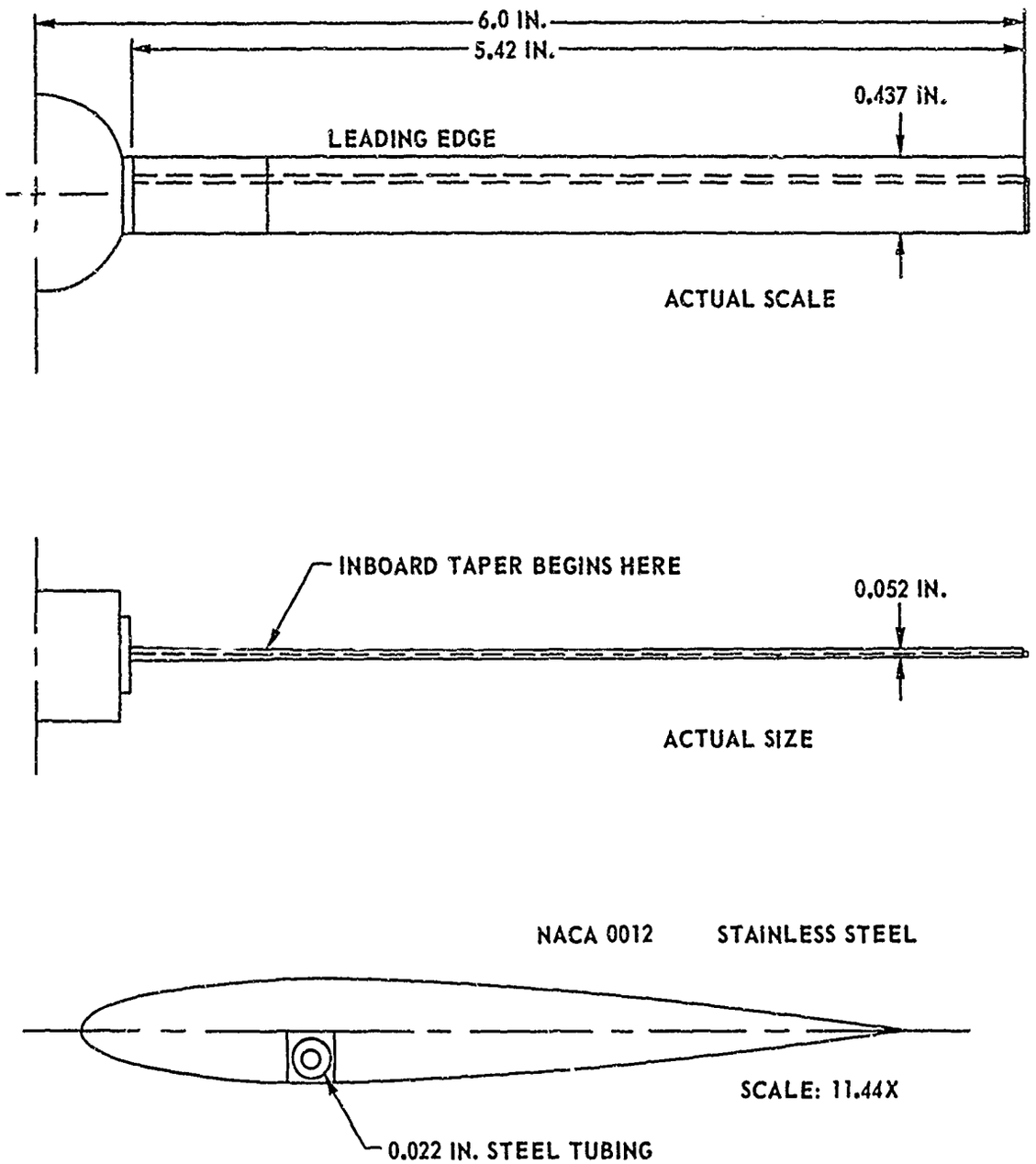

Figure 8. Three-View Drawing of Oceanics Model Rotor Blade.

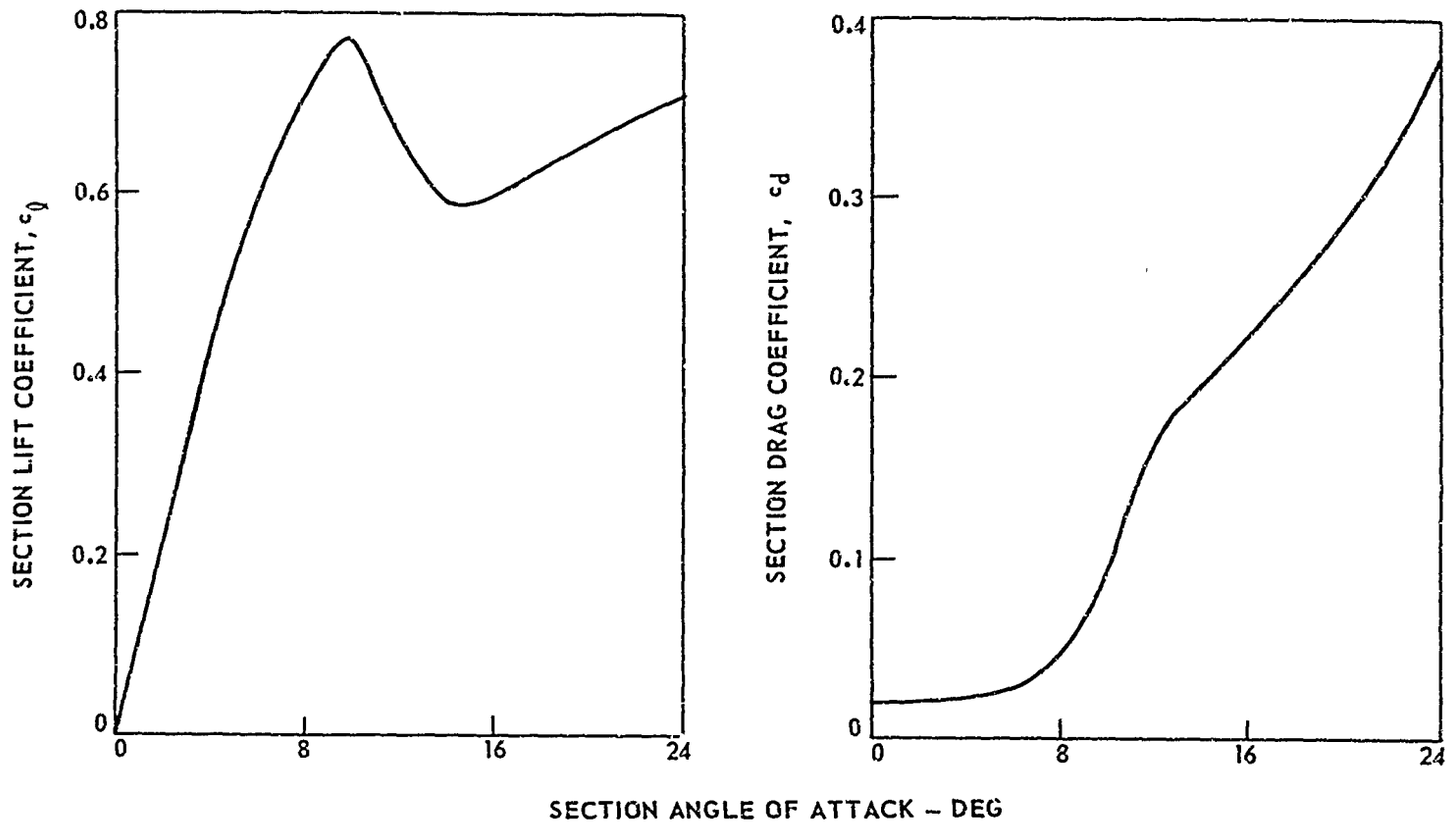

Figure 9. NACA 0012 Airfoil Data Used for Model Blade in UARL Rotor Analysis -- Mach Number = 0.13, Reynolds Number = 110,000.

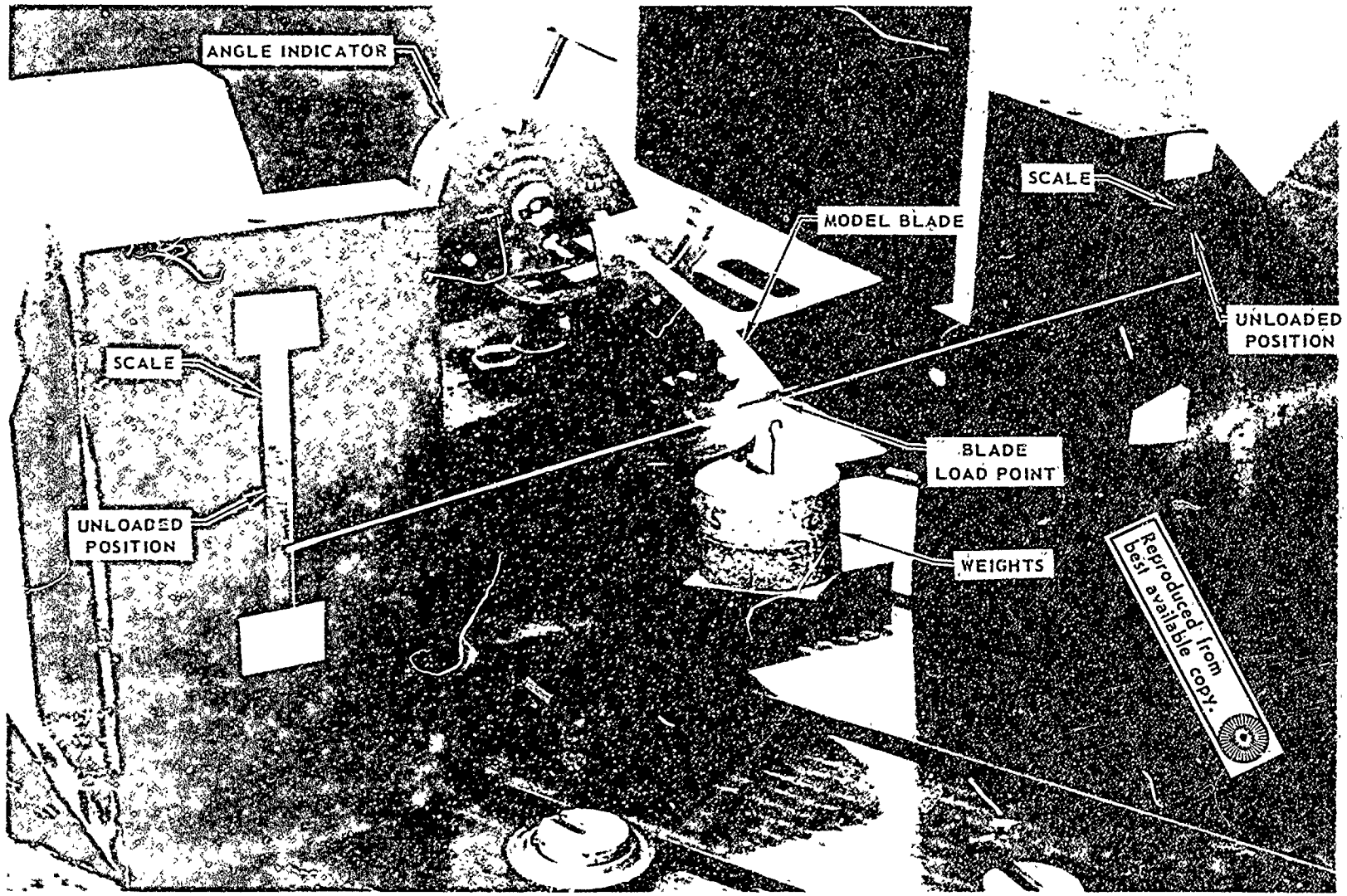

Reproduced from best available copy.

Figure 10. Model Blade Static Calibration Rig.

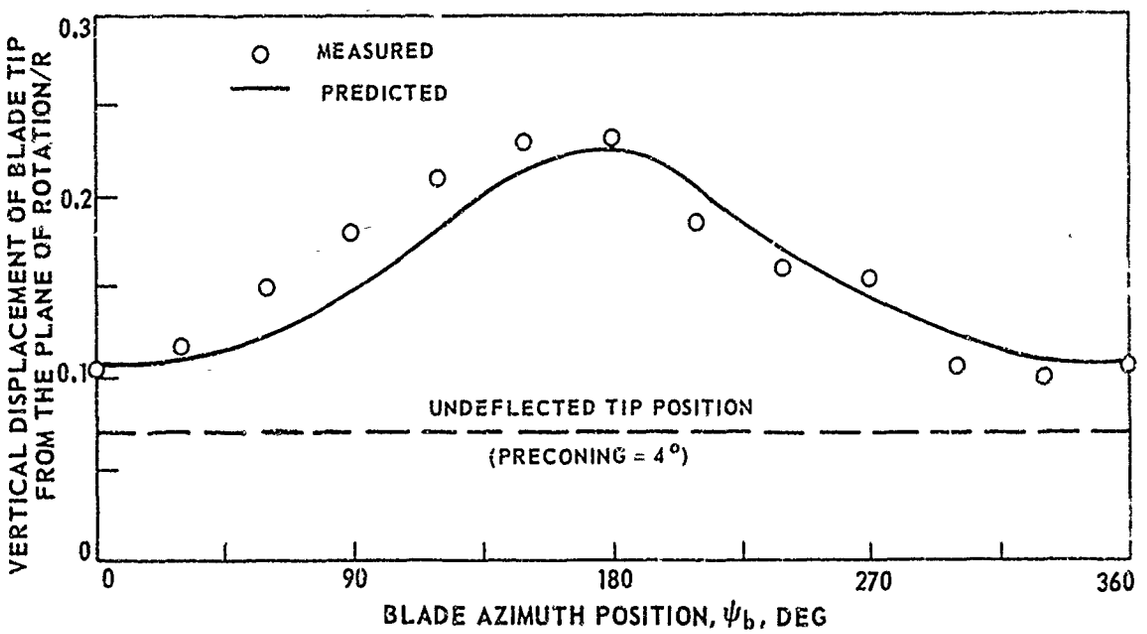

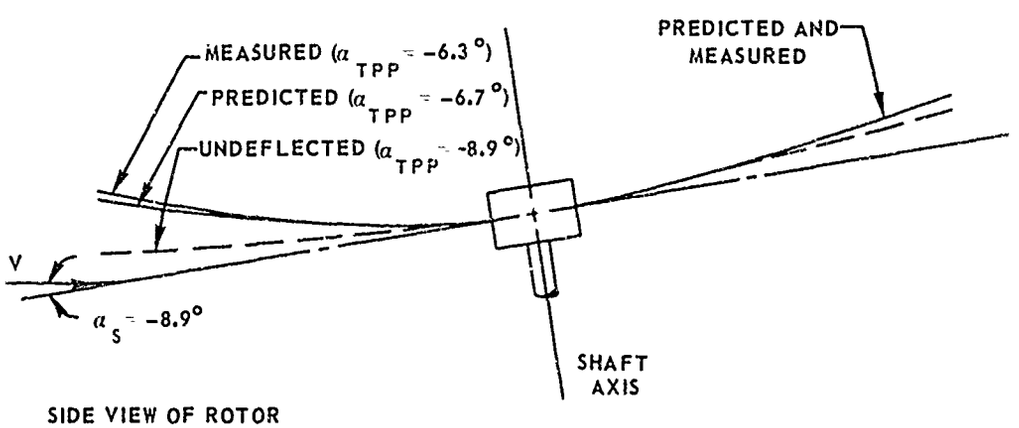

Figure 11. Comparison of Measured and Predicted Bending Deflections of Model Blade in Water -- Simulated 90 Kt, 10,000-Lb Lift.

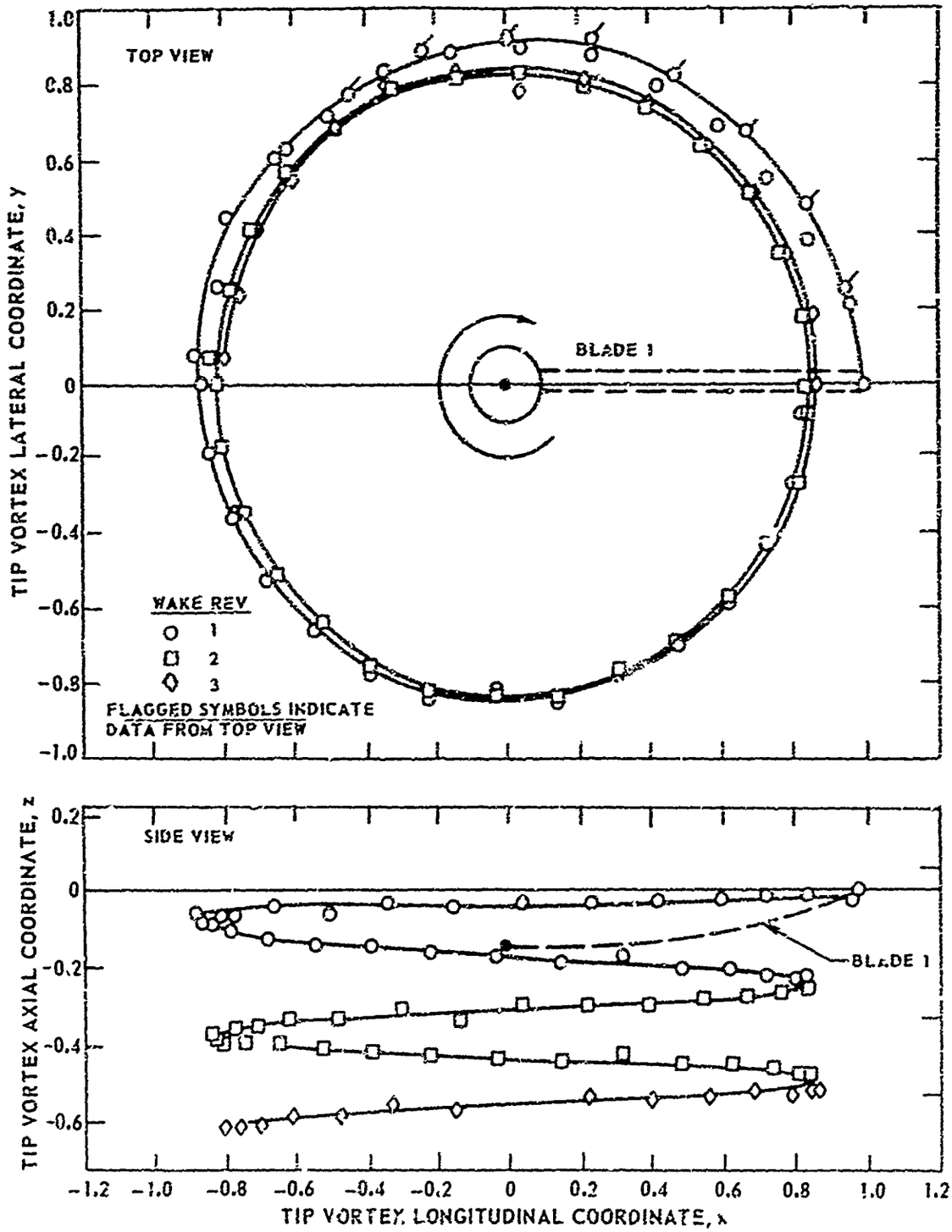

Figure 12. Water Tunnel Tip Vortex Pattern From Blade 1 -- Model Rotor, Hover, Simulated 10,000-Lb Lift, $\psi_{b0,1}$ = 0 deg.

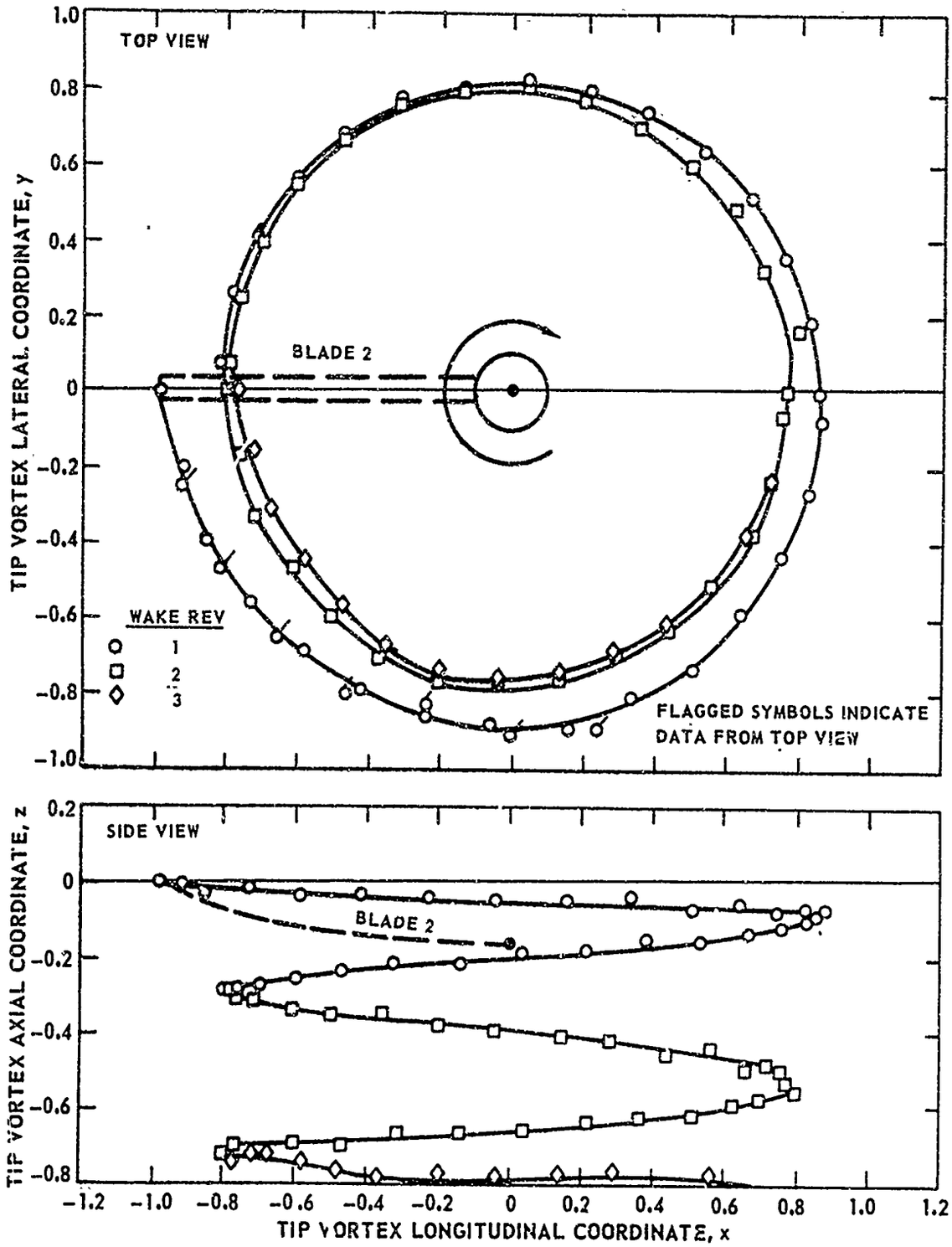

Figure 13. Water Tunnel Tip Vortex Pattern From Blade 2 -- Model Rotor, Hover, Simulated 10,000-Lb Lift, $\psi_{b_{0,1}}$ = 180 deg.

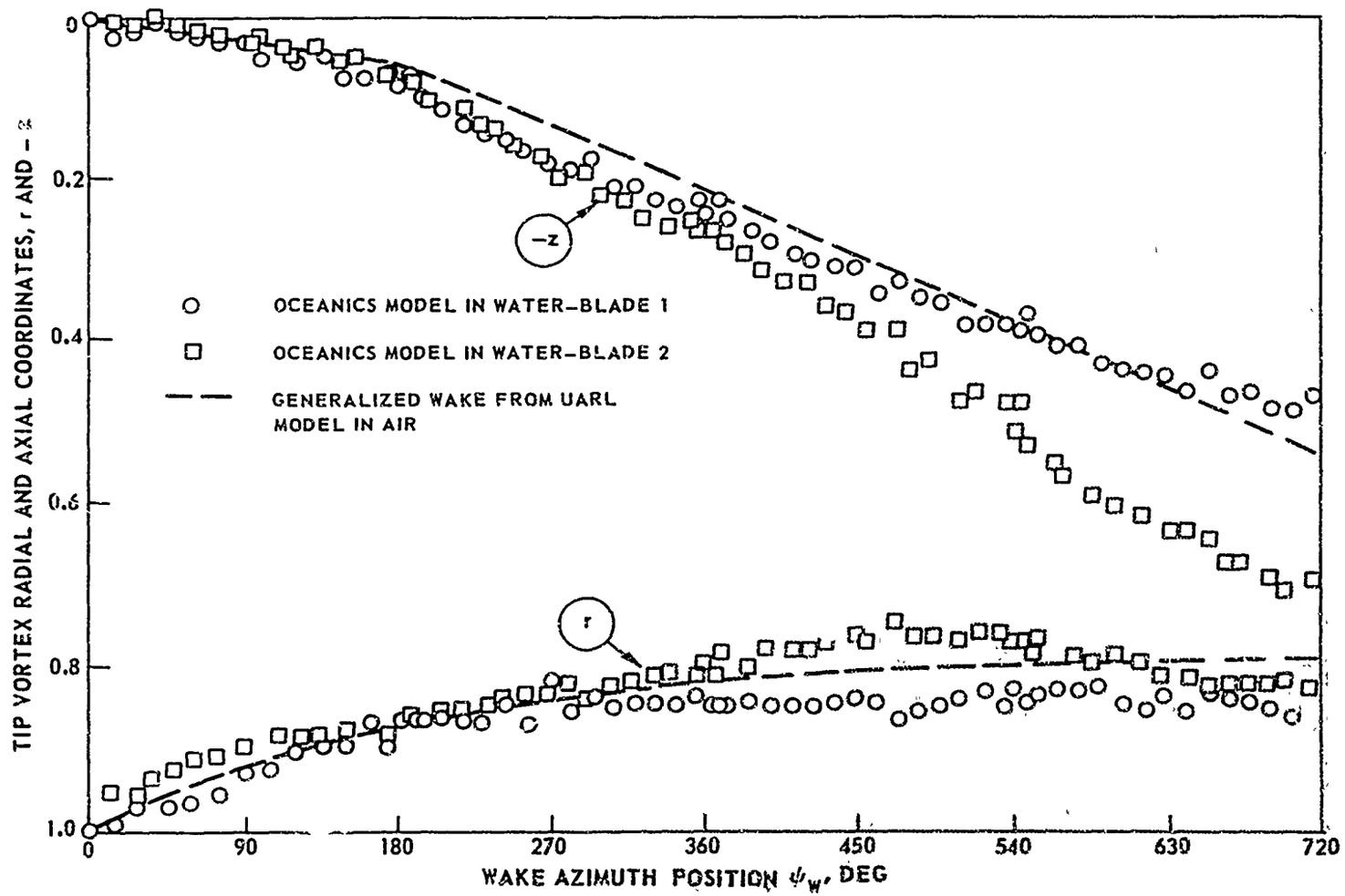

Figure 14. Comparison of Water Tunnel Tip Vortex Coordinates With UARL Test Results -- Hover, Simulated 10,000-Lb Lift.

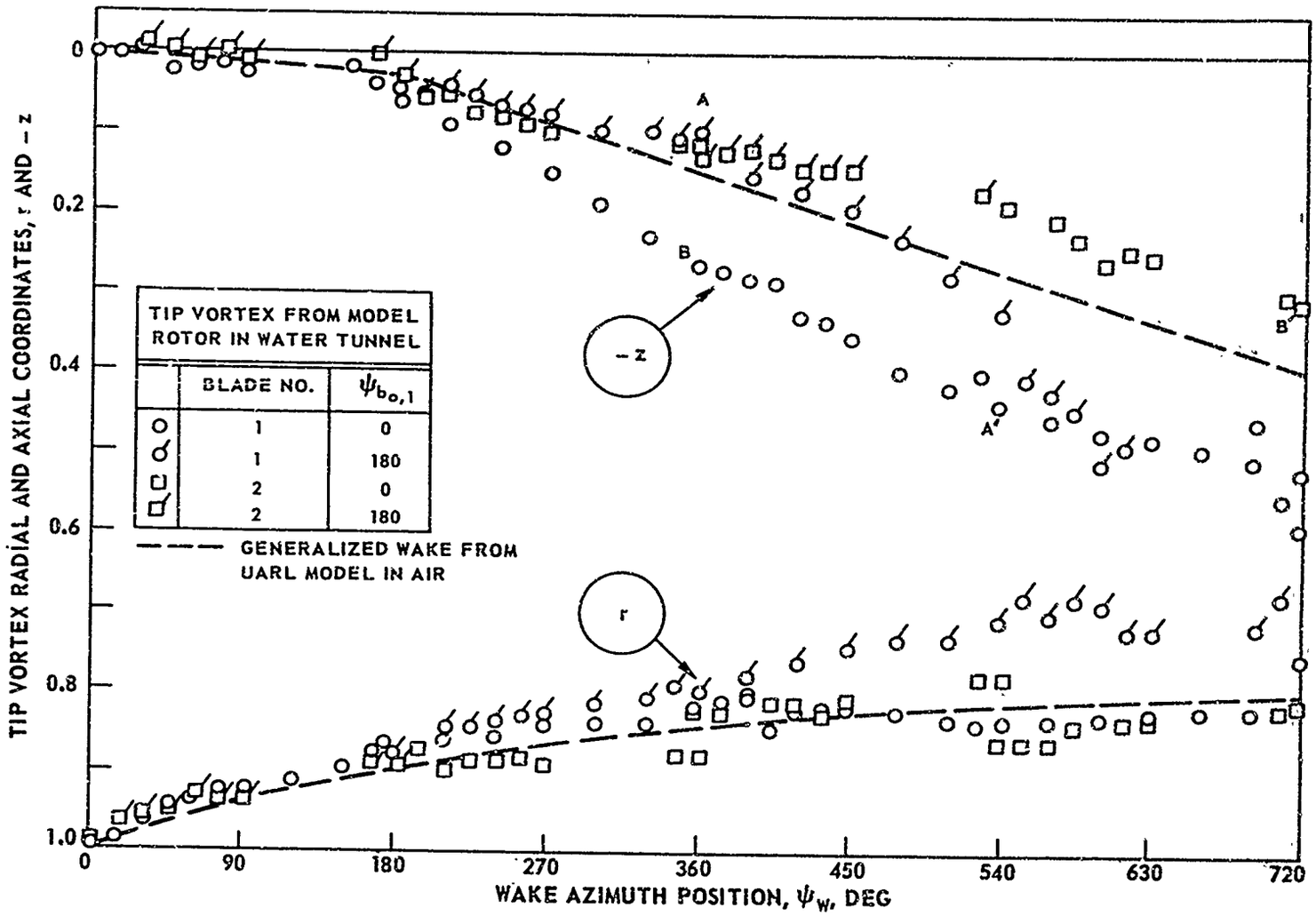

Figure 15. Comparison of Water Tunnel Tip Vortex Coordinates With UARL Test Results -- Hover, Simulated 6,000-Lb Lift.

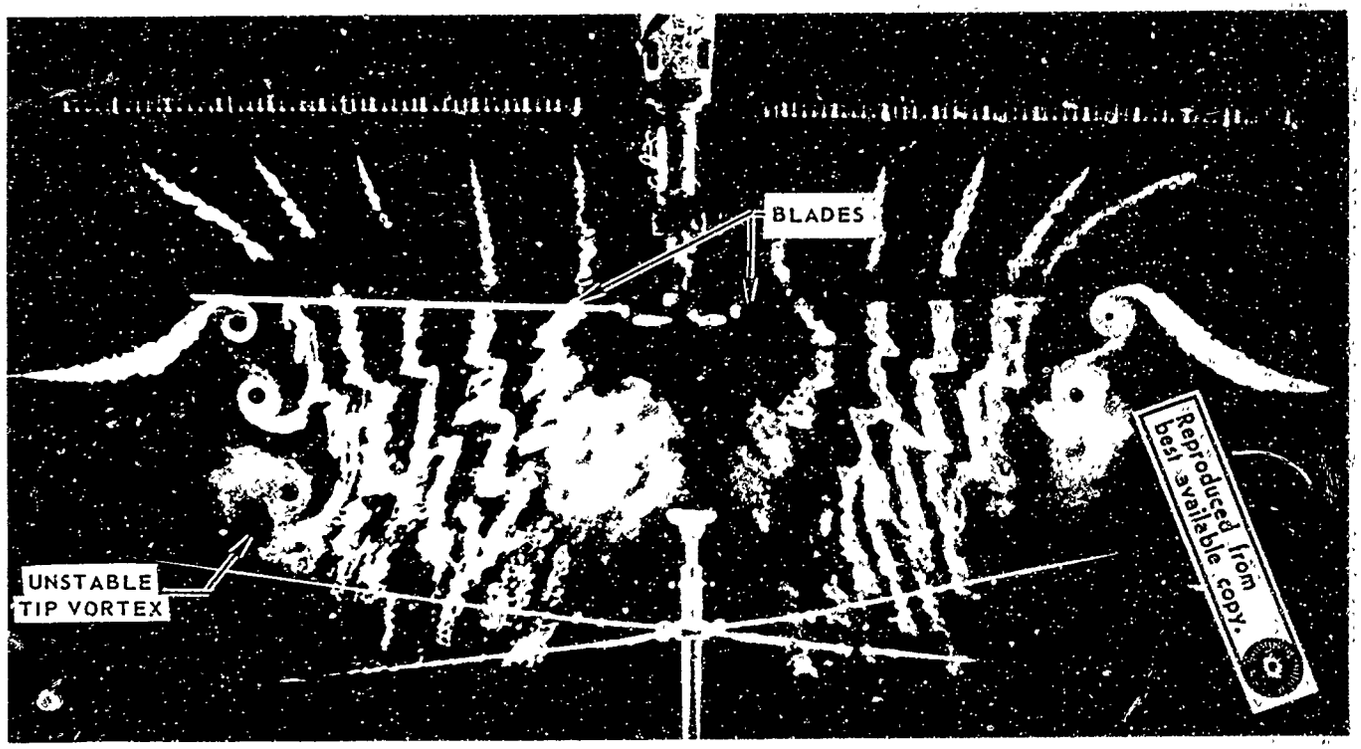

Reproduced from best available copy.

Figure 16. Photograph of Wake Instability of a Hovering Model Rotor in Air.

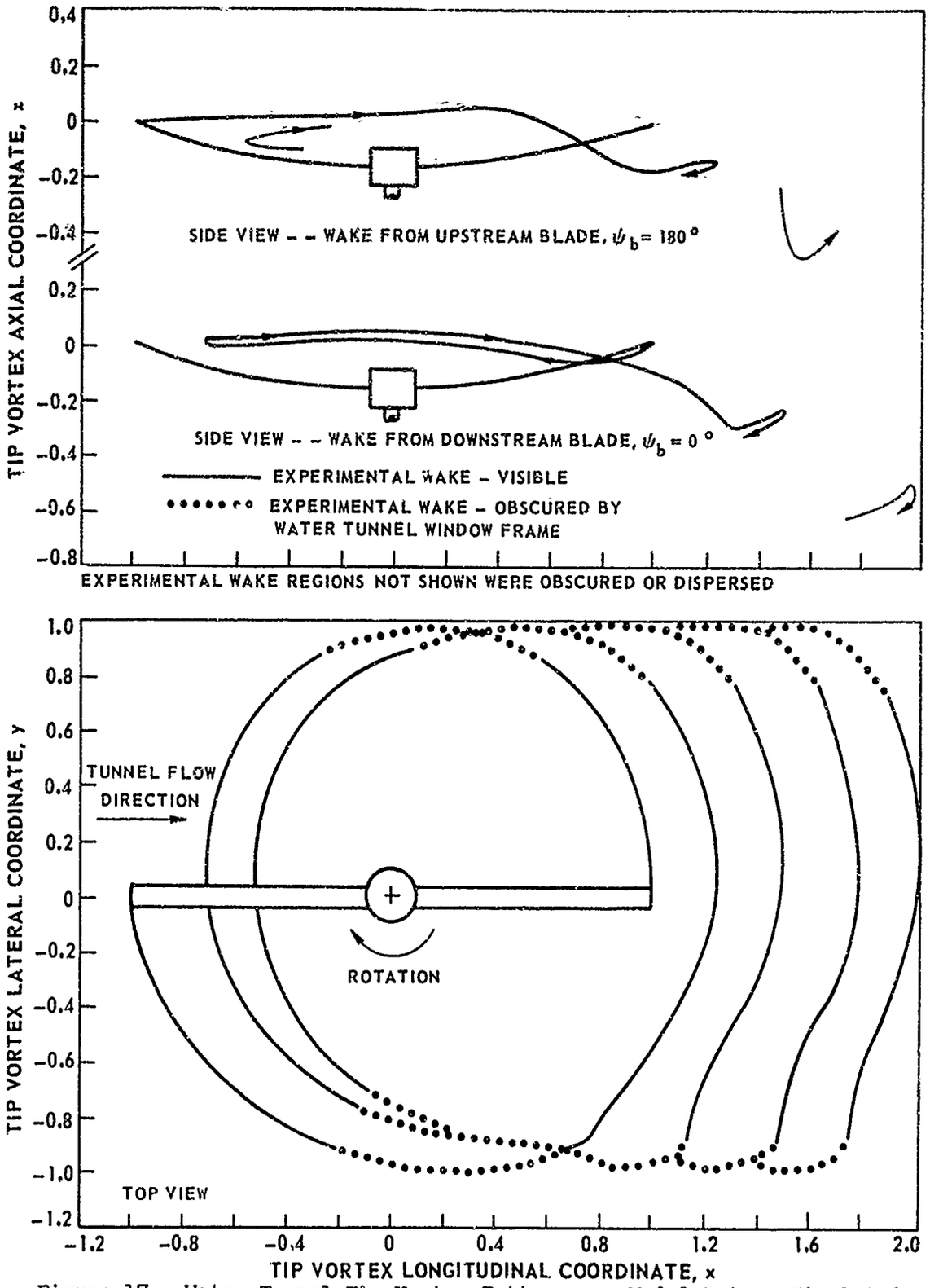

Figure 17. Water Tunnel Tip Vortex Patterns -- Model Rotor, Simulated 35 Kt, 10,000-Lb Lift.

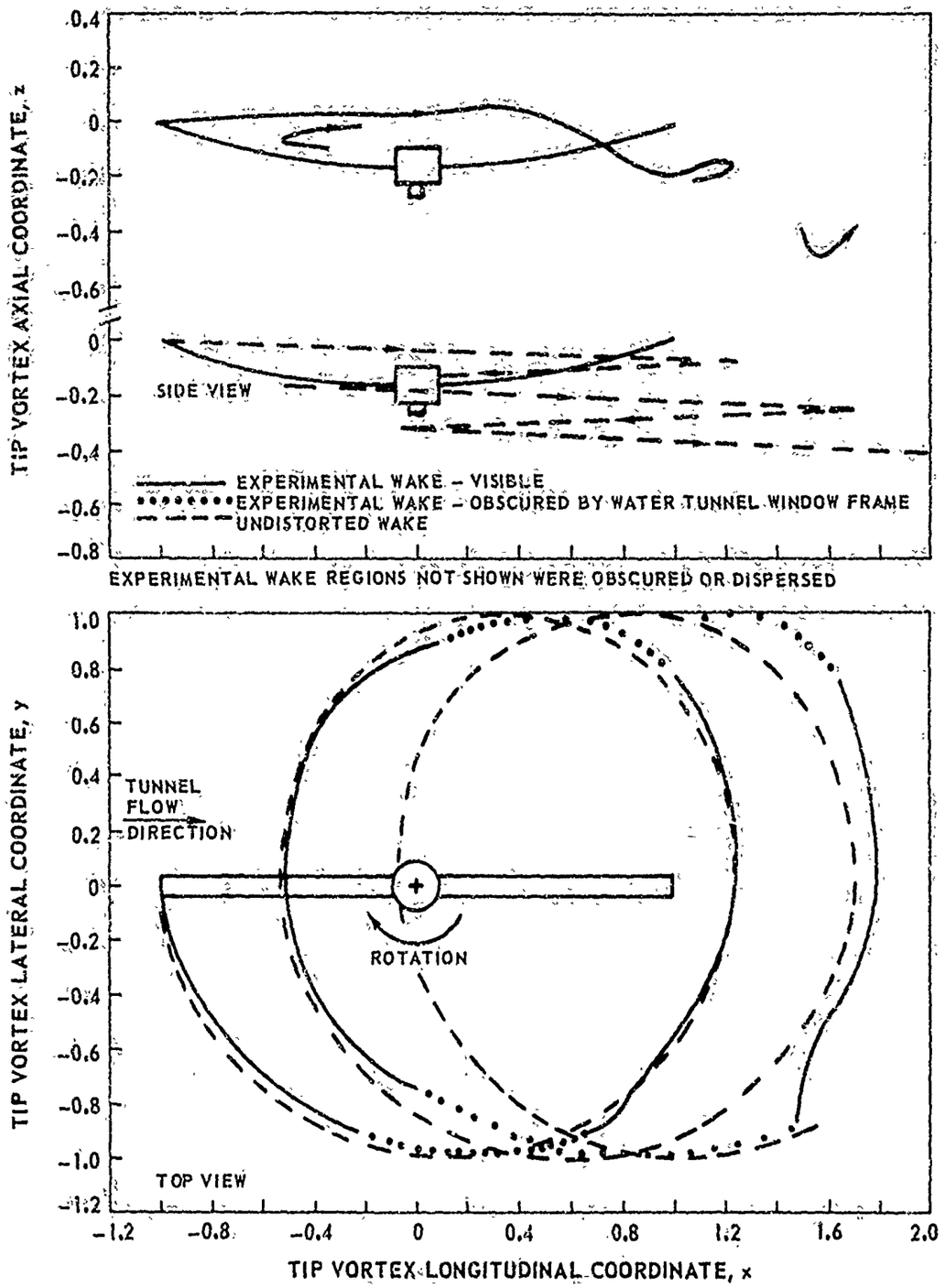

Figure 18. Comparison of Experimental and Undistorted Wake Patterns -- Model Rotor, Simulated 35 Kt, 10,000-Lb Lift.

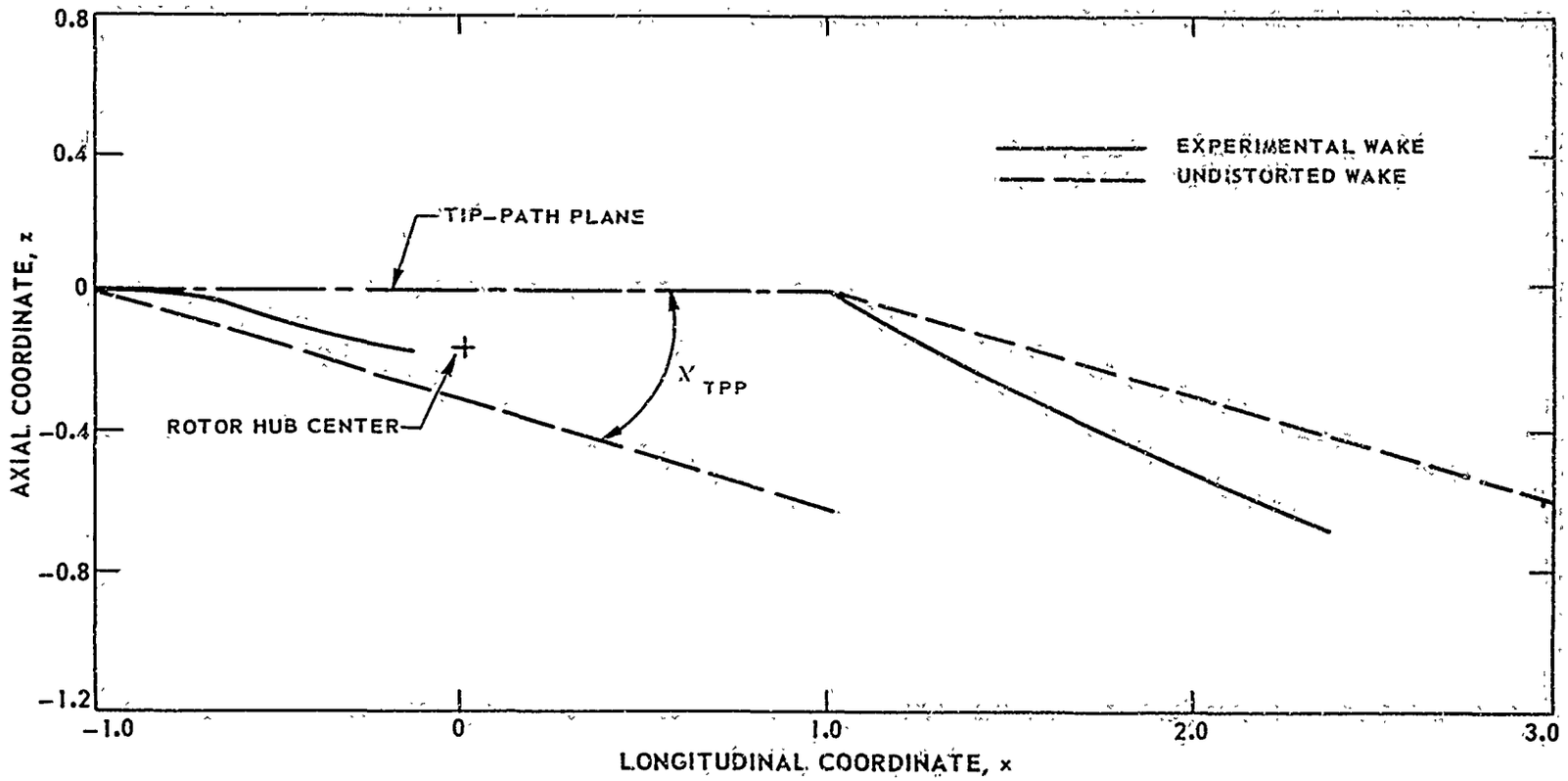

Figure 19. Comparison of Experimental and Undistorted Wake Boundaries -- Model Rotor, Simulated 35 Kt, 10,000-Lb Lift.

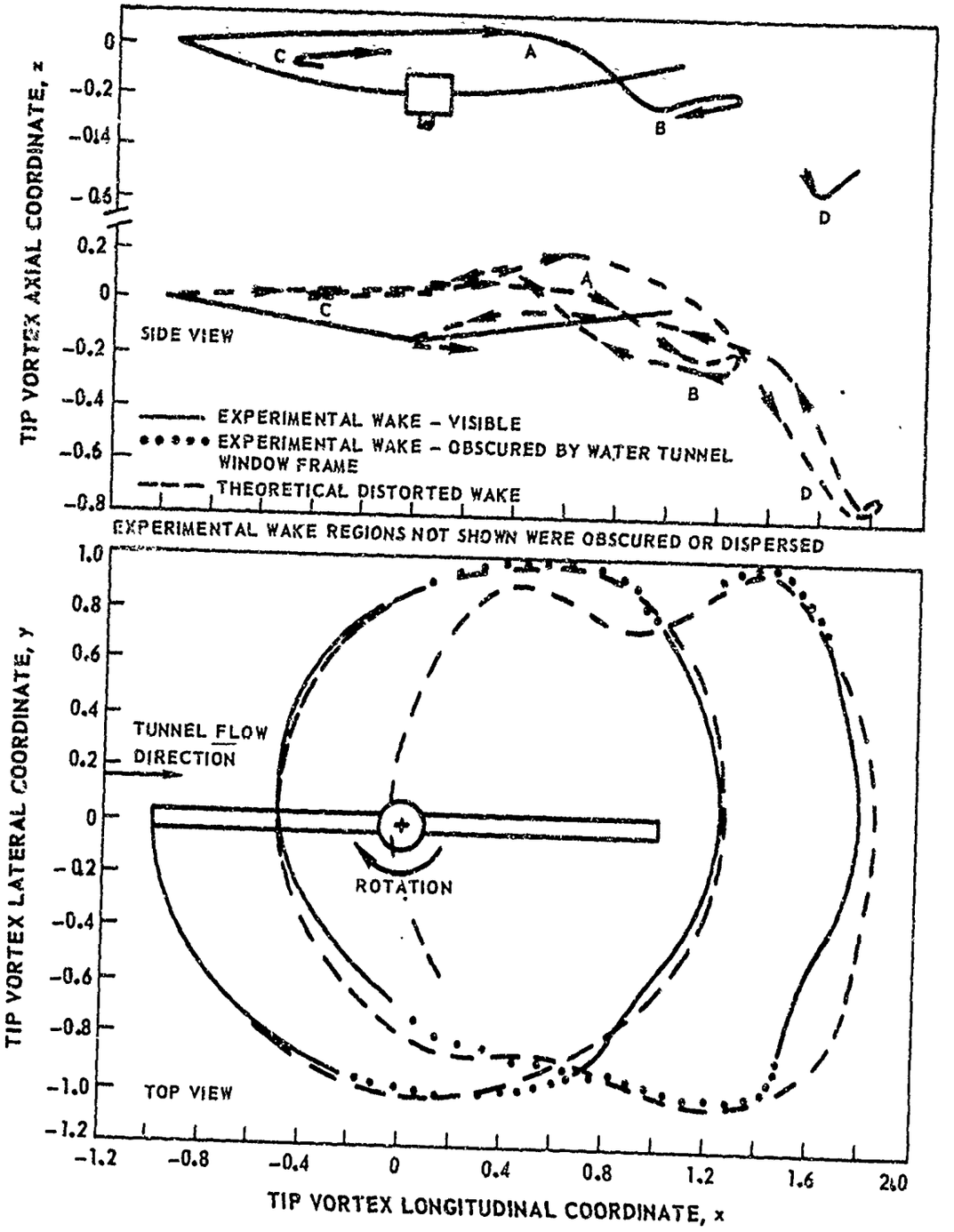

Figure 20. Comparison of Experimental and Theoretical Wake Patterns -- Model Rotor, Simulated 35 Kt, 10,000-Lb Lift.

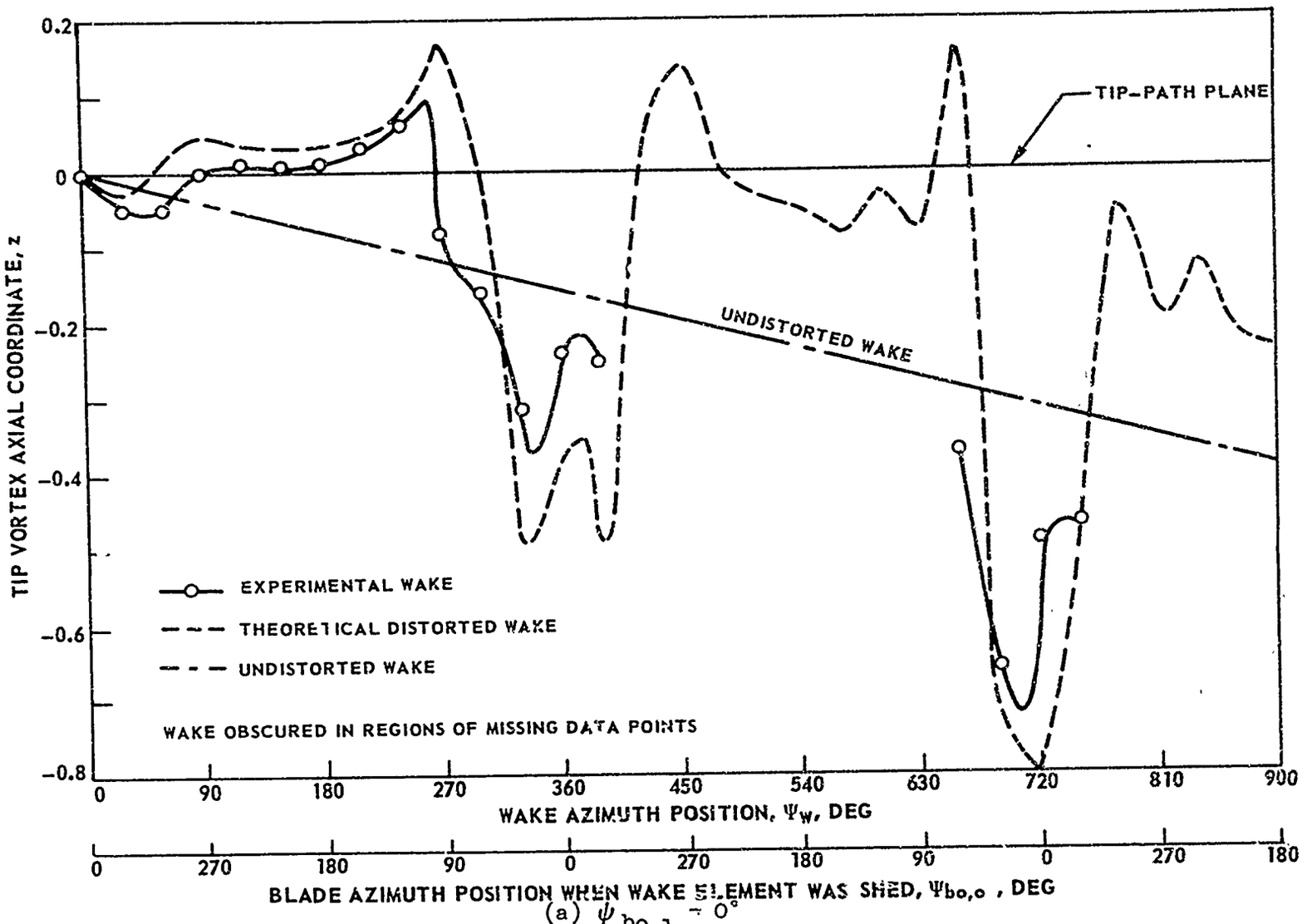

(a) $\psi_{b_{0,1}} = 0°$

Figure 21. Comparison of Experimental and Theoretical Wake Axial Coordinates -- Model Rotor, Simulated 35 Kt, 10,000-Lb Lift.

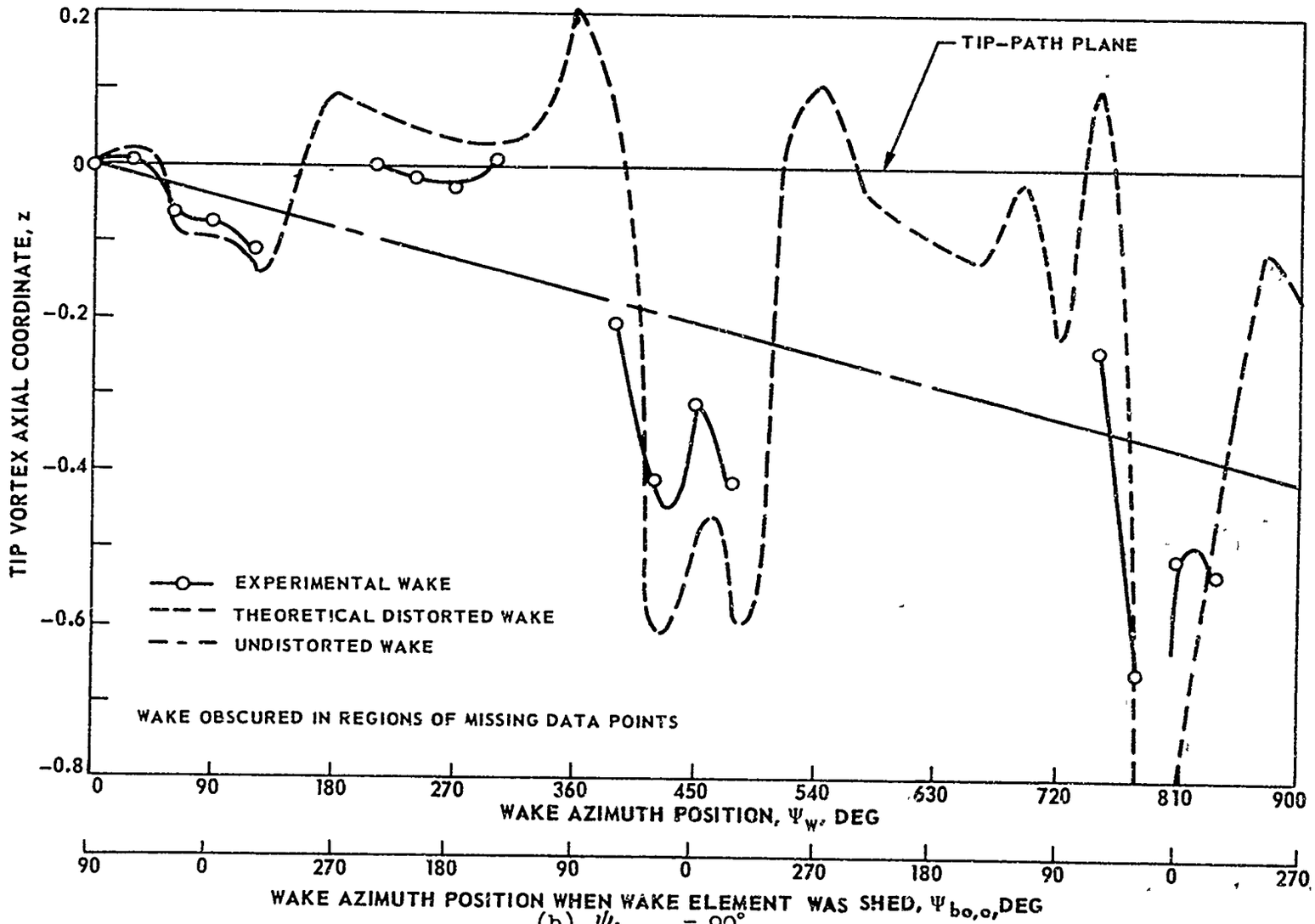

(b) $\psi_{b0,1} = 90°$

Figure 21. Continued.

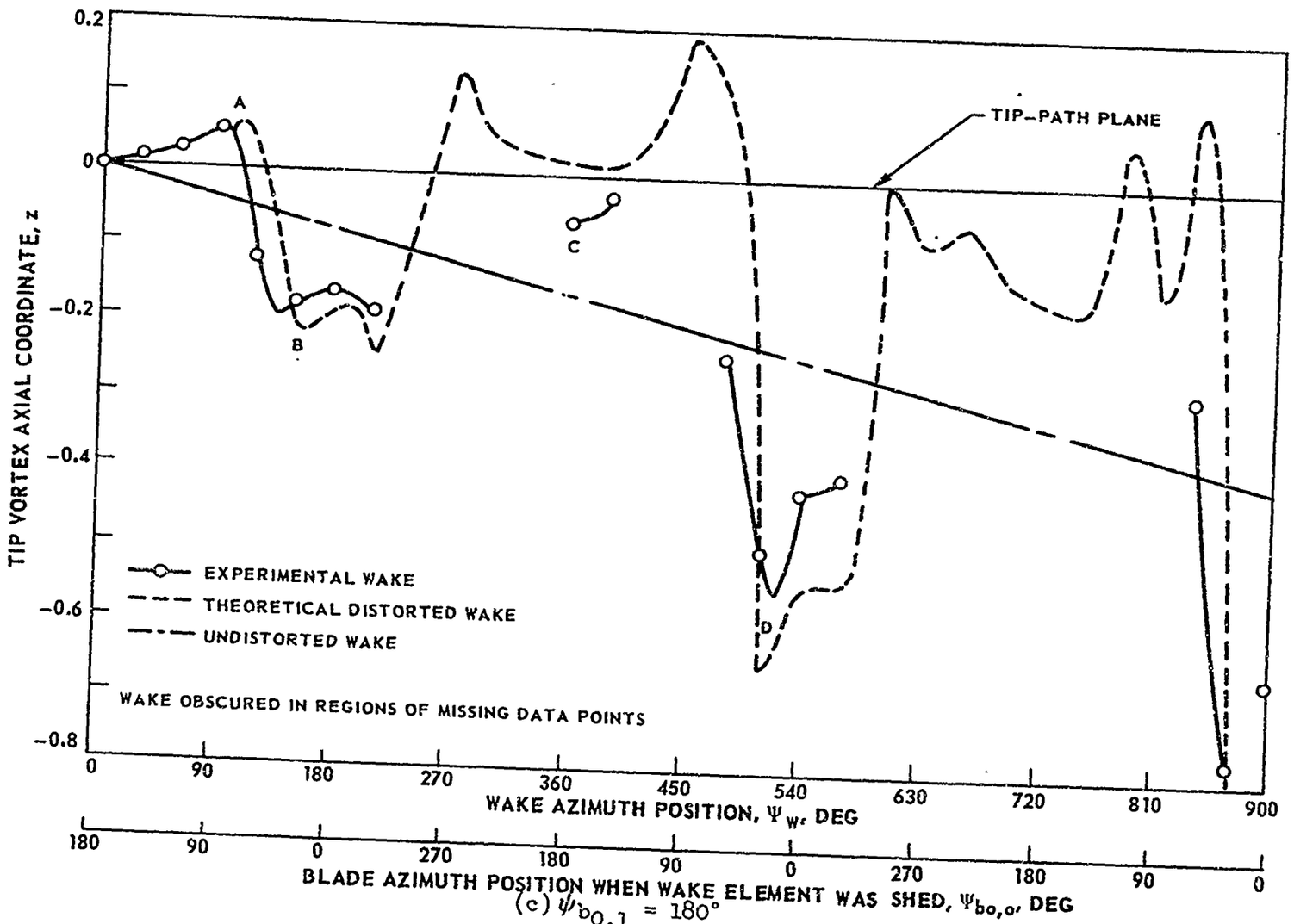

(c) $\psi_{b_{0,1}} = 180°$

Figure 21. Continued.

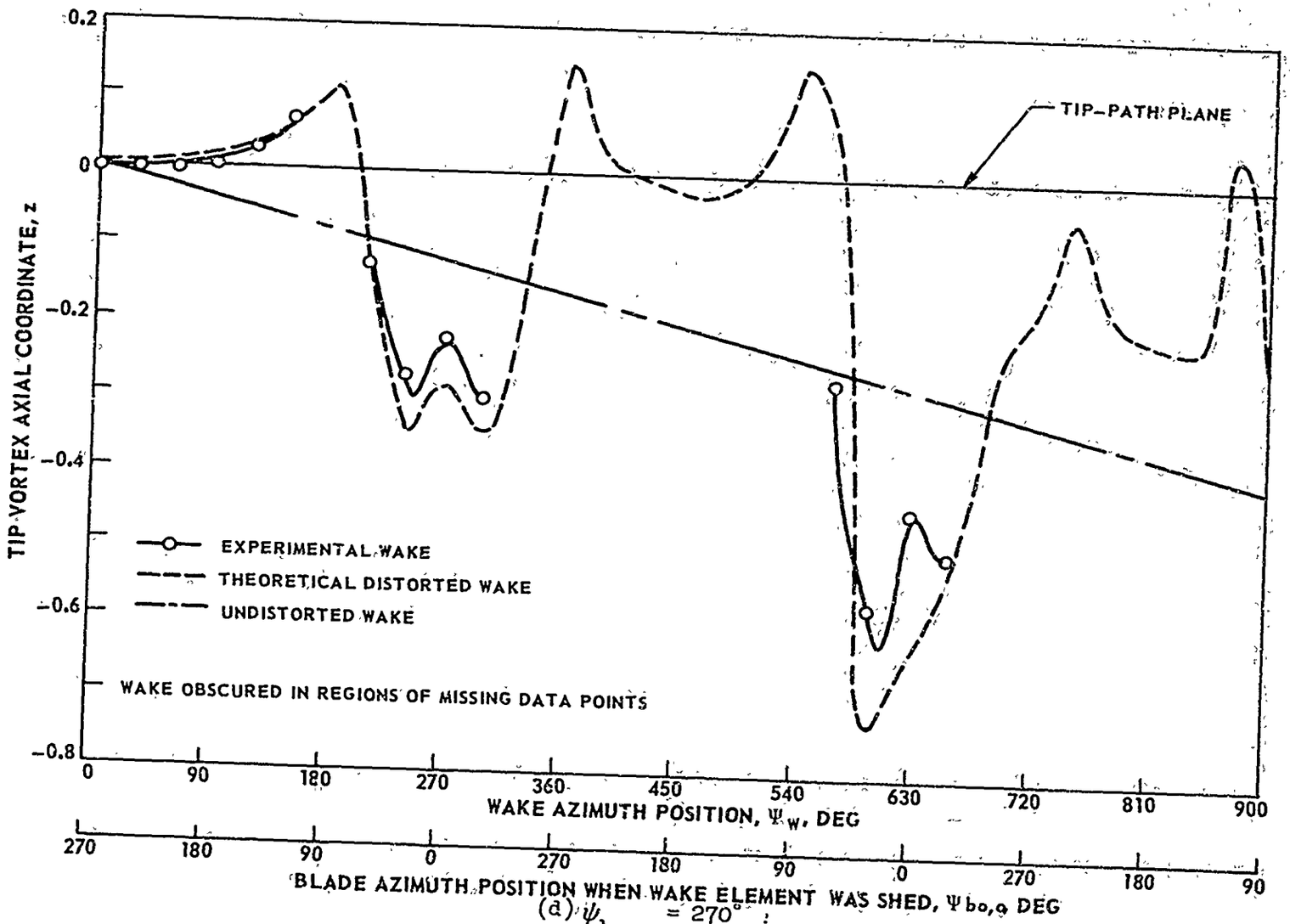

(d) $\psi_{b_{0,1}} = 270°$

Figure 21. Concluded.

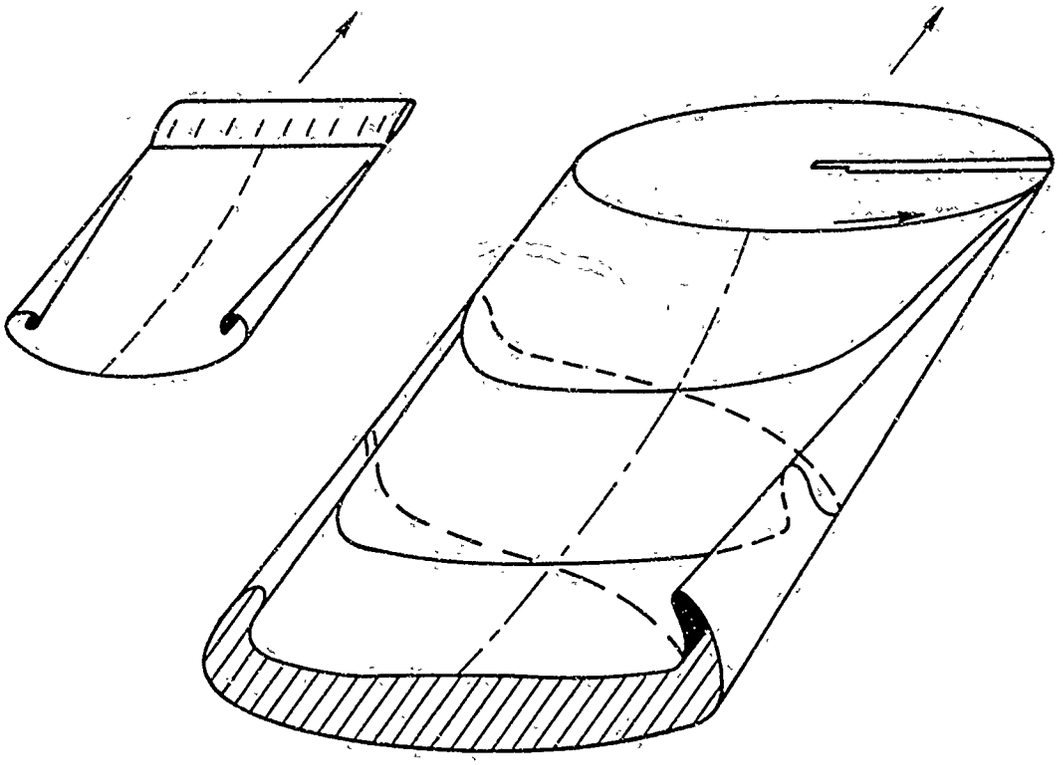

Figure 22. Schematic of Rotor and Fixed-Wing Wakes.

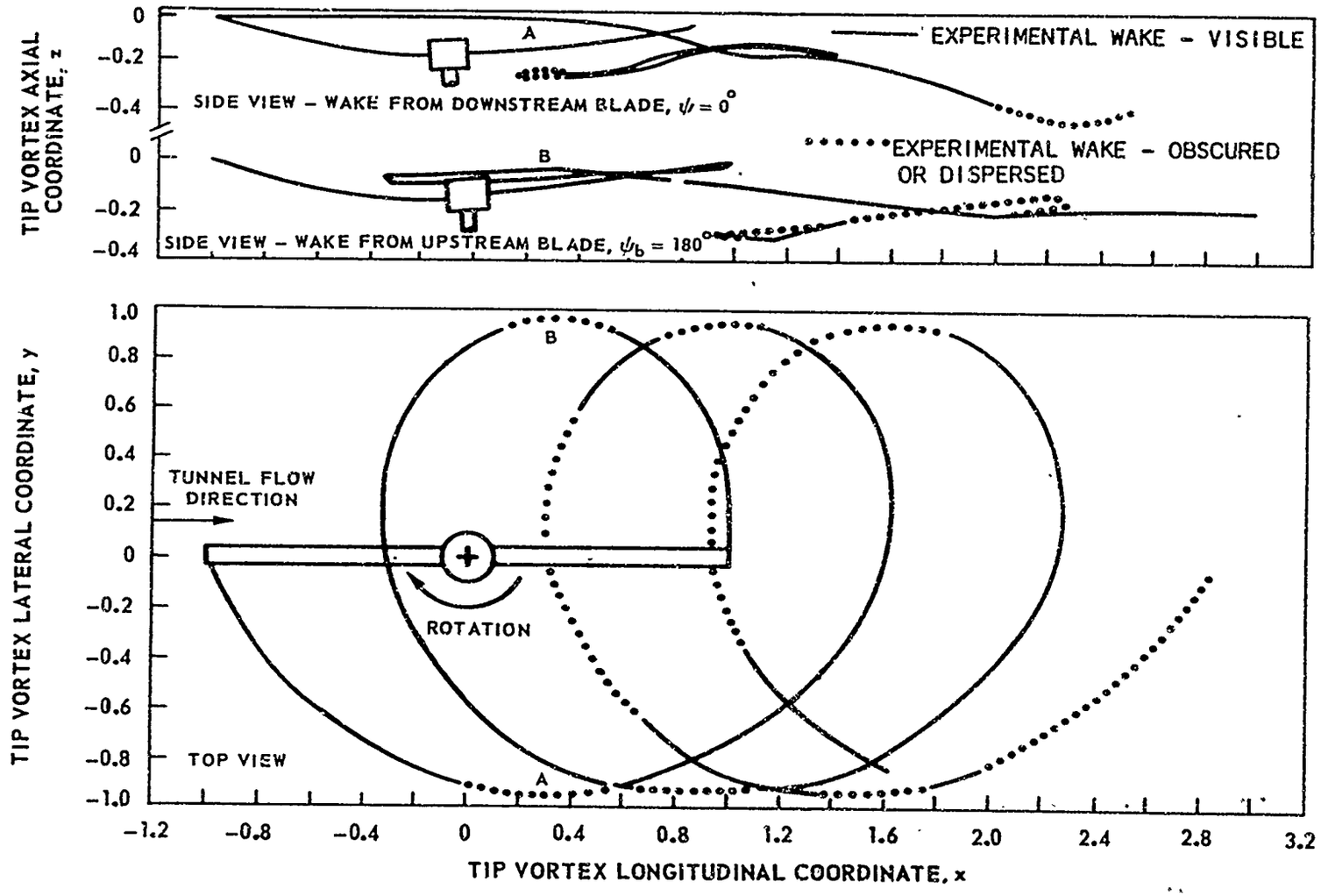

Figure 23. Water Tunnel Tip Vortex Patterns -- Model Rotor, Simulated 90 Kt, 10,000-Lb Lift.

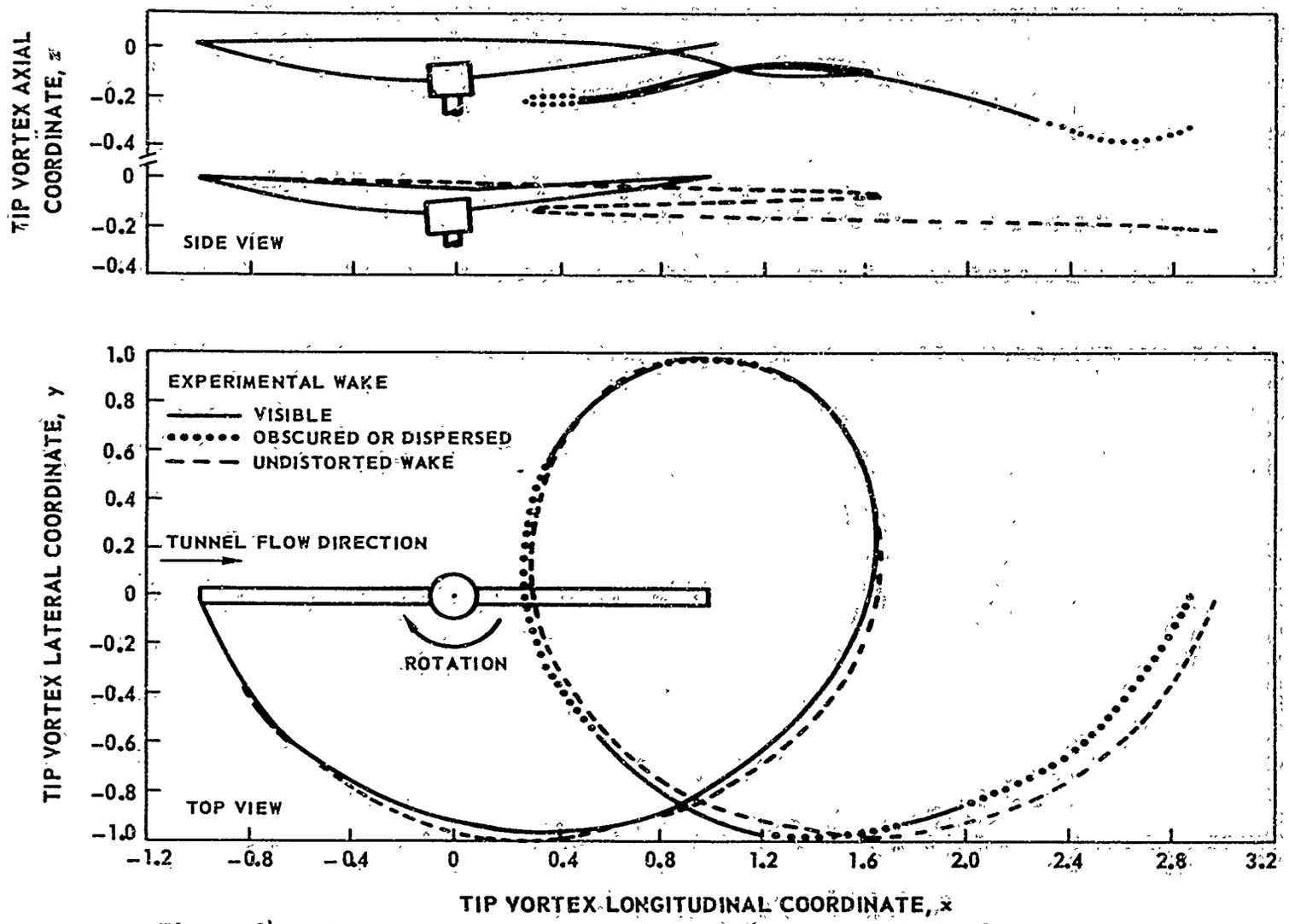

Figure 24. Comparison of Experimental and Undistorted Wake Patterns -- Model Rotor, Simulated 90 Kt, 10,000-Lb Lift.

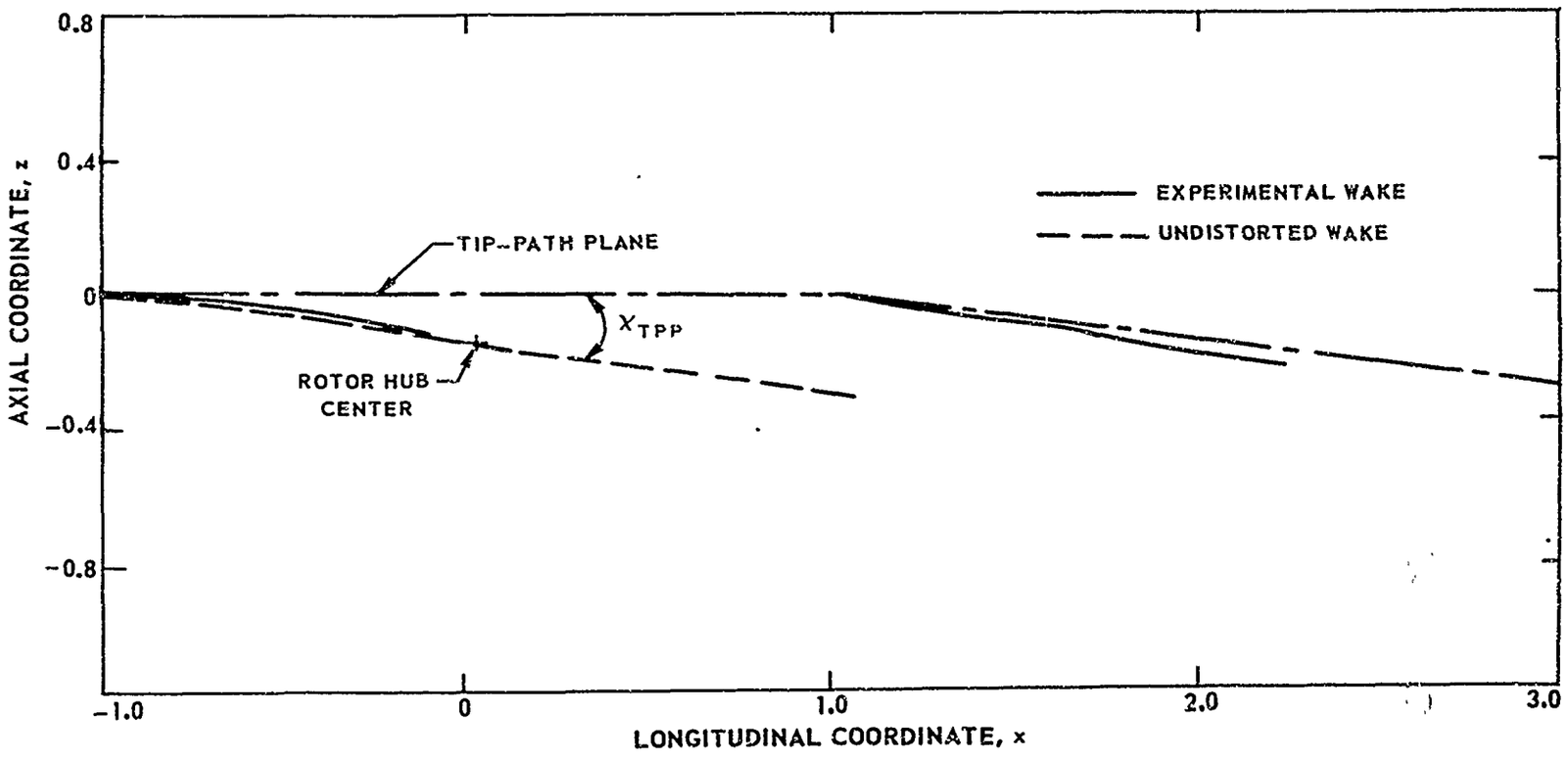

Figure 25. Comparison of Experimental and Undistorted Wake Boundaries -- Model Rotor, Simulated 90 Kt, 10,000-Lb Lift.

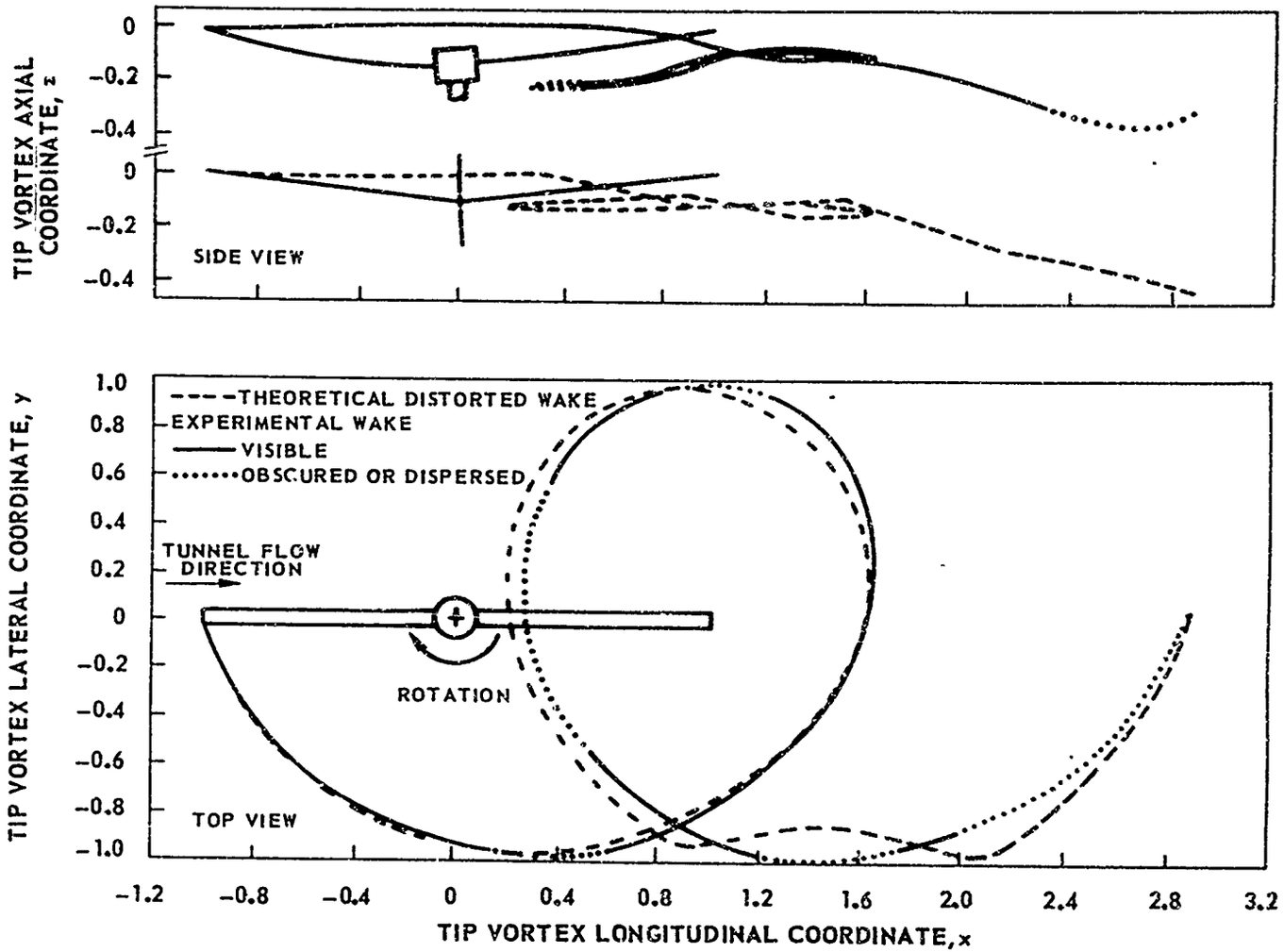

Figure 26. Comparison of Experimental and Theoretical Wake Patterns -- Model Rotor, Simulated 90 Kt, 10,000-Lb Lift.

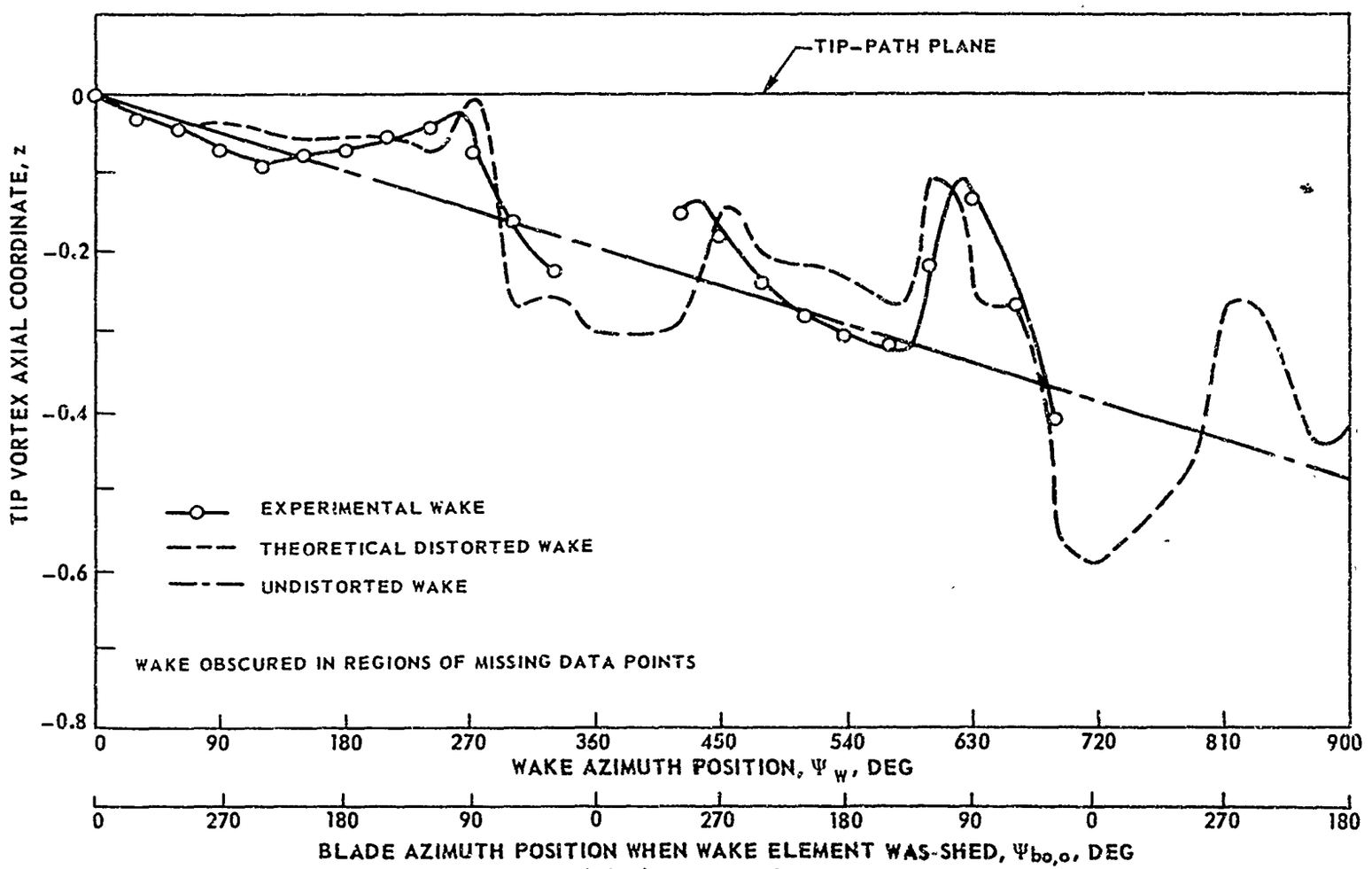

(a) $\psi_{b_{0,1}} = 0°$

Figure 27. Comparison of Experimental and Theoretical Wake Axial Coordinates -- Model Rotor, Simulated 90 Kt, 10,000-Lb Lift.

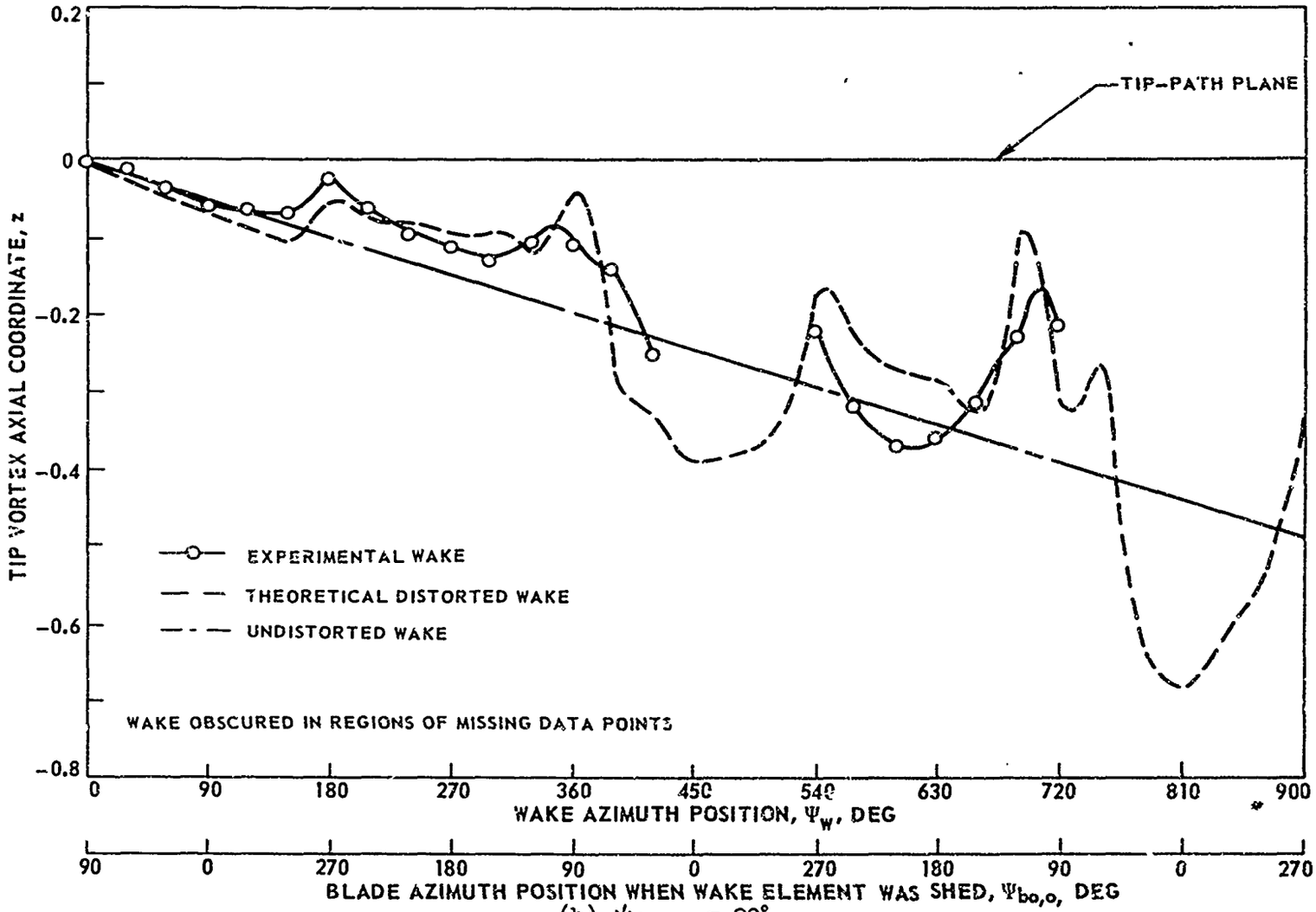

(b) $\psi_{bo,1} = 90°$

Figure 27. Continued.

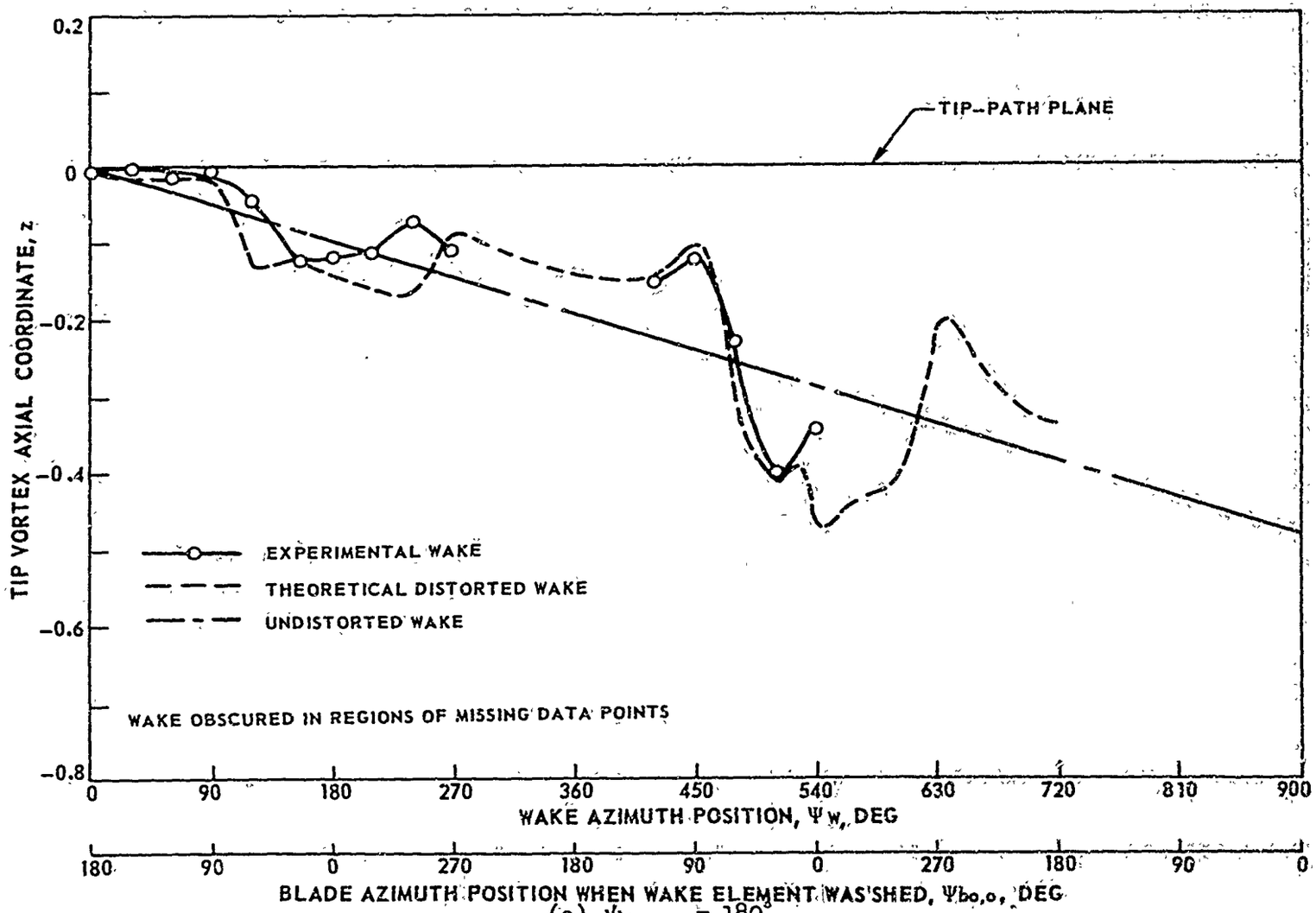

(c) $\psi_{b_{0,1}} = 180°$

Figure 27. Continued.

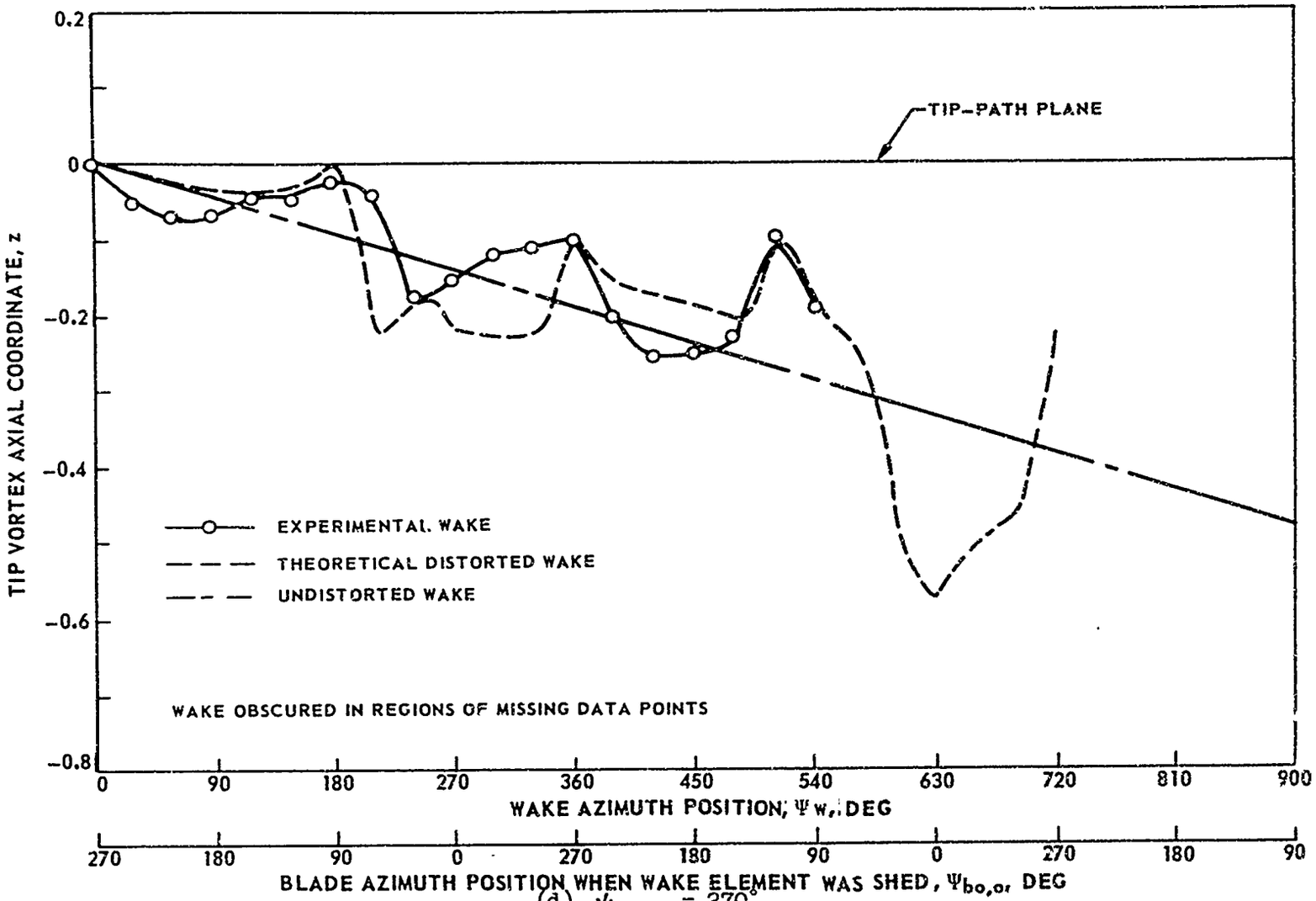

(d) $\psi_{b_{0,1}} = 270°$

Figure 27. Concluded.

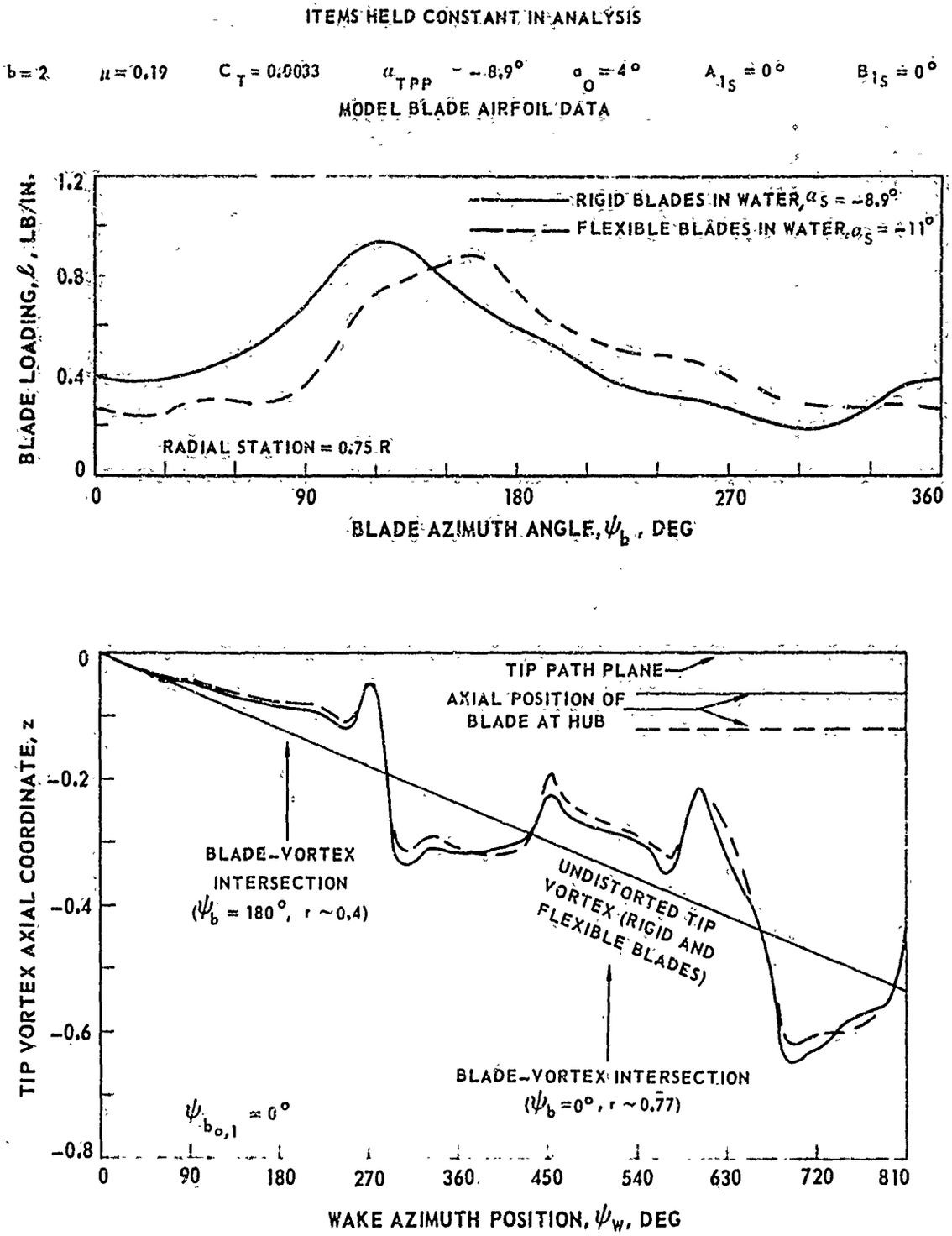

Figure 28. Effect of Blade Flexibility on Model Rotor Loading and Wake Geometry for Constant Rotor Tip-Path Plane Angle.

ITEMS HELD CONSTANT IN ANALYSIS

$b = 2$ $\mu = 0.19$ $C_T = 0.0033$ $\alpha_{TPP} = -8.9°$ $A_{1_S} = 0°$ $B_{1_S} = 0°$ RIGID BLADES MODEL AIRFOIL DATA

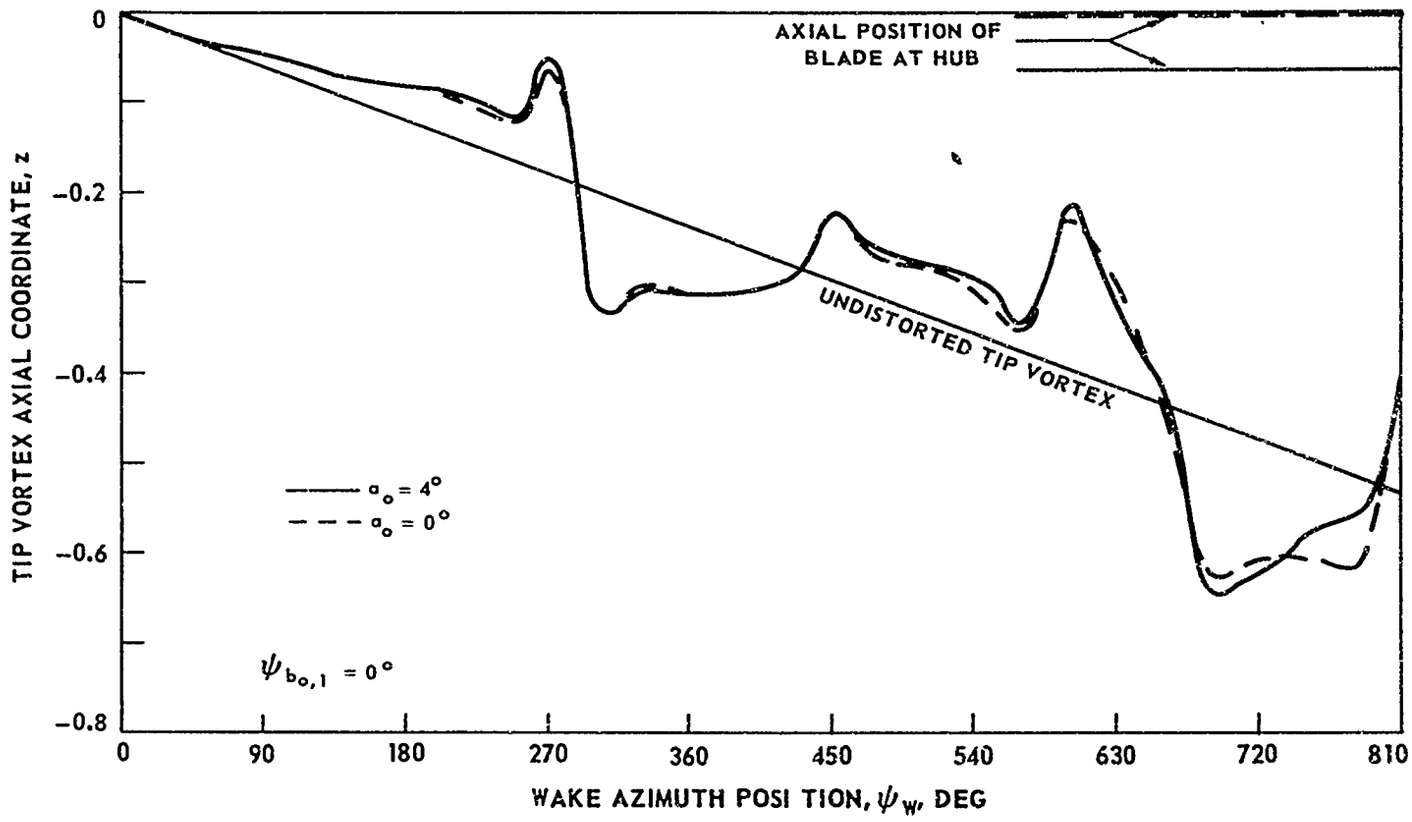

Figure 29. Effect of Blade Coning on Model Rotor Wake Geometry.

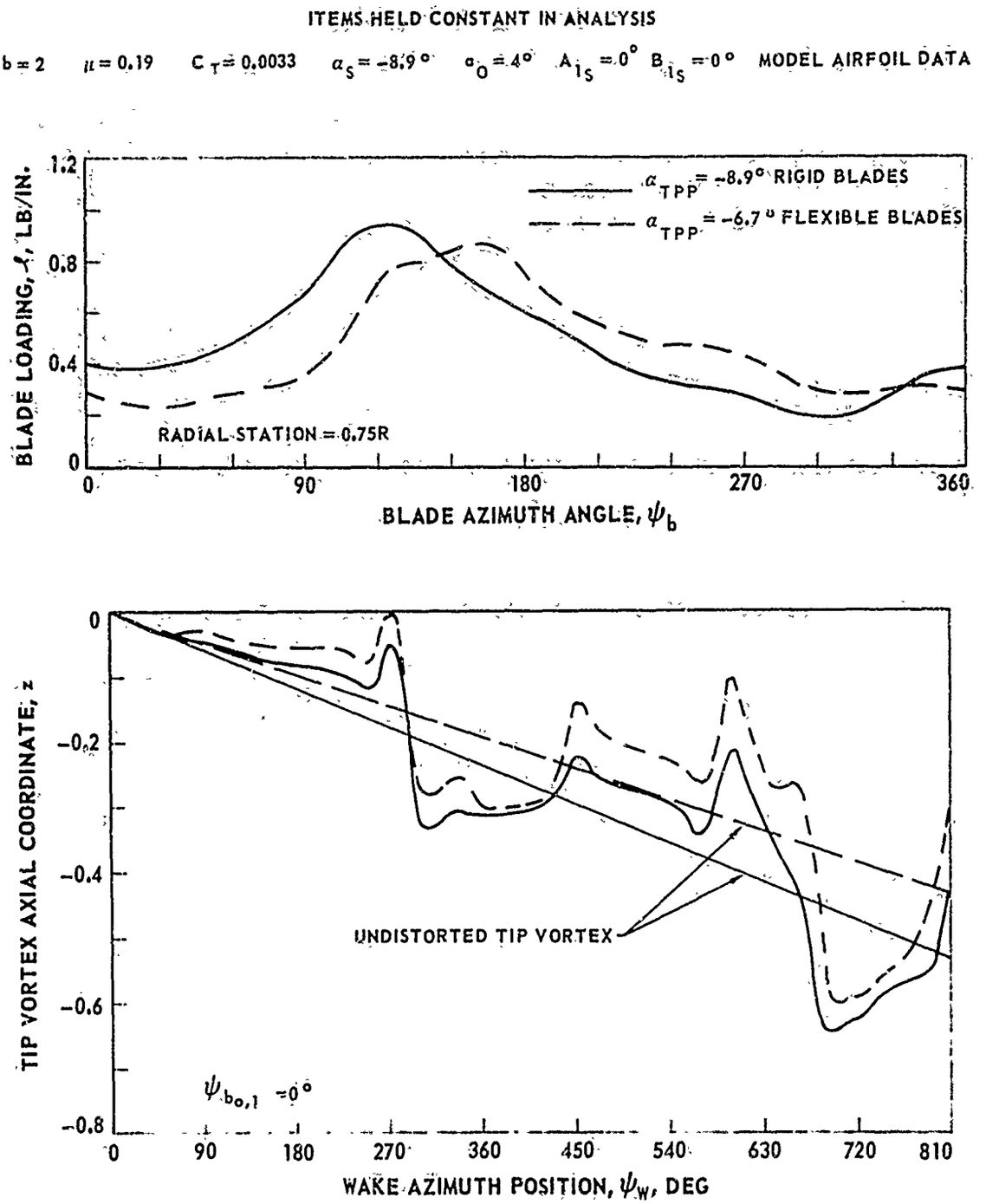

Figure 30. Effect of Rotor Tip-Path Plane Angle on Model Rotor Loading and Wake Geometry.

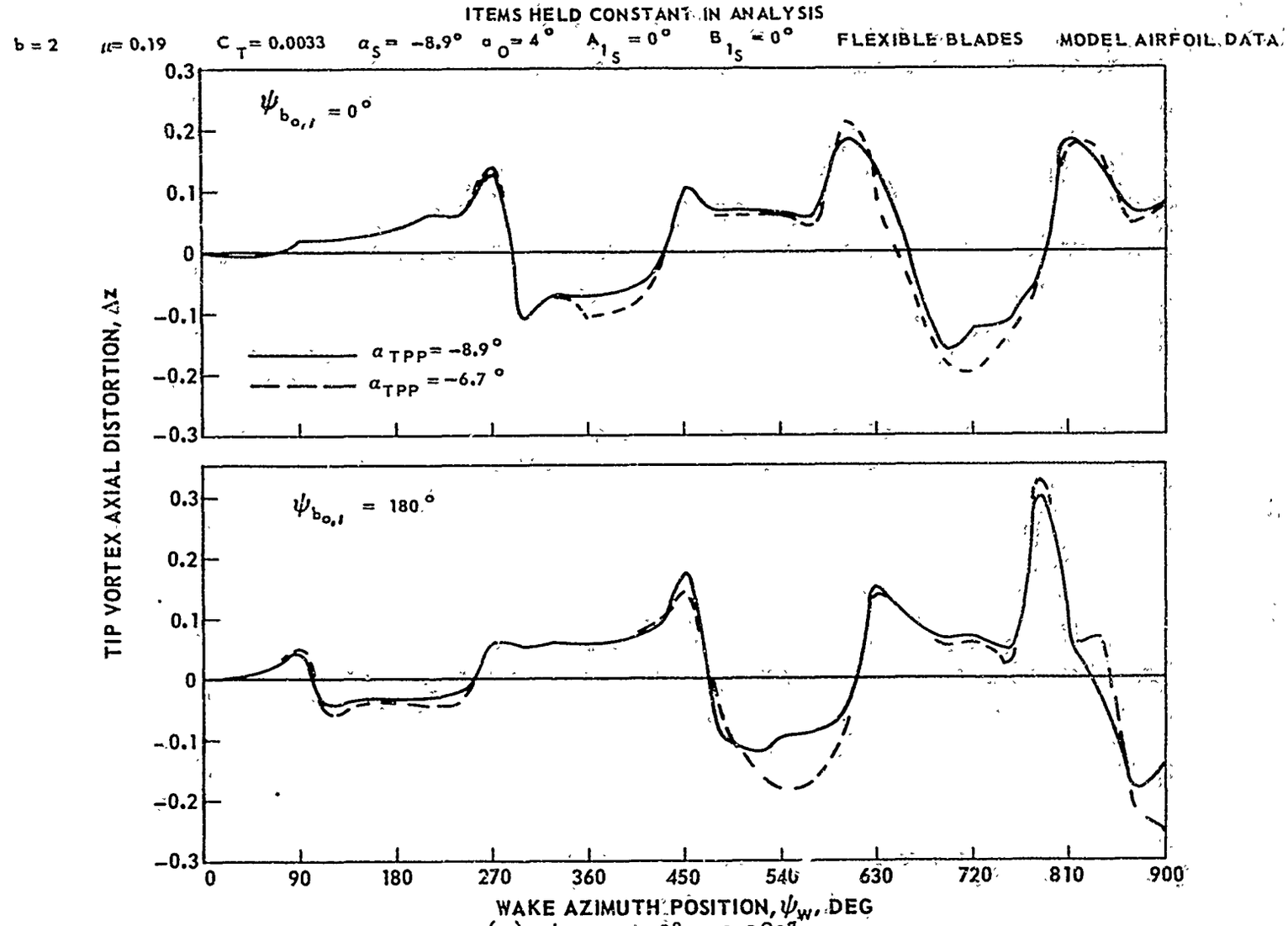

(a) $\psi_{b_{0,1}} = 0°$ and 180°.

Figure 31. Effect of Rotor Tip-Path Plane Angle on Model Rotor Wake Distortions.

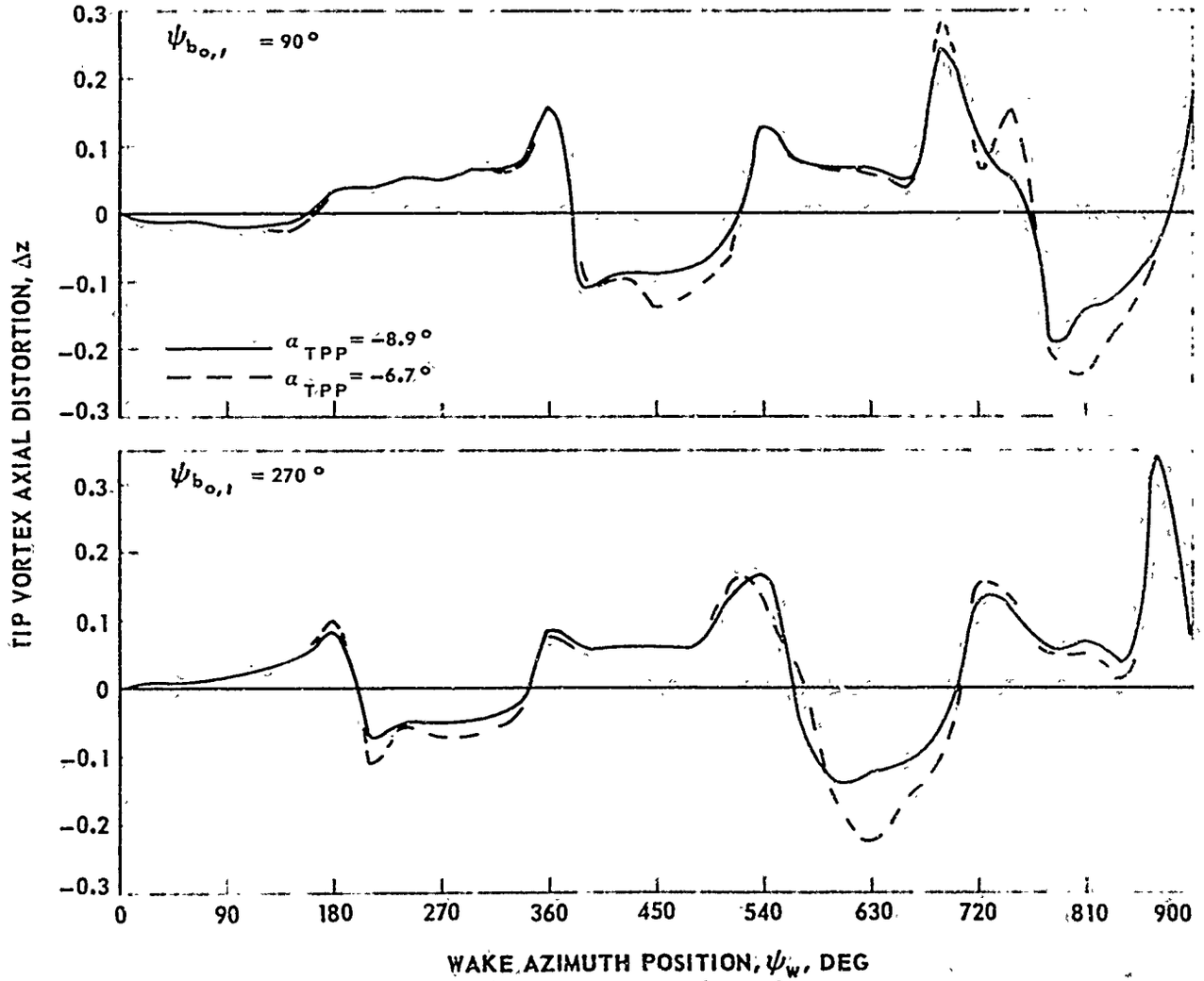

(b) $\psi_{b_{0,1}}$ = 90° and 270°

Figure 31. Concluded.

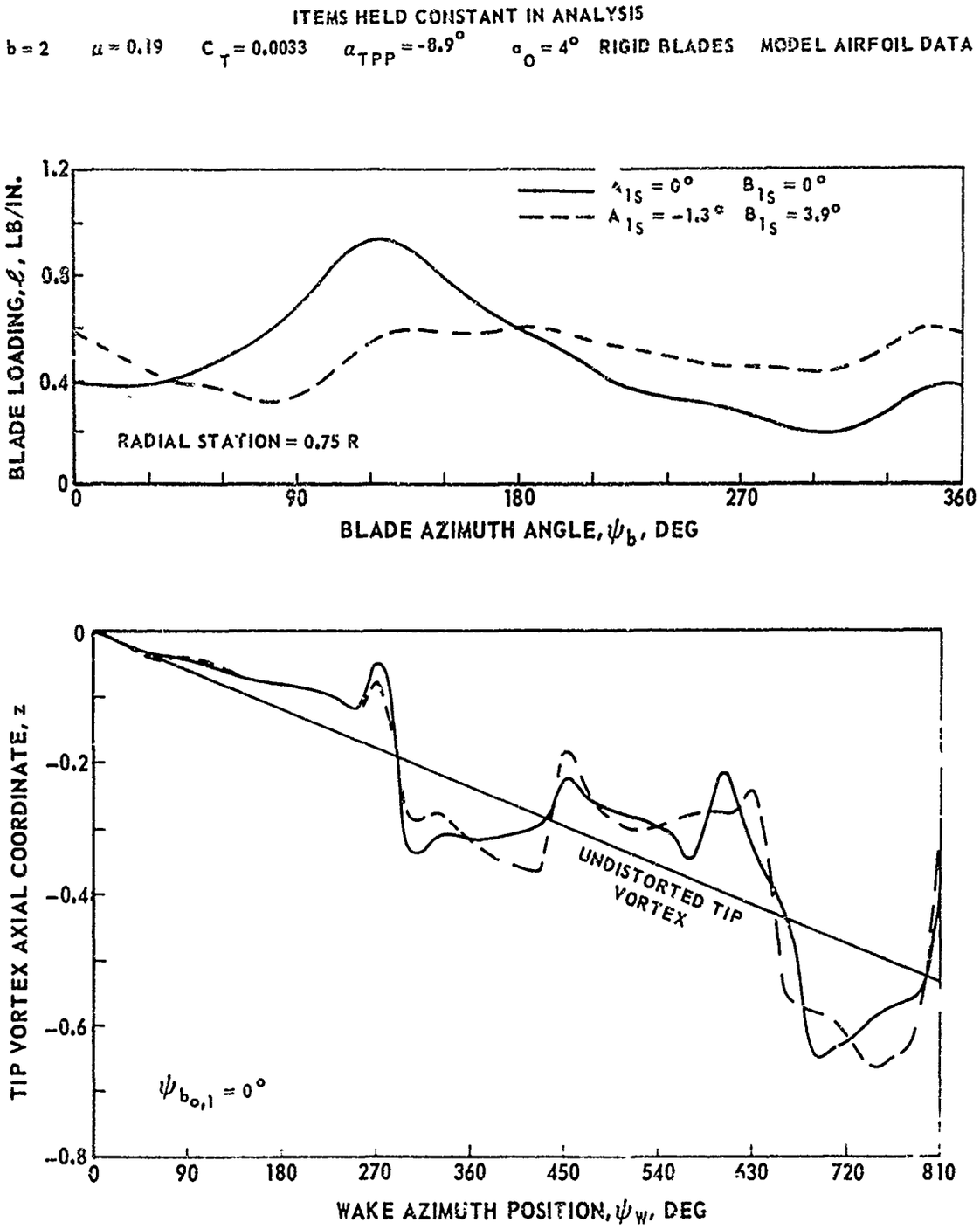

Figure 32. Effect of Cyclic Pitch on Model Rotor Loading and Wake Geometry.

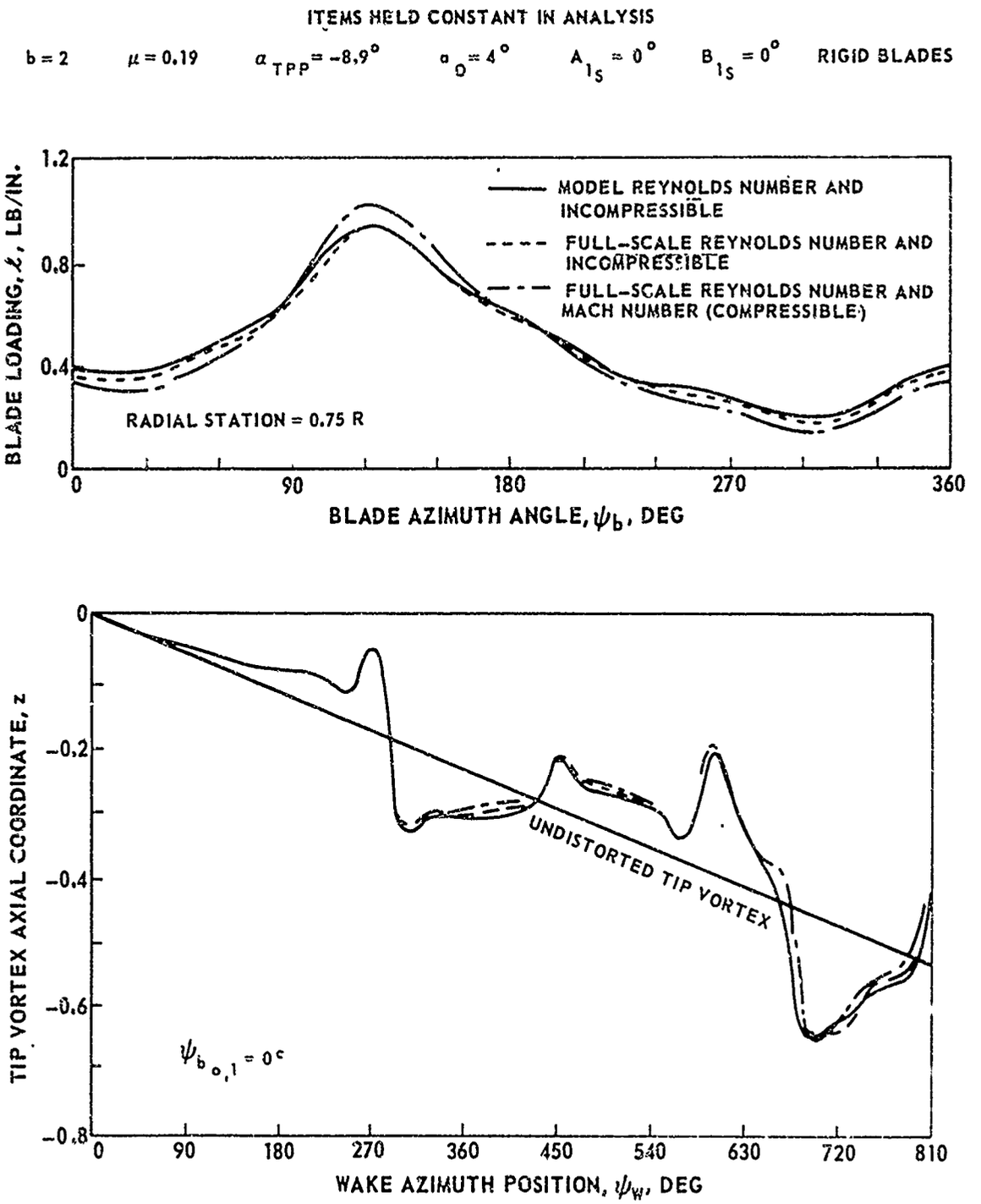

Figure 33. Effect of Reynolds Number and Mach Number on Model Rotor Loading and Wake Geometry.

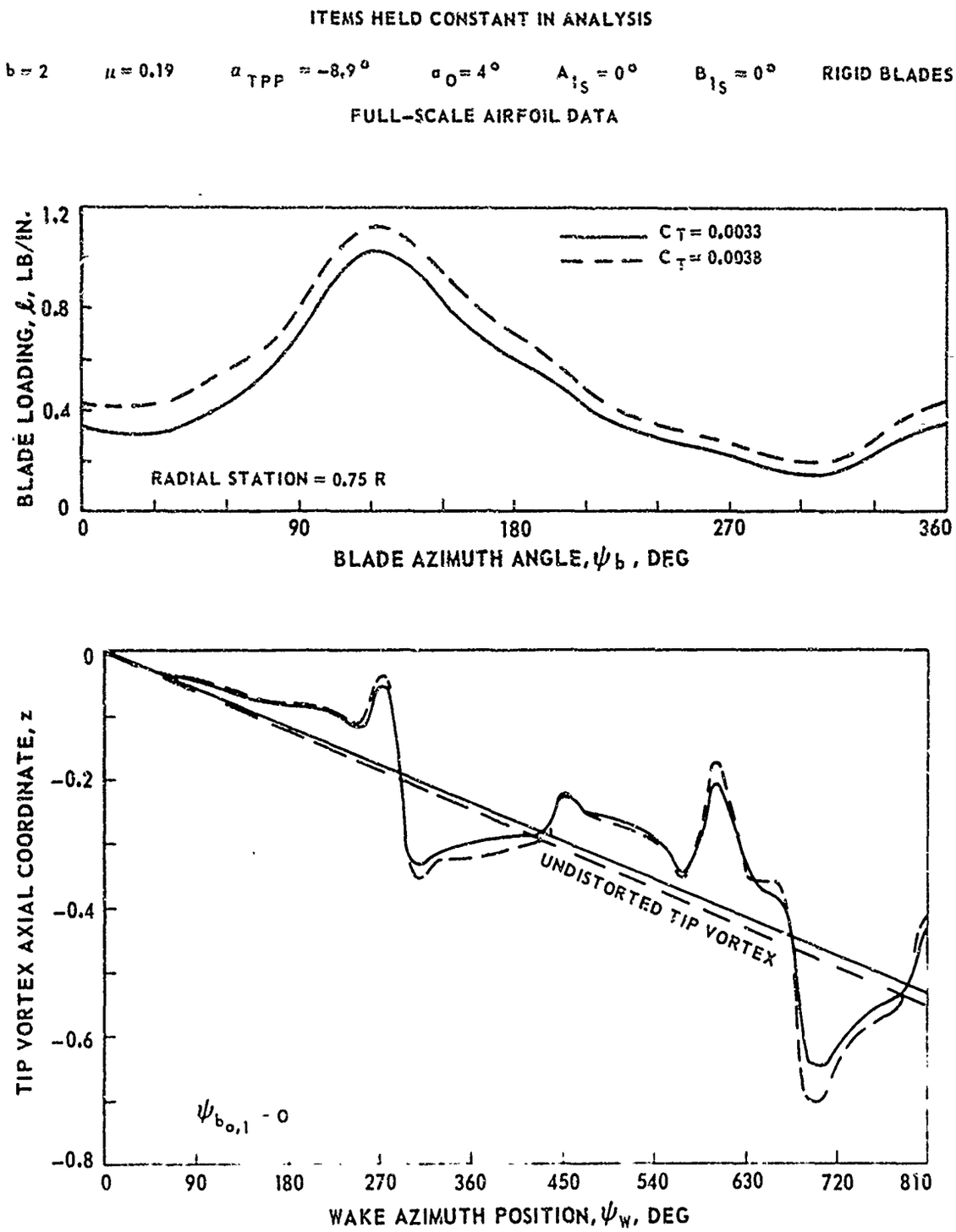

Figure 34. Effect of Thrust Coefficient on Model Rotor Loading and Wake Geometry.

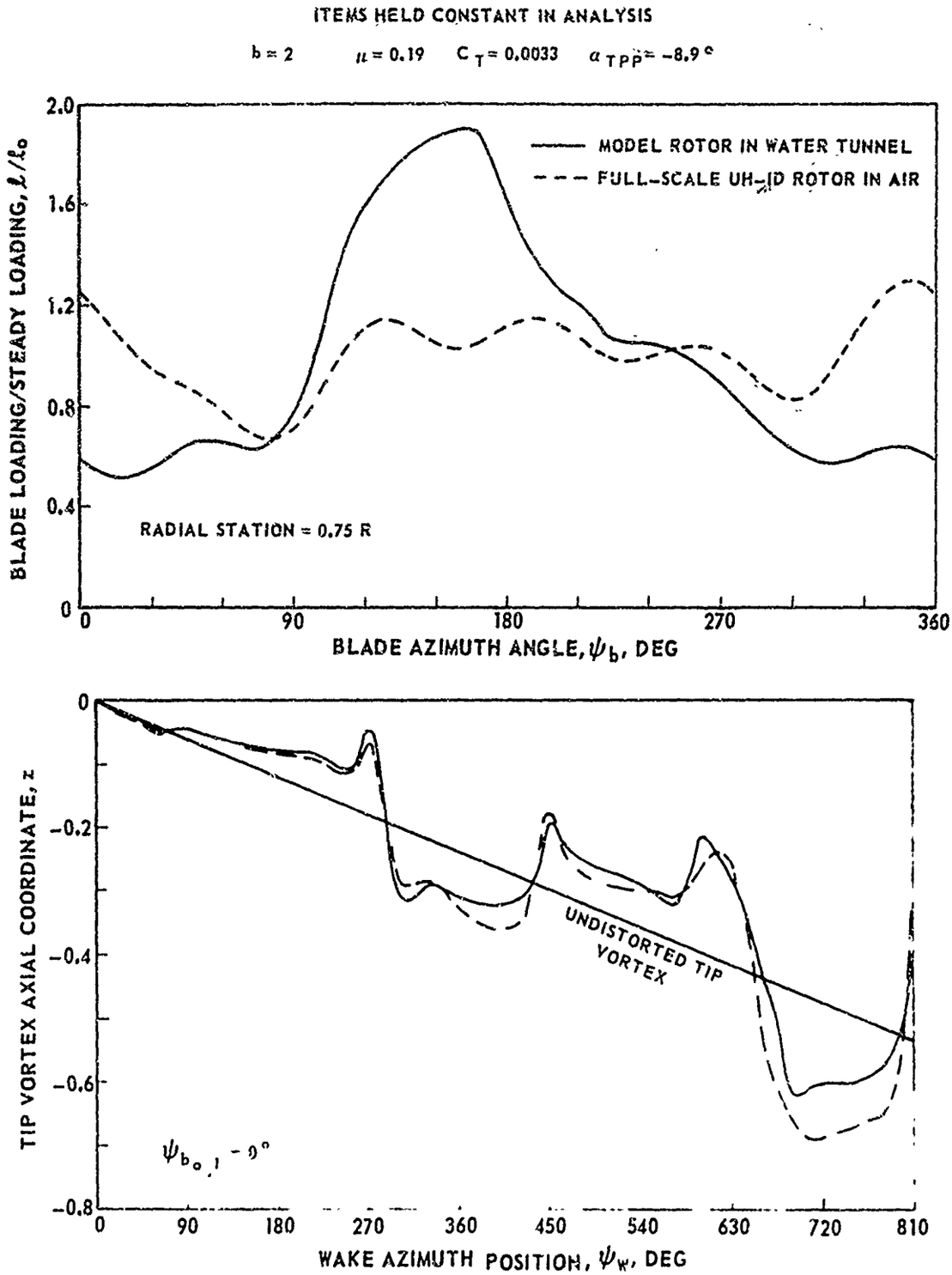

Figure 35. Comparison of Predicted Loading and Wake Geometry of the Full-Scale UH-1D Rotor and Water Tunnel Model Rotor.

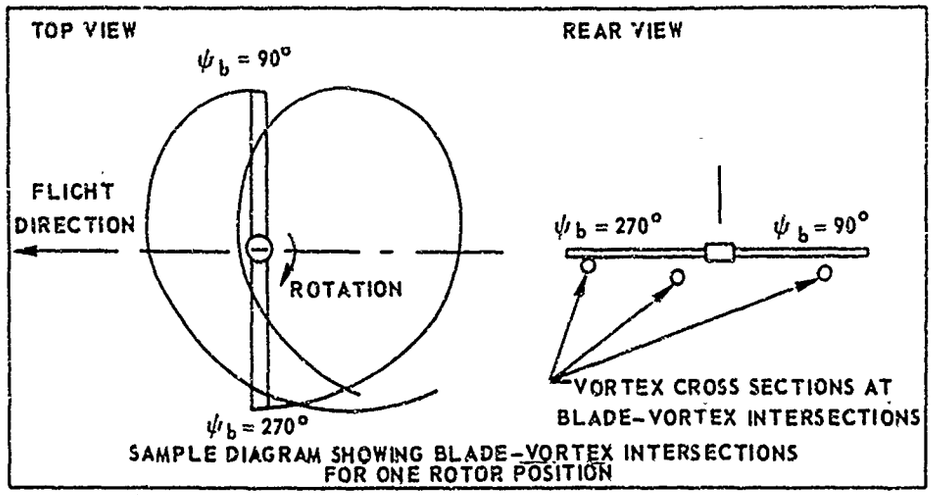

SAMPLE DIAGRAM SHOWING BLADE-VORTEX INTERSECTIONS FOR ONE ROTOR POSITION

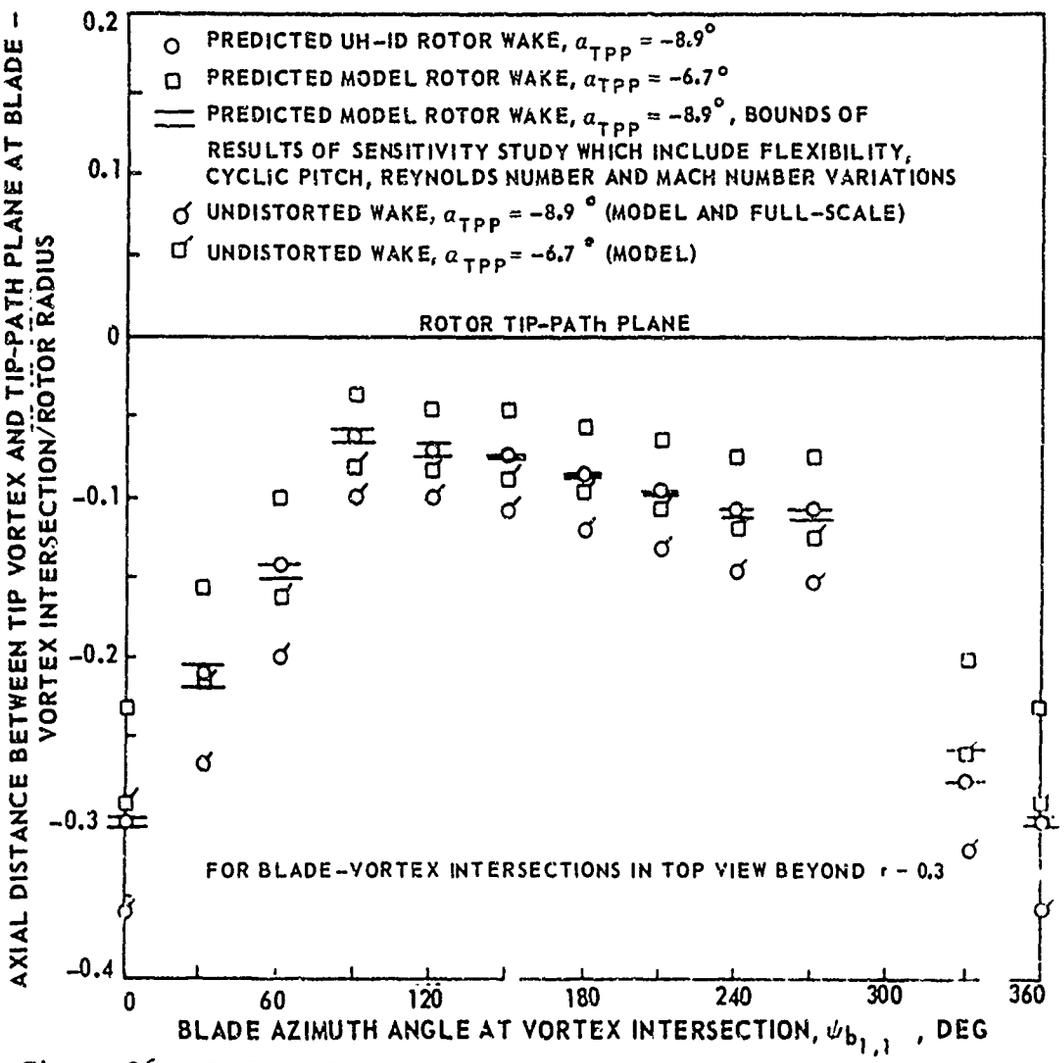

Figure 36. Predicted Wake Geometry Sensitivity Results at Blade-Vortex Intersections -- $\mu = 0.19$, $C_T = 0.0033$.

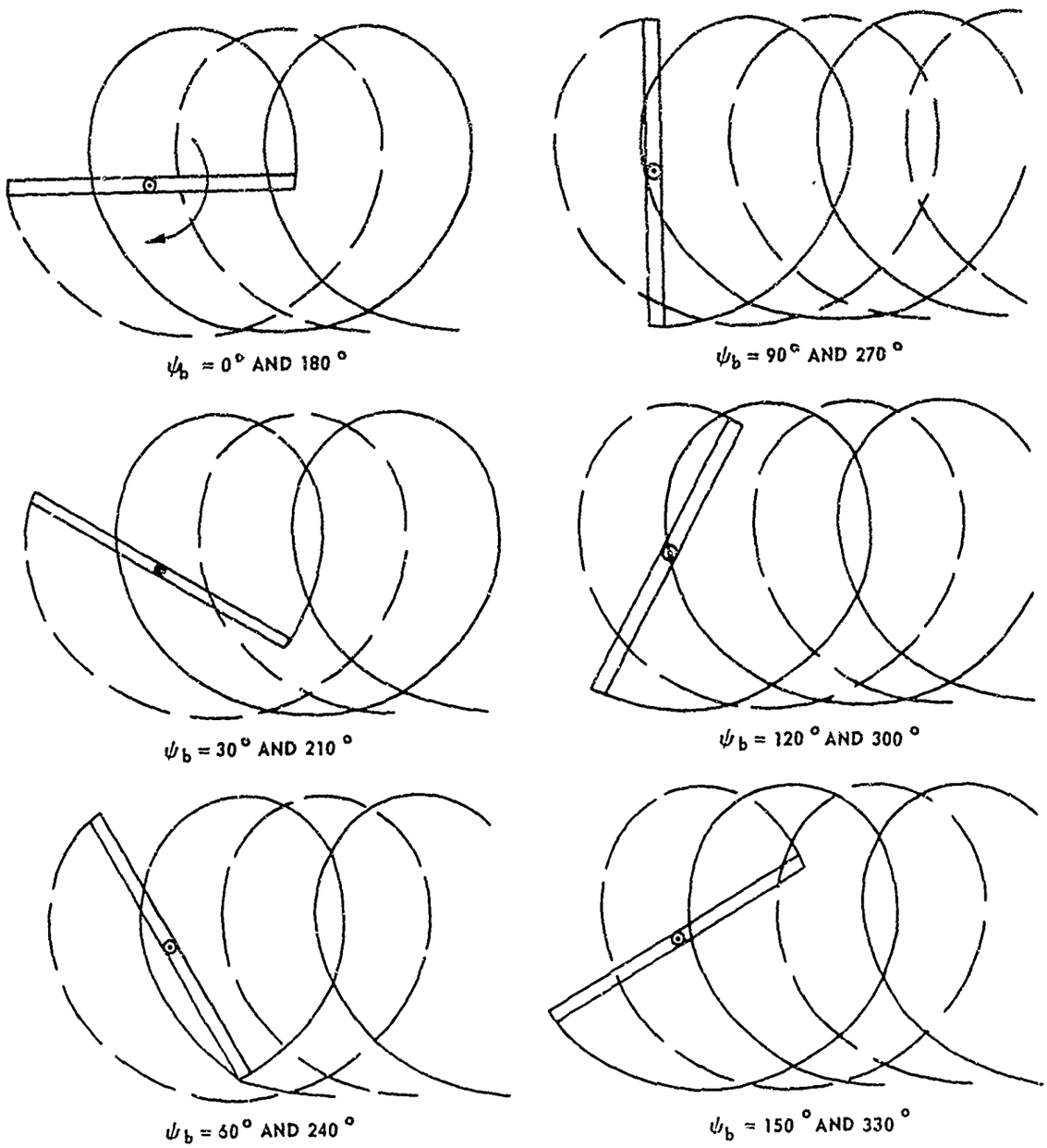

Figure 37. Top View of Undistorted Wake Patterns -- b = 2, μ = 0.19.

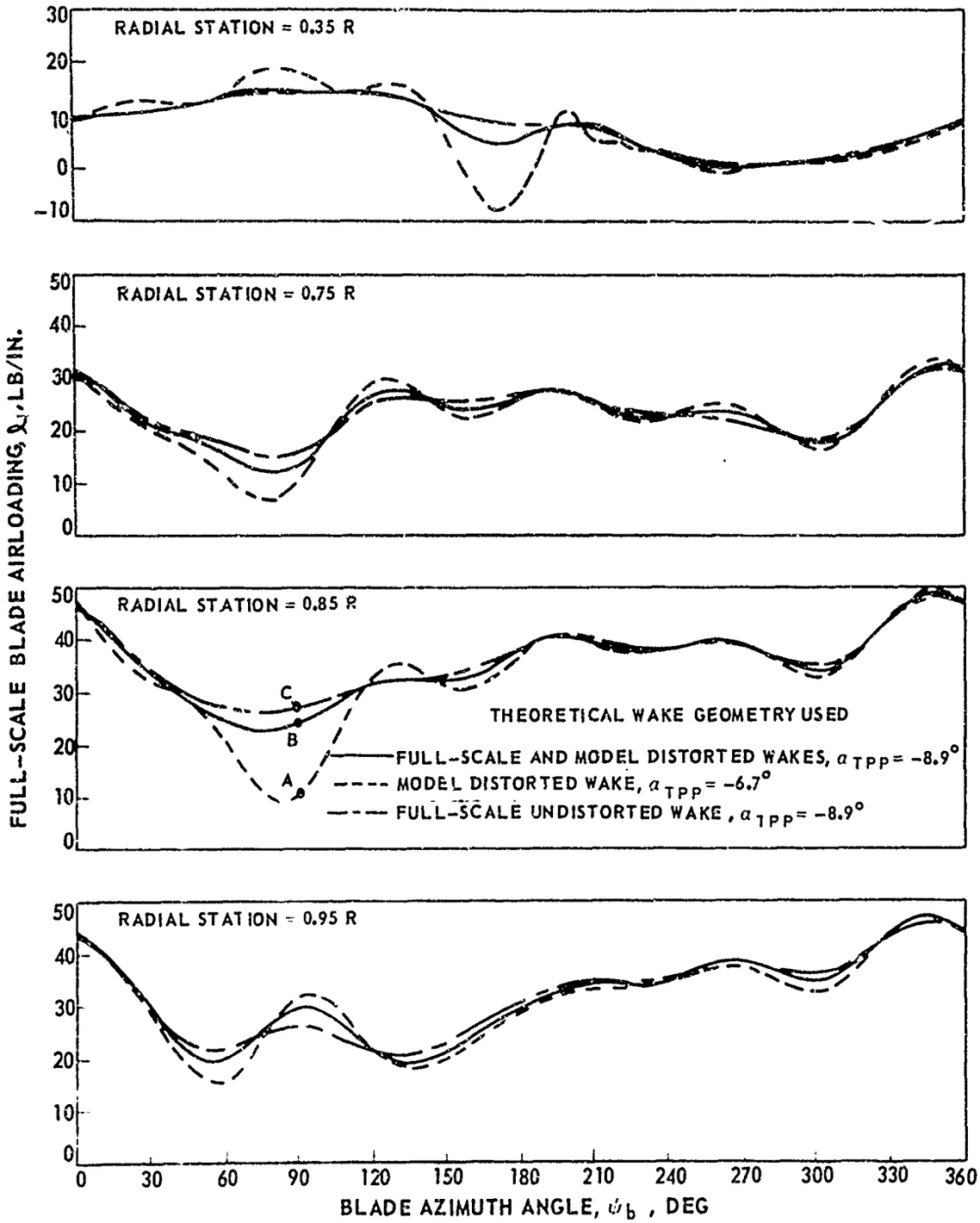

Figure 38. Sensitivity of Predicted Full-Scale Rotor Airloads to Wake Geometry -- UH-1D Rotor, V = 90 Kt, μ = 0.19, C_T = 0.0033.

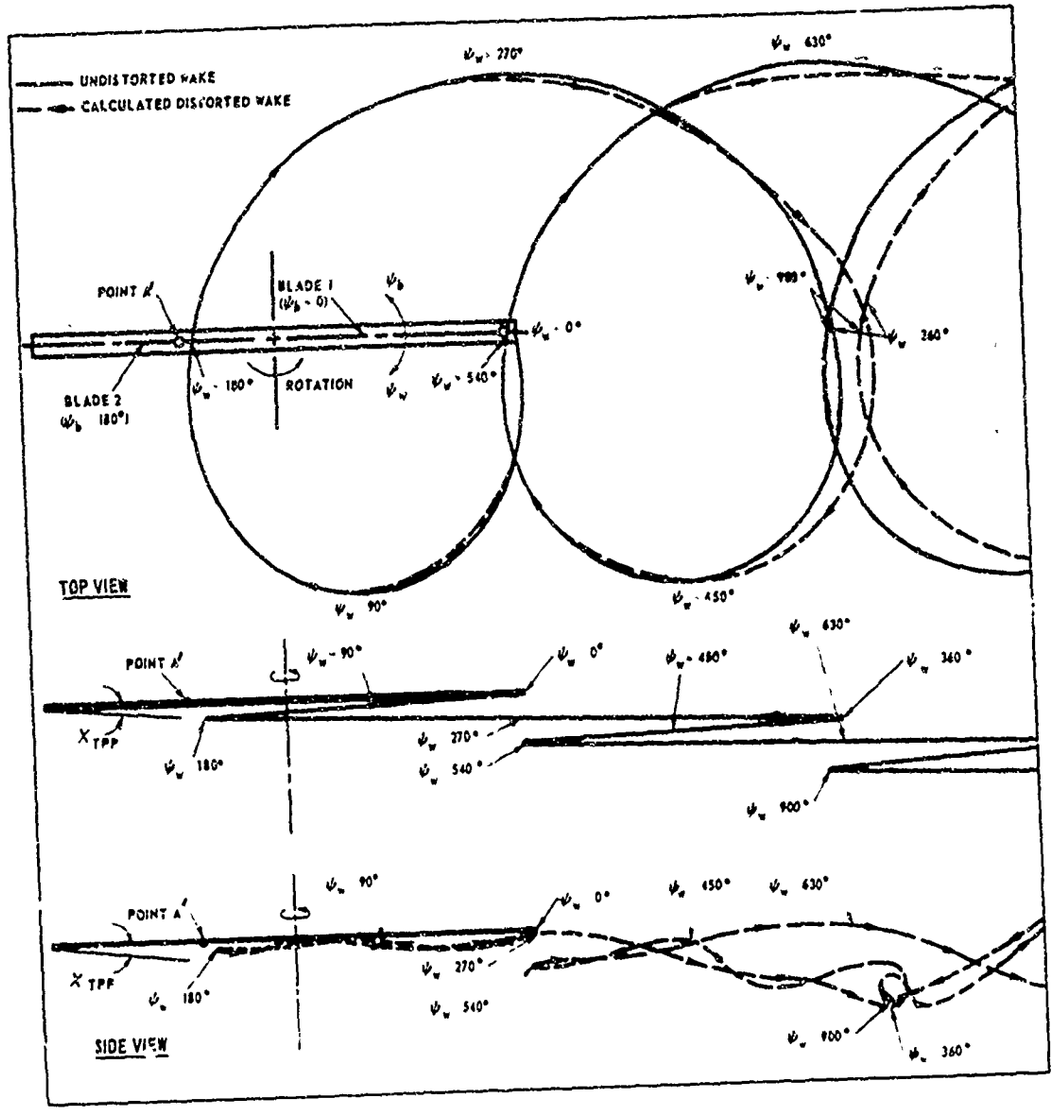

Figure 39. Theoretical Wake Pattern From One Blade of the UH-1A Rotor, V = 89 Kt, μ = 0.21, C_T = 0.0037.

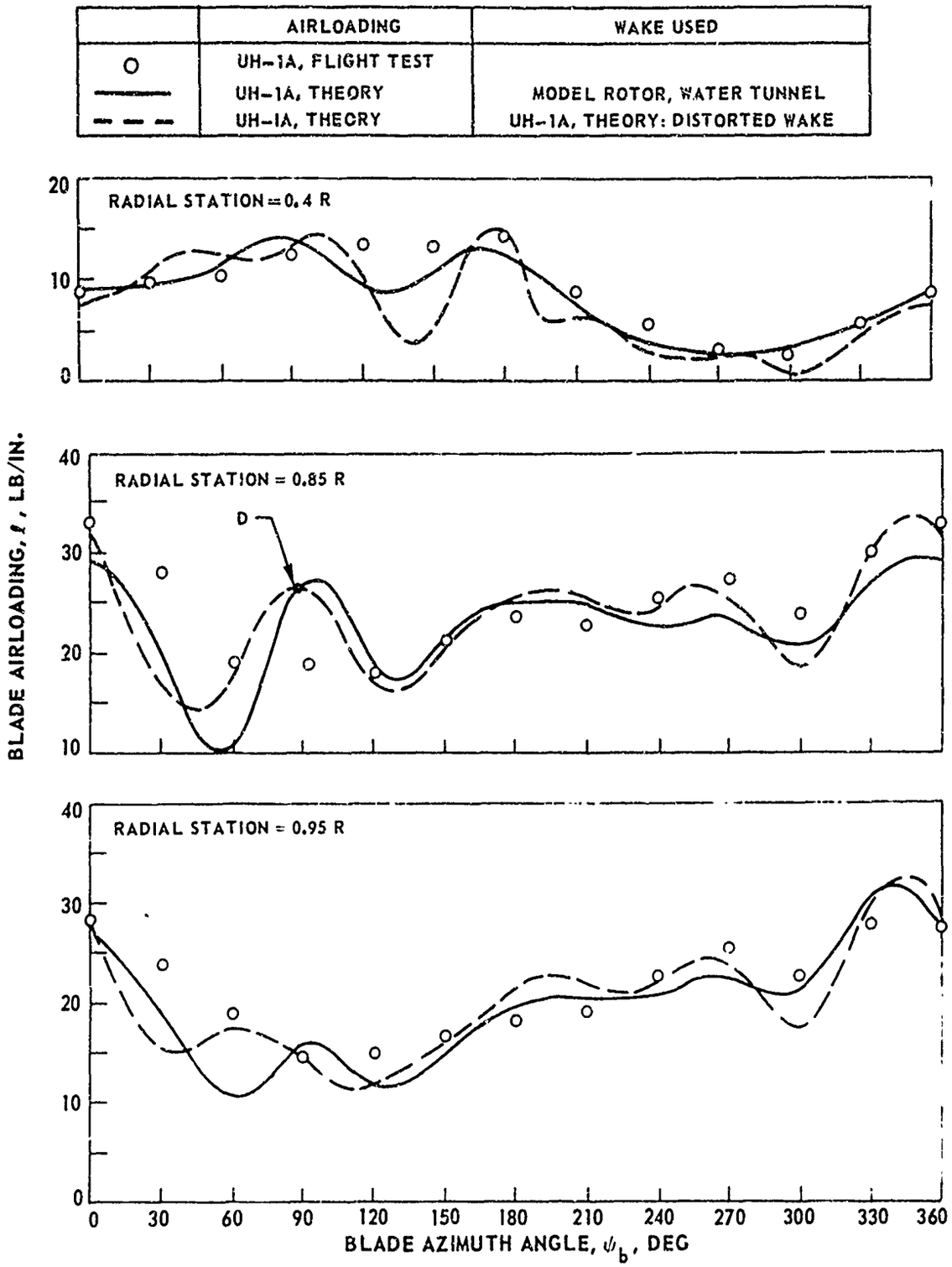

Figure 40. Comparison of Predicted Full-Scale Rotor Airloads Based on Experimental and Theoretical Wake Coordinates With Flight Test Data -- UH-1A Rotor.

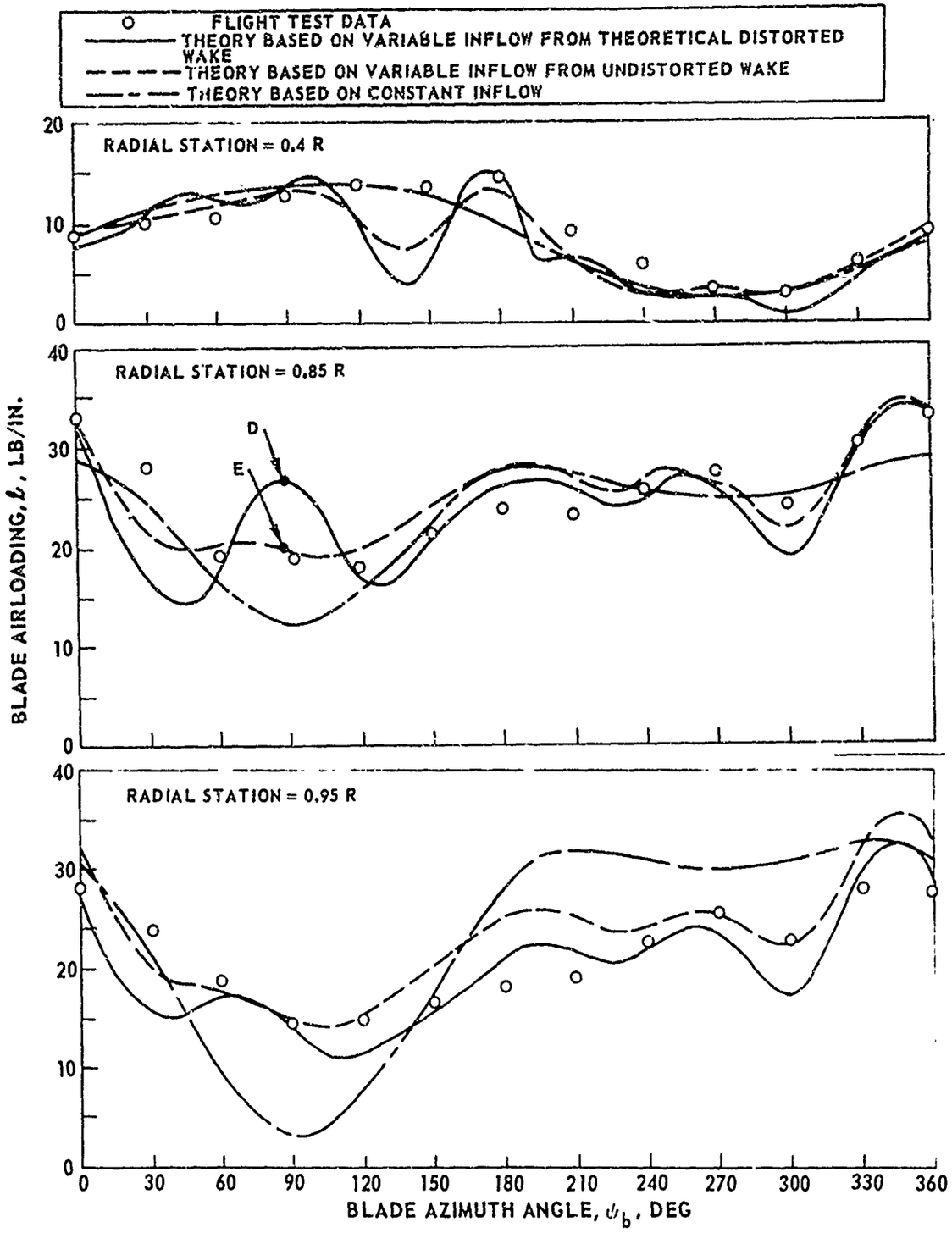

Figure 41. Comparison of Predicted Full-Scale Rotor Airloads Based on Various Theoretical Inflow Sources With Flight Test Data -- UH-1A Rotor, μ = 0.21, C_T = 0.0037, α_{TPP} = 3.6 deg.

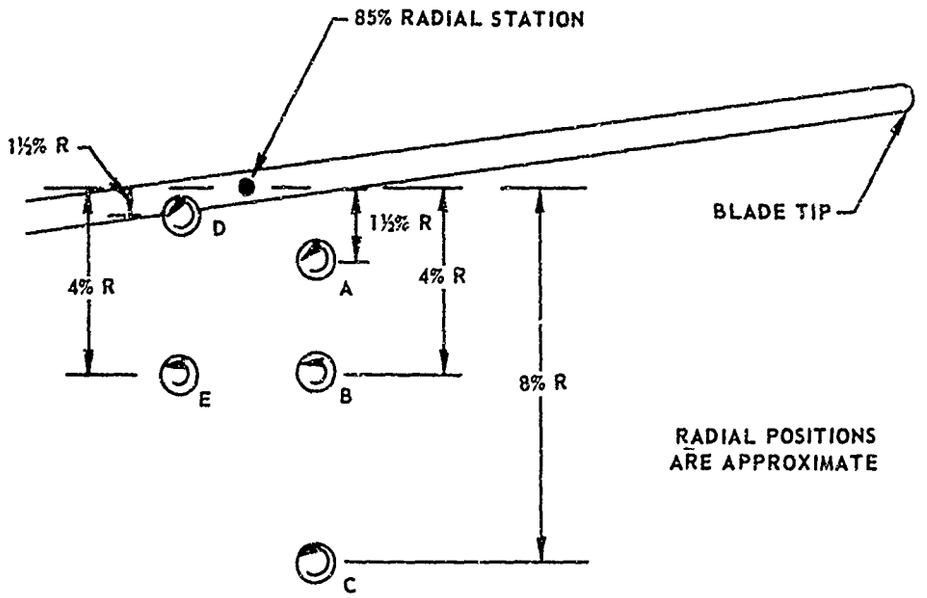

A – MODEL ROTOR THEORETICAL DISTORTED TIP VORTEX, $\alpha_{TPP} = -6.7°$

B – UH-1D THEORETICAL DISTORTED TIP VORTEX, $\alpha_{TPP} = -8.9°$

C – UH-1D UNDISTORTED TIP VORTEX, $\alpha_{TPP} = -8.9°$

D – UH-1A THEORETICAL DISTORTED TIP VORTEX, $\alpha_{TPP} = -3.6°$

ALSO, MODEL ROTOR EXPERIMENTAL TIP VORTEX, $\alpha_{TPP} = -6.3°$

E – UH-1A UNDISTORTED TIP VORTEX, $\alpha_{TPP} = -3.6°$

Figure 42. Tip Vortex Positions Relative to the 85 Percent Radial Station of the Following Blade, ψ_b = 90 deg.

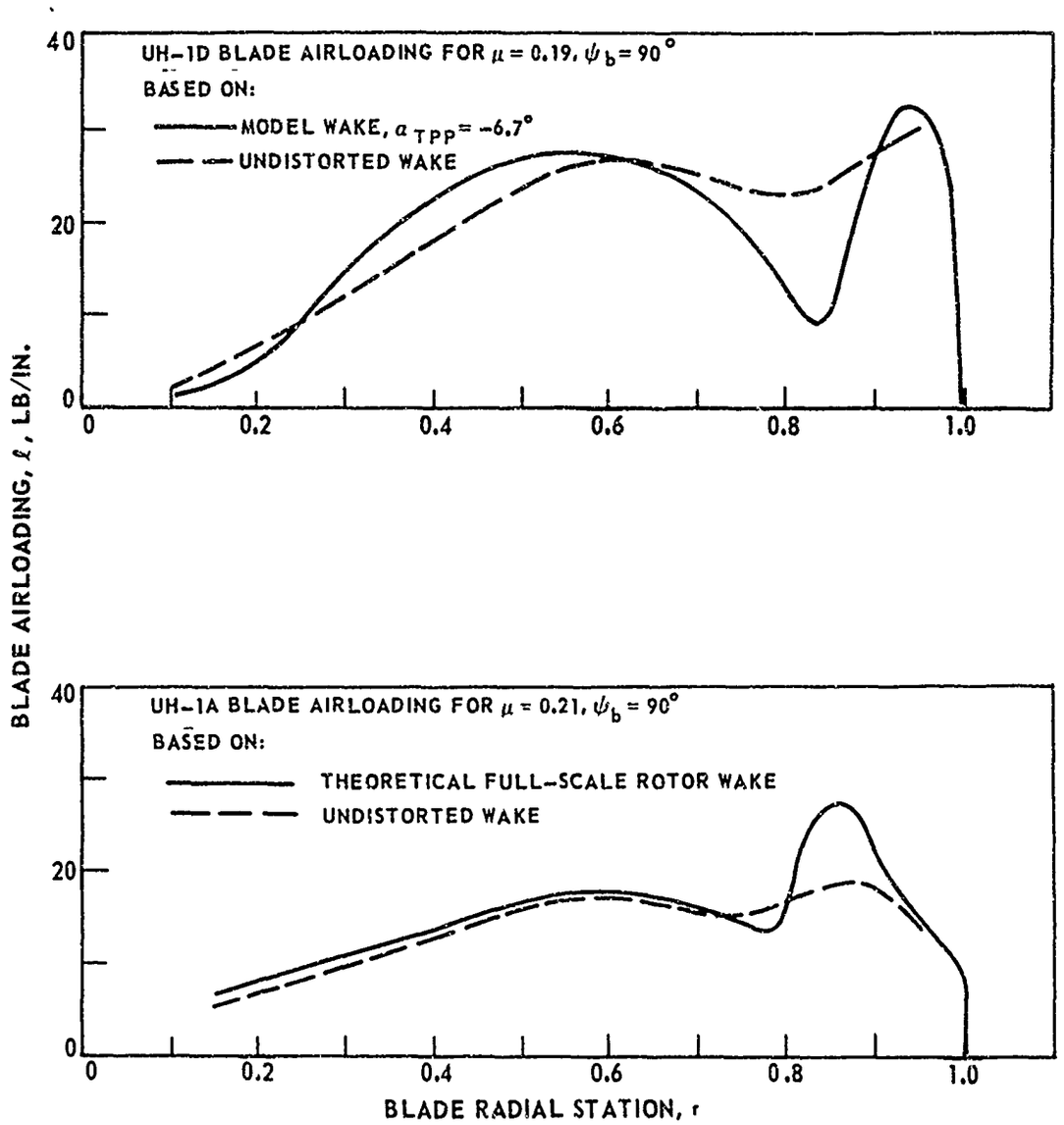

Figure 43. Radial Airloading Distributions at the 90-deg Azimuth Position.

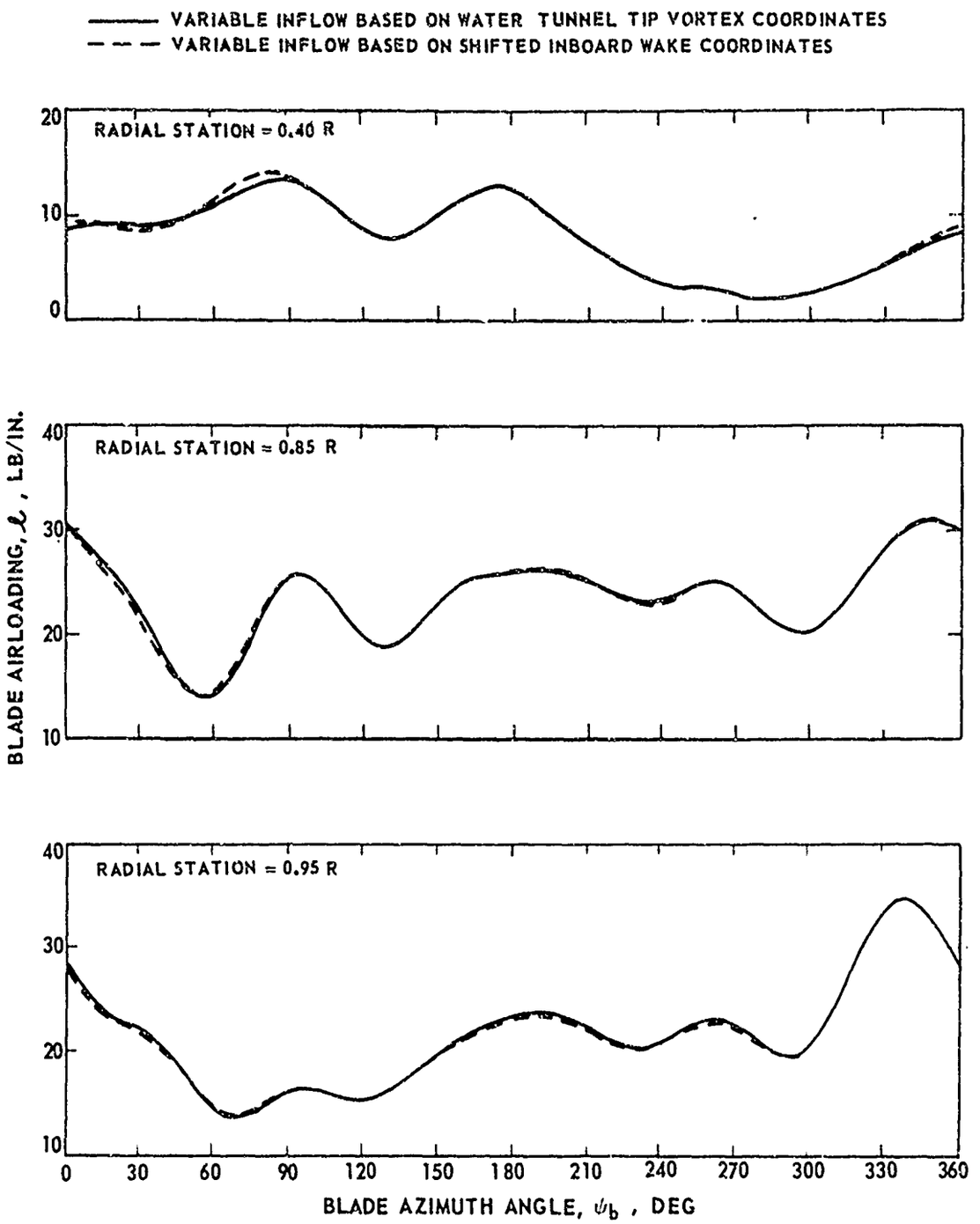

Figure 44. Sensitivity of UH-1A Airloads to Deviations of the Inboard Wake Coordinates, V = 89 Kt, μ = 0.21, C_T = 0.0037.

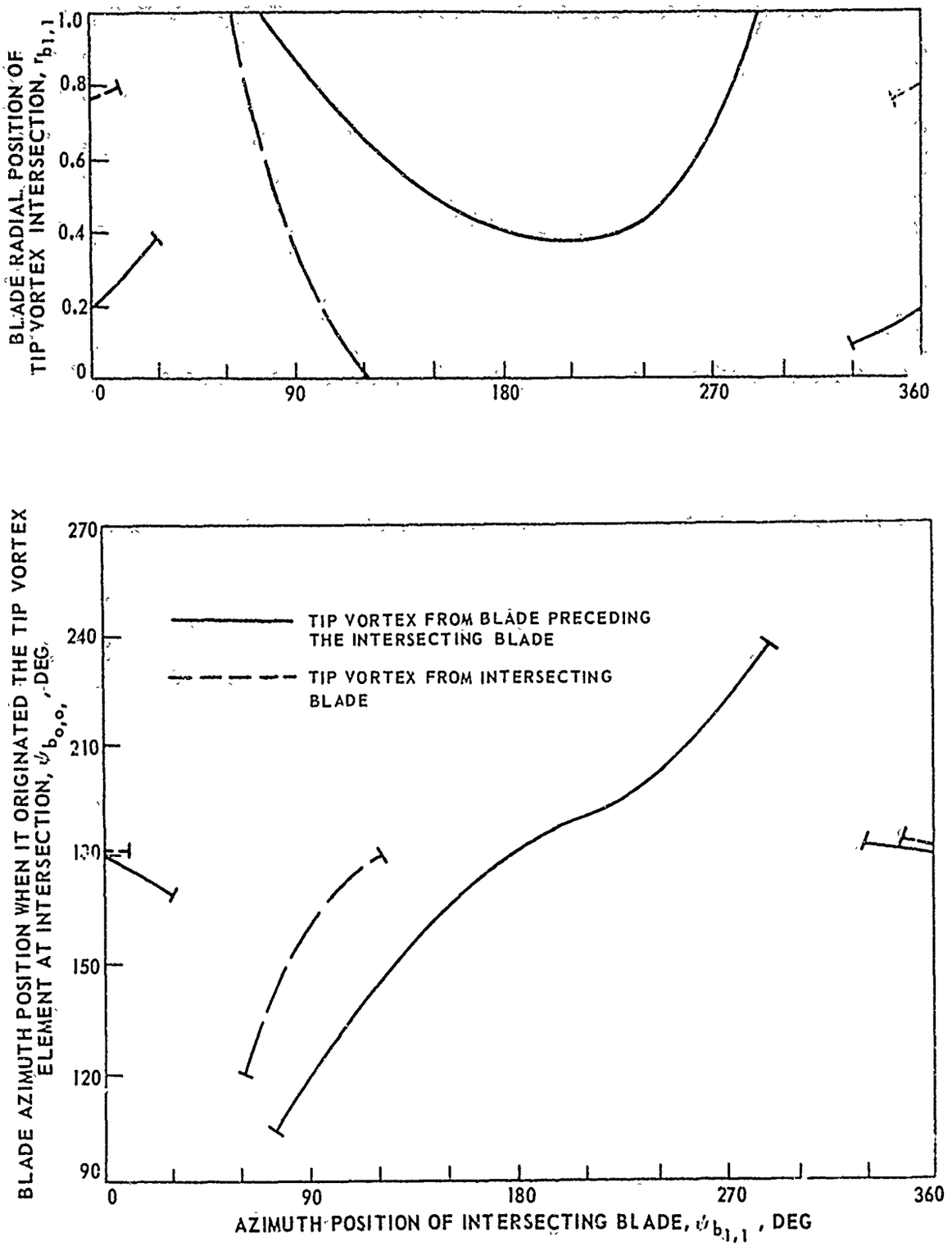

Figure 45. Radial and Azimuthal Coordinates Associated With Blade-Vortex Intersections -- b = 2, μ = 0.19.

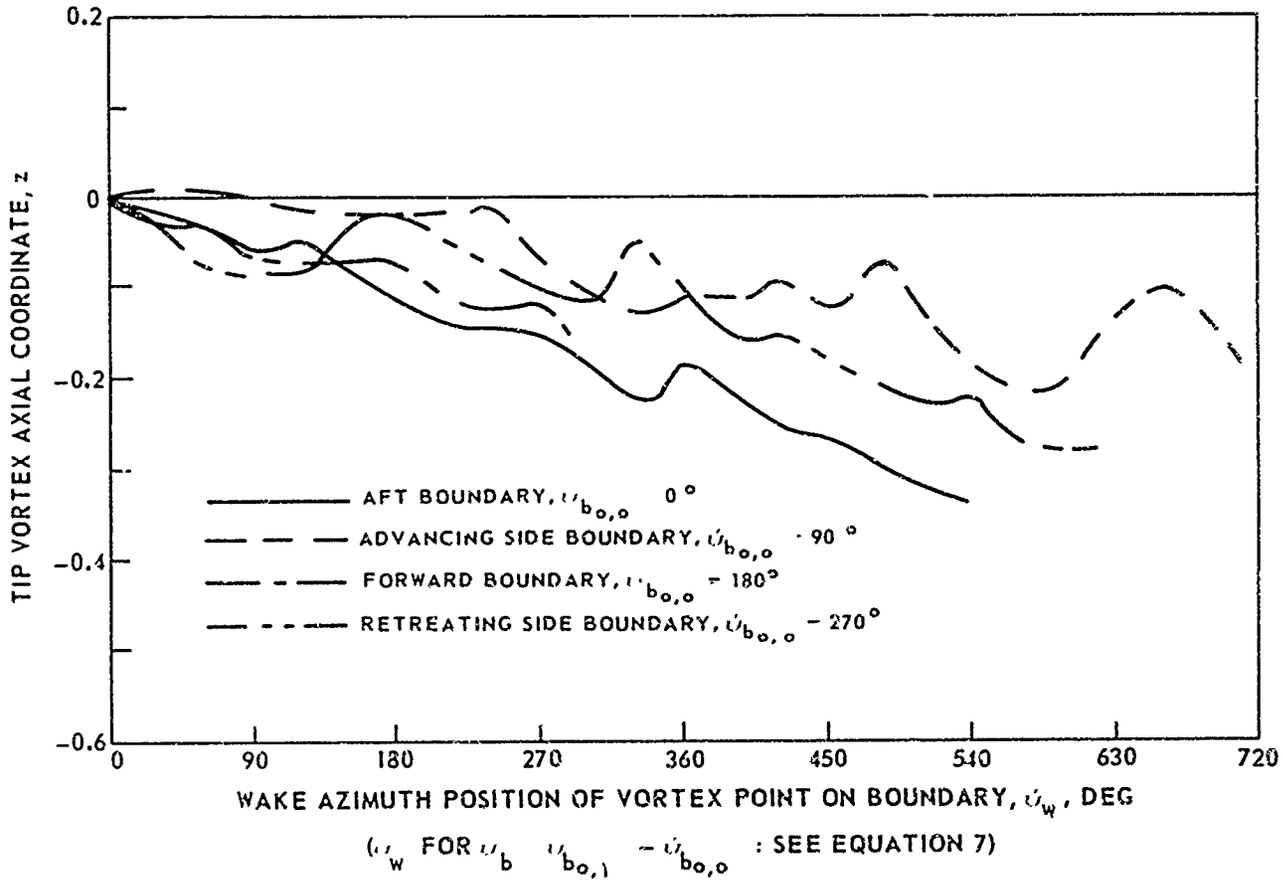

Figure 46. Axial Coordinates of Experimental Wake Boundaries Versus Wake Azimuth Position -- Model Rotor, Simulated 90 Kt, 10,000-lb Lift.

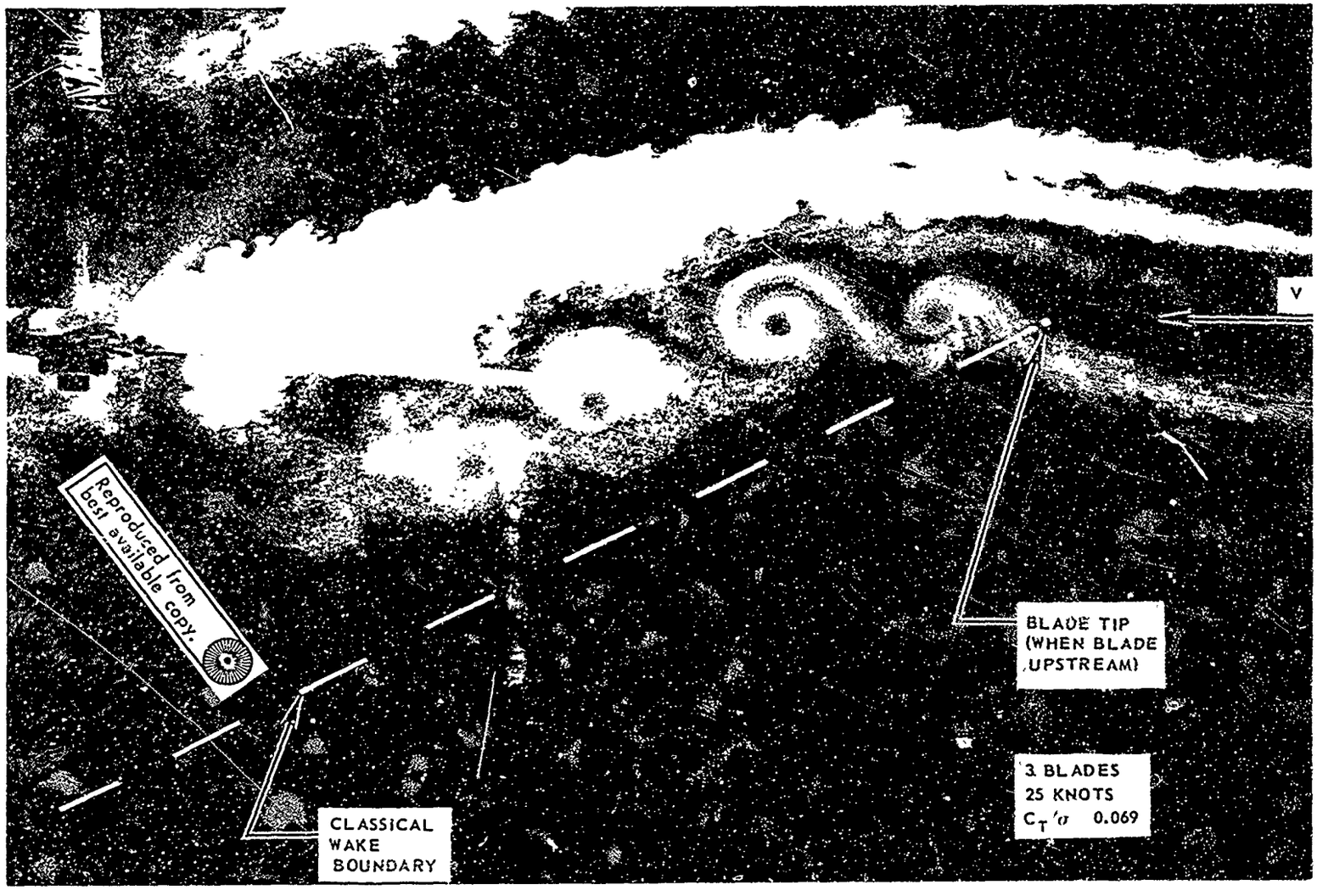

Reproduced from best available copy.

Figure 47. Sample Photograph of Wake Flow Visualization for a Model Rotor Operating in Air.

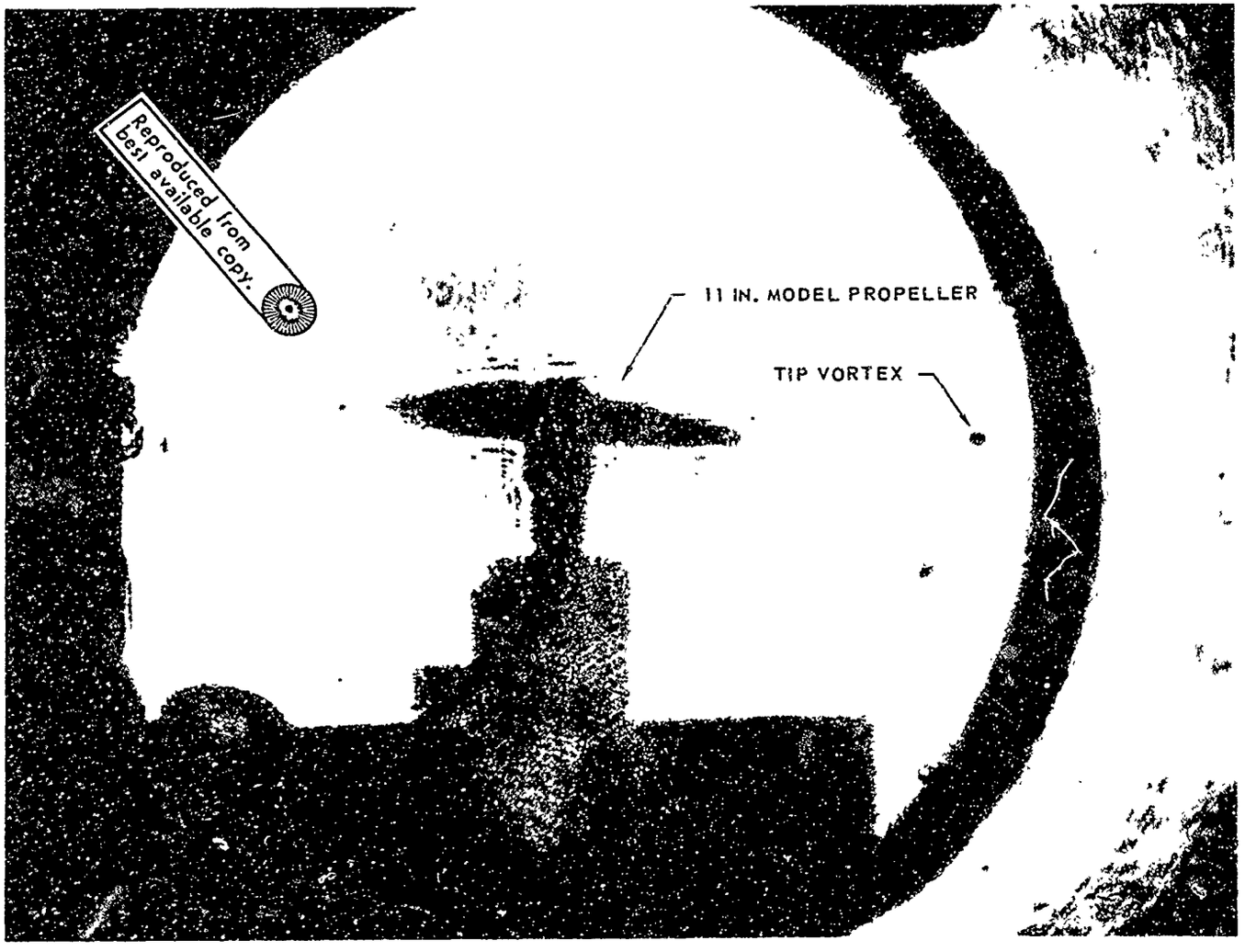

Reproduced from best available copy.

Figure 48. Sample Shadowgraph of Wake of a Model Propeller Obtained Using Laser Holography Techniques.

LITERATURE CITED

1. Lehman, August F., MODEL STUDIES OF HELICOPTER ROTOR FLOW PATTERNS, Oceanics Inc.; USAAVLABS Technical Report 68-17, U. S. Army Aviation Materiel Laboratories, Fort Eustis, Virginia, April 1968, AD 671670.

2. Lehman, August F., MODEL STUDIES OF HELICOPTER ROTOR FLOW PATTERNS, Oceanics Inc., Paper Presented at the 24th Annual National Forum of the American Helicopter Society, Paper No. 207, May 1968.

3. Lehman, August F., and Besold, Jeffrey A., TEST SECTION SIZE INFLUENCE ON MODEL HELICOPTER ROTOR PERFORMANCE, Oceanics Inc.; USAAVLABS Technical Report 71-6, Eustis Directorate, U. S. Army Air Mobility Research and Development Laboratory, Fort Eustis, Virginia, March 1971, AD 724191.

4. Landgrebe, Anton J., AN ANALYTICAL METHOD FOR PREDICTING ROTOR WAKE GEOMETRY, United Aircraft Research Laboratories; Journal of the American Helicopter Society, Vol. 14, No. 4, October 1969, pp. 20-32.

5. Landgrebe, Anton J., AN ANALYTICAL AND EXPERIMENTAL INVESTIGATION OF HELICOPTER ROTOR HOVER PERFORMANCE AND WAKE GEOMETRY CHARACTERISTICS, United Aircraft Research Laboratories; USAAMRDL Technical Report 71-24, Eustis Directorate, U. S. Army Air Mobility Research and Development Laboratory, Fort Eustis, Virginia, June 1971.

6. Clark, David R., and Landgrebe, Anton J., WAKE AND BOUNDARY LAYER EFFECTS IN HELICOPTER ROTOR AERODYNAMICS, United Aircraft Corp.; Paper presented at the AIAA Fluid and Plasma Dynamics Conference, June 1971.

7. Jenney, David S., Olson, John R., and Landgrebe, Anton J., A REASSESSMENT OF ROTOR HOVERING PERFORMANCE PREDICTION METHODS, United Aircraft Corp.; Journal of the American Helicopter Society, Vol. 13, No. 2, April 1968, pp. 1-26.

8. Bellinger, E. D., ANALYTICAL INVESTIGATION OF THE EFFECTS OF BLADE FLEXIBILITY, UNSTEADY AERODYNAMICS, AND VARIABLE INFLOW ON HELICOPTER ROTOR STALL CHARACTERISTICS; United Aircraft Research Laboratories, Presented at the 27th Annual National V/STOL Forum of the American Helicopter Society, Preprint No. 520, May 1971.

9. Bisplinghoff, Raymond L., Ashley, Holt, and Halfman, Robert L., AEROELASTICITY, Reading, Mass., Addison-Wesley Publishing Co., 1955.

10. Arcidiacono, Peter J., PREDICTION OF ROTOR INSTABILITY AT HIGH FORWARD SPEEDS, VOL. I: STEADY FLIGHT DIFFERENTIAL EQUATIONS OF MOTION FOR A FLEXIBLE HELICOPTER ROTOR BLADE WITH CHORDWISE MASS UNBALANCE, Sikorsky Aircraft Division, United Aircraft Corp.; USAAVLABS Technical Report 68-18A, U. S. Army Aviation Materiel Laboratories, Fort Eustis, Virginia, February 1969, AD 685860.

11. Gessow, Alfred, and Myers, Gary C., Jr., AERODYNAMICS OF THE HELICOPTER, New York, Frederick Ungar Publishing Co., 1952.

12. Piziali, Raymond A., and DuWaldt, Frank A., A METHOD FOR COMPUTING ROTARY-WING AIRLOAD DISTRIBUTIONS IN FORWARD FLIGHT, Cornell Aeronautical Laboratories; TCREC Technical Report 62-44, U. S. Army Transportation Research Command, Fort Eustis, Virginia, November 1962.

13. Gray, Robin B., AN AERODYNAMIC ANALYSIS OF A SINGLE-BLADED ROTOR IN HOVERING AND LOW SPEED FLIGHT AS DETERMINED FROM SMOKE STUDIES OF THE VORTICITY DISTRIBUTION IN THE WAKE, Princeton University Aeronautical Engineering Department, Report No. 356, Princeton University, Princeton, New Jersey, September 1956.

14. Tararine, V. S., EXPERIMENTAL AND THEORETICAL STUDY OF LOCAL INDUCED VELOCITIES OVER A ROTOR DISC FOR ANALYTICAL EVALUATION OF THE PRIMARY LOADS ACTING ON HELICOPTER ROTOR BLADES, Department Army Report No. DE 2012, European Research Office, October 1960.

15. Jones, J. P., Simons, I. A., and Pacifico, R., THE MOVEMENT, STRUCTURE, AND BREAKDOWN OF TRAILING VORTICES FROM A ROTOR BLADE, University of Southampton, CAL/USAAVLABS Symposium Proceedings on Aerodynamic Problems Associated With V/STOL Aircraft, Vol. 1, Cornell Aeronautical Laboratory, Inc., Buffalo, New York, June 1966.

16. Werle, Henri, and Armand, Claude, MESURES ET VISUALISATIONS INSTATIONAIRES SUR LES ROTORS, Office National D'Etudes Et De Recherches Aerospatiales, Chatillon, France, November 1969.

17. Tanner, W. H., CHARTS FOR ESTIMATING ROTARY WING PERFORMANCE IN HOVER AND HIGH FORWARD SPEEDS, United Aircraft Corp., Sikorsky Aircraft Division; NASA Contractor Report CR-114, 1965.

18. Burpo, F. B., et al., MEASUREMENT OF DYNAMIC AIRLOADS ON A FULL-SCALE SEMI-RIGID ROTOR, Bell Helicopter Co.; TCREC Technical Report 62-42, U. S. Army Transportation Research Command, Fort Eustis, Virginia, December 1962.

19. Ward, John F., and Snyder, William J., THE DYNAMIC RESPONSE OF A FLEXIBLE ROTOR BLADE TO A TIP-VORTEX INDUCED MOVING FORCE, Paper presented at the AIAA/AHS VTOL Research, Design and Operations Meeting, AIAA Paper No. 69-203, February 1969.

20. Heyson, Harry H., LINEARIZED THEORY OF WIND-TUNNEL JET-BOUNDARY CORRECTIONS AND GROUND EFFECT FOR VTOL/STOL MODELS, NASA Technical Report TR R-124, NASA Langley Research Center, Hampton, Virginia, 1962.

21. Heyson, Harry H., THE FLOW THROUGHOUT A WIND TUNNEL CONTAINING A ROTOR WITH A SHARPLY DEFLECTED WAKE, NASA Langley Research Center, Proceedings of the Third CAL/AVLABS Symposium, Vol. II, Cornell Aeronautical Laboratories, Buffalo, New York, June 1969.

22. Lehman, August F., MODEL STUDIES OF HELICOPTER TAIL ROTOR FLOW PATTERNS IN AND OUT OF GROUND EFFECT, Oceanics Inc.; USAAVLABS Technical Report 71-12, Eustis Directorate, U. S. Army Air Mobility Research and Development Laboratory, Fort Eustis, Virginia, April 1971.

23. Cassarino, Sebastian J., EFFECT OF ROOT CUTOUT ON HOVER PERFORMANCE, United Aircraft Corp., Sikorsky Aircraft Division; AFFDL Technical Report AFFDL-TR-70-70, Air Force Flight Dynamics Laboratory, Wright-Patterson Air Force Base, Ohio, June 1970.

24. Tanner, W. H., and Wohlfeld, R. M., VORTEX FIELD, TIP VORTEX, AND SHOCK FORMATION ON A MODEL PROPELLER, Bell Helicopter Co., Paper Presented at the Third CAL/AVLABS Symposium on Aerodynamics of Rotary Wing and VTOL Aircraft, Cornell Aeronautical Laboratories, Buffalo, New York, 1969.